SVHEAT SVENVIRO

1D/2D/3D FINITE ELEMENT
FREEZE/THAW MODELING

Verification Manual

Written by:
The Bentley Systems Team

Last Updated: Wednesday, August 28, 2019

Bentley Systems Incorporated

COPYRIGHT NOTICE

TRADEMARK NOTICE

1 INTRODUCTION

The word “Verification”, when used in connection with computer software can be defined as “the ability of the computer code to provide a solution consistent with the physics defined by the governing partial differential equation, PDE”. There are also other factors such as initial conditions, boundary conditions, and control variables that also affect the accuracy of the code to perform as stated.

“Verification” is generally achieved by solving a series of so-called “benchmark” problems. “Benchmark” problems are problems for which there is a closed-form solution or for which the solution has become “reasonably certain” as a result of long-hand calculations that have been performed. Publication of the “benchmark” solutions in research journals or textbooks also lends credibility to the solution. There are also example problems that have been solved and published in the User Manual documentation associated with other comparable software packages. While these are valuables checks to perform, it must be realized that it is possible that errors can be transferred from one’s software solution to another. Consequently, care must be taken in performing the “verification” process on a particular software package. It must also be remembered there is never such a thing as complete software verification for “all” possible problems. Rather, it is an ongoing process that establishes credibility with time.

Bentley Systems takes the process of “verification” most seriously and has undertaken a wide range of steps to ensure that the SVHEAT software will perform as intended by the theory of saturated-unsaturated freezing and thawing.

The following models represent comparisons made to textbook solutions, hand calculations, and other software packages. We at Bentley Systems are dedicated to providing our clients with reliable and tested software. While the following list of example models is comprehensive, it does not reflect the entirety of models, which may be posed to the SVHEAT software. It is our recommendation that water balance checking be performed on all model runs prior to presentation of results. It is also our recommendation that the modeling process moves from simple to complex models with simpler models being verified through the use of hand calculations or simple spreadsheet calculations.

2 ONE-DIMENSIONAL HEAT TRANSFER

2.1 LU ET AL. (2007), TARNAWSKI ET AL. (2009): VERIFY THERMAL CONDUCTIVITY OF SOILS

Project: Geothermal
Model: Verify_ThermalConductivity_Johansen_Metric,
Verify_ThermalConductivity_Johansen_Imperial,
Verify_ThermalConductivity_Lu_Metric,
Verify_ThermalConductivity_Lu_Imperial,
Verify_ThermalConductivity_DeVries_Metric,
Verify_ThermalConductivity_DeVries_Imperial

SVHEAT has implemented several methods to estimate the thermal conductivity of soils, including the approach presented by De Vries (1963), Johansen (1975), and Lu et al. (2007). Based on experimental data, Lu et al. (2007) improved the Johansen approach so that the thermal conductivity can be reasonably predicted with the full range of water content. Tarnawski et al. (2009) adjusted the fitting parameter for Lu et al. (2007) model according to the quartz content effect on the thermal conductivity.

2.1.1 Purpose

Verify the calculation of thermal conductivity with the Johansen (1975) model, Lu et al. (2007) model, and De Vries (1963) model that has been implemented in the SVHEAT software. The behavior of thermal conductivity changing with water content, dry density and temperature is also presented in the benchmark.

2.1.2 Geometry and Boundary Conditions

To compare the calculated thermal conductivity in metric and imperial unit for each approach of Johansen (1975), Lu et al. (2007), and De Vries (1963). Six models were created with the same geometry as shown in Figure 1.

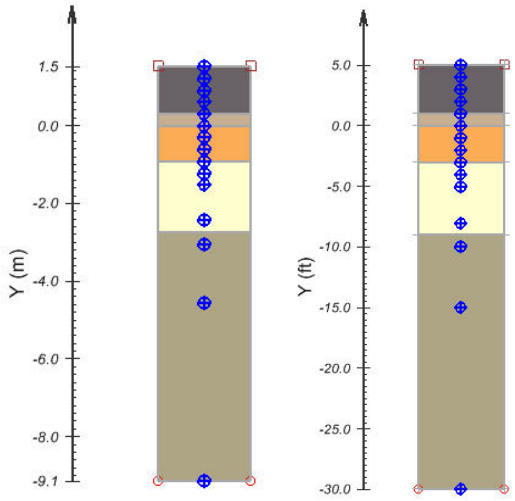

Figure 1 Model geometry for the verification of thermal conductivity (the left model is in metric and the right model in imperial)

2.1.3 Material Properties

The soil properties to calculate thermal conductivity were originally presented by Lu et al. (2007). Tarnawski et al. (2009) analyzed the quartz content for the same soils used in Lu et al. (2007) experimental data as given in the Table 1:

Table 1 Soil properties presented by Lu et al. (2007) and Tarnawski et al. (2009)

Soil No	Material name	Material type	Quartz content (%)	Dry density (kg/m^3)	Dry density (lb/ft^3)
1	Sand 1	Coarse	74	1,600	99.88
2	Sand 2	Coarse	51	1,600	99.88
5	Silty loam	Fine	47	1,330	83.03
8	Silty clay loam	Fine	36	1,300	81.16

2.1.4 Results and Discussions

The thermal conductivity can be calculated and previewed by the graphing in the material properties dialog of the SVHEAT software.

2.1.4.1 Water content effect on the thermal conductivity

Figure 2 and Figure 3 are the results of thermal conductivity calculated for different approaches compared with the experimental data. Figure 2 is obtained from the SVHEAT model with metric units, and Figure 3 is from the SVHEAT model with imperial units.

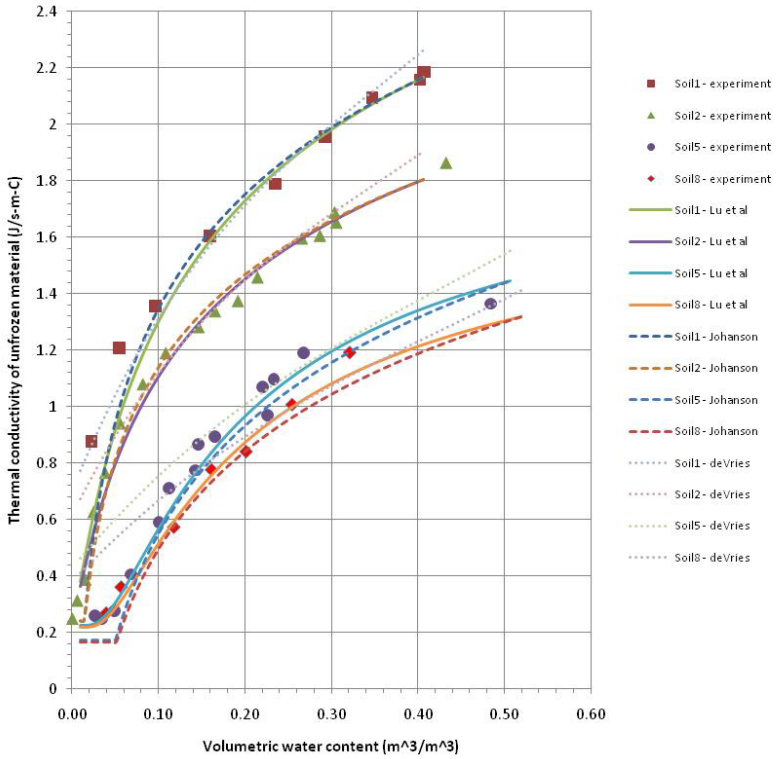

Figure 2 Comparison of the thermal conductivity in metric calculated by the SVHEAT software for Johansen (1975), Lu et al. (2007) and De Vries (1963) approach to the experimental data after Lu et al. (2007)

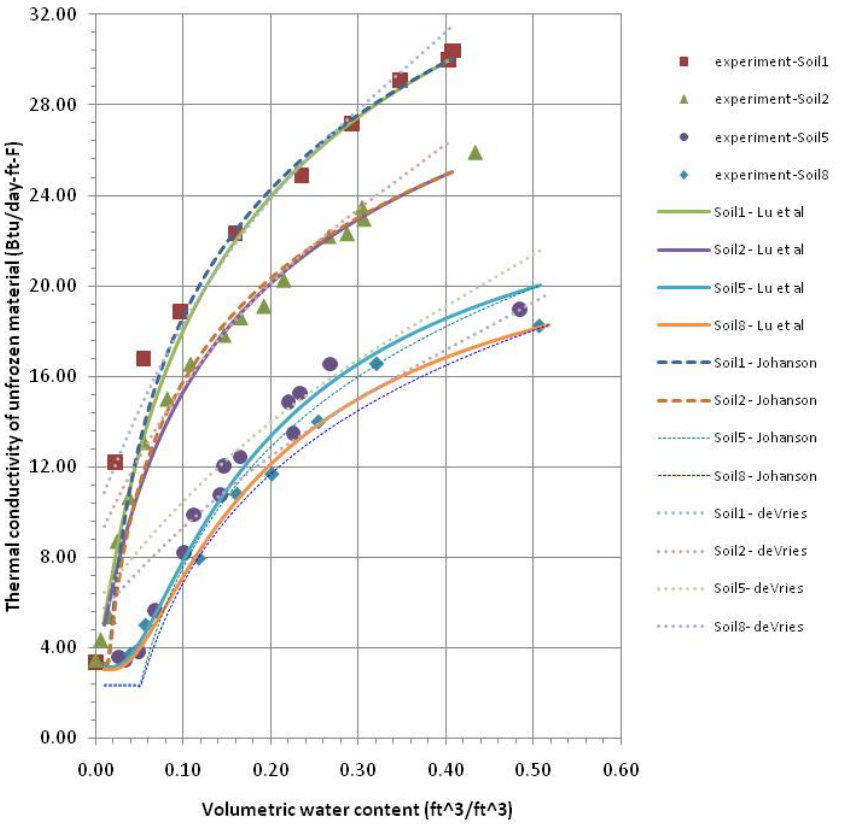

Figure 3 Comparison of the thermal conductivity in imperial unit calculated by the SVHEAT software for Johansen (1975), Lu et al. (2007) and De Vries (1963) approach to the experimental data after Lu et al. (2007)

It can be seen from Figure 2 and Figure 3 that the calculated thermal conductivity for the Johansen (1975) and Lu et al. (2007) approach is very close, but Lu et al. (2007) approach can predict the thermal conductivity at the very low degree of water saturation. Therefore, SVHEAT recommends Lu et al. (2007) or Johansen (1975) approach to estimate the thermal conductivity.

It should be noted that the only thermal conductivity for the unfrozen soil was available in the original experimental data (Lu et al., 2007).

2.1.4.2 Temperature effect on the thermal conductivity

Because the thermal conductivity of ice is larger than the water, the thermal conductivity of the frozen soil is greater than the unfrozen soil, as shown in Figure 4.

2.1.4.3 Dry density effect on the thermal conductivity

The thermal conductivity changes with the dry density and water content is shown in Figure 5 and Figure 6.

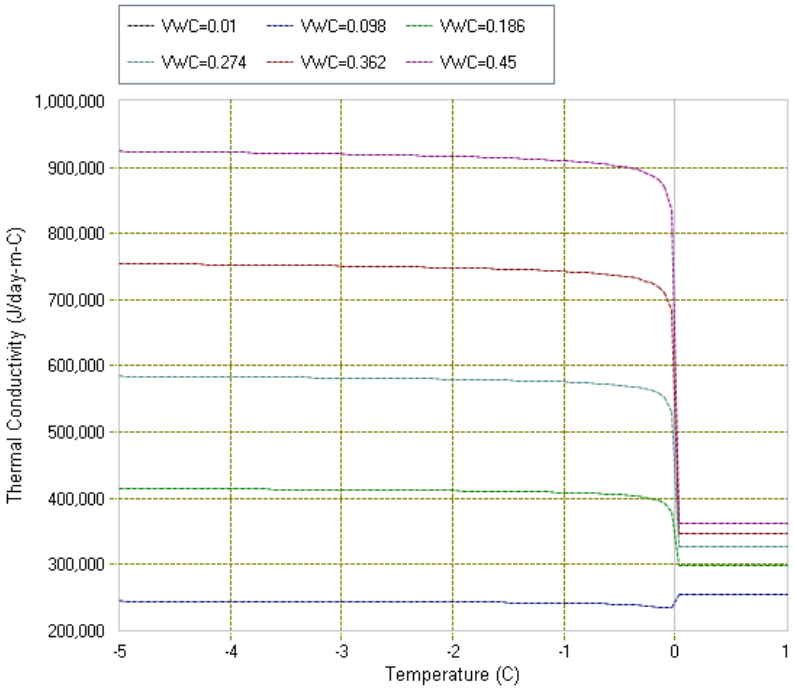

Figure 4 Temperature effect on the thermal conductivity at different water contents

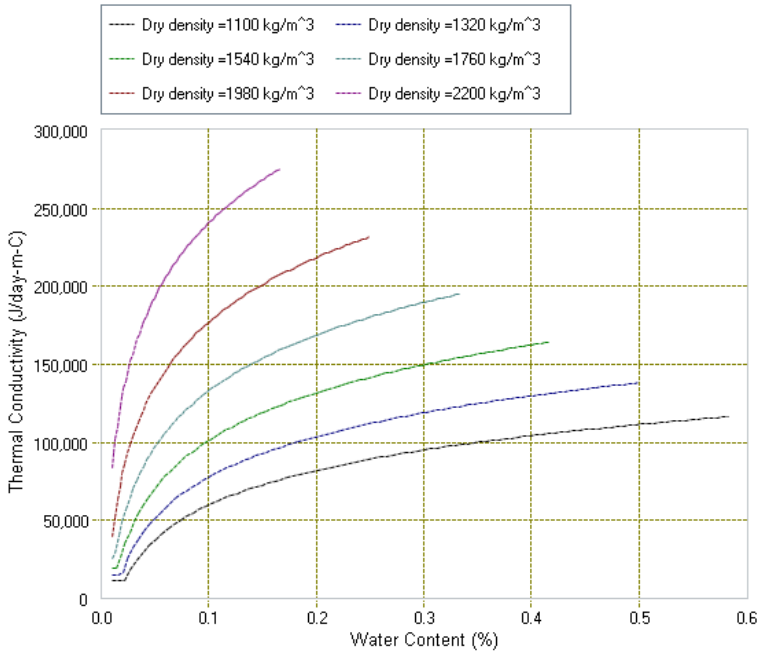

Figure 5 Thermal conductivity changing with water contents and dry densities at a temperature of 1 °C

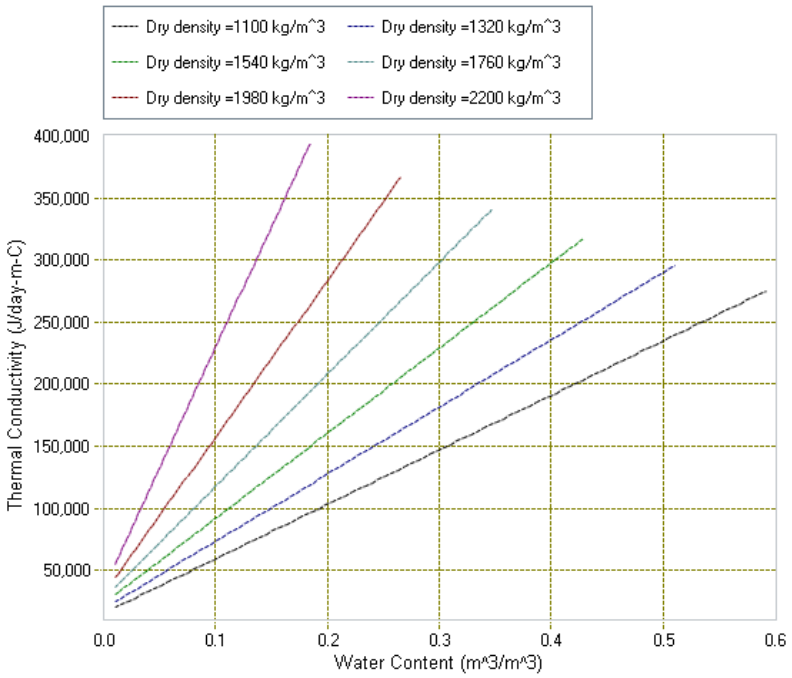

Figure 6 Thermal conductivity changing the water content and dry density at a temperature of -5 °C

2.2 METRIC VS IMPERIAL UNITS

Project: Geothermal
Model: Verify_SVHEAT_Metric, Verify_SVHEAT_Imperial

SVHEAT can support both the metric and imperial systems. If a model has the same material properties and boundary condition settings, the model should have the same results of simulation for both metric and imperial units.

2.2.1 Purpose

The model is used to compare the value of spreadsheet based calculation and SVHEAT simulation for the material properties of thermal conductivity, heat capacity, soil freezing characteristic curve (SFCC). The simulation results for both models with metric and imperial unit are also verified.

2.2.2 Geometry and Boundary Conditions

The model geometry, material properties, and boundary conditions are the same, but only the units are different. One model is in metric units, another is in imperial units, as shown in Figure 7. The model has 5 regions, and each region has the different material properties.

The ambient air temperature, which changes with time as described in equation [1] or equation [2], is applied to the upper boundary of the soil column.

$$Te = -2 + 20\sin\left(\frac{2\pi t}{365} + \frac{\pi}{2}\right) \quad (^{\circ}\mathrm{C}) \qquad [1]$$

$$Te = 28.4 + 36\sin\left(\frac{2\pi t}{365} + \frac{\pi}{2}\right) \quad (^{\circ}\mathrm{F}) \qquad [2]$$

On the bottom of the model, a constant thermal flux with a value of 5,148 J/day-m^2 is applied in the metric model, and the thermal flux of 0.45 Btu/day-ft^2 is applied in the imperial model.

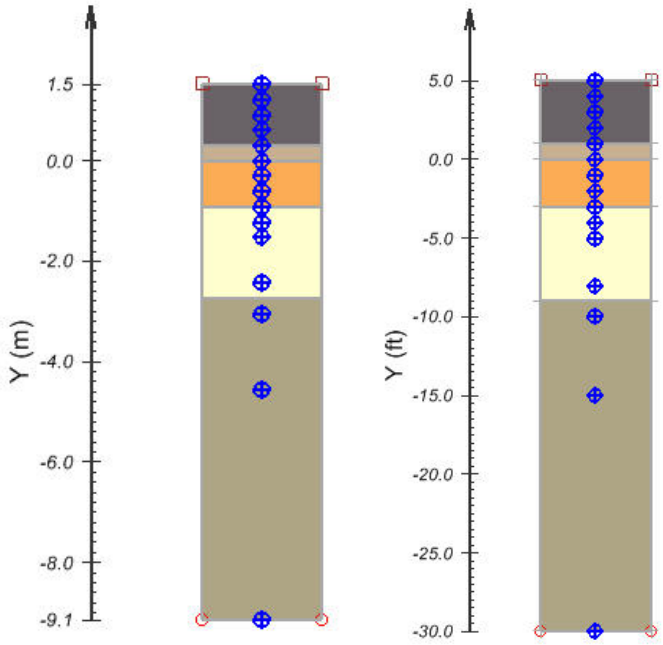

Figure 7 Model geometry in metric and imperial units

2.2.3 Material Properties

The material properties used in the model for the metric and imperial units are presented in Table 2 and Table 3.

Table 2 Parameters of thermal properties used in metric units

Material name	Thermal Properties	Method	Parameters	Value	Units
Asphalt	Thermal conductivity	Constant		128,603	J/day-m-°C
	Heat capacity	Constant		2,521,731	J/m^3-°C
	SFCC	None			
	VWC		SatVWC	0.001	
			VWC	0.001	
Embank Fill	Thermal conductivity	Johansen-Lu et al.	Material type	fine	
			Quartz content	60	
	Heat capacity	Jame-Newman	Soil dry density	2,242	kg/m^3
			Heat capacity of solid component	711	J/kg-°C
	SFCC	Tice & Anderson	Tef	-0.03	°C
			Tep	-0.1	°C
	VWC		SatVWC	0.15	
			VWC	0.15	
Sand	Thermal conductivity	De Vries	Solid phase	736,128	J/day-m-°C
	Heat capacity	Jame-Newman	Dry density	1,601	kg/m^3
	SFCC	Exponential Function	Residual uvwc	0.025	
			Param W	0.2	
	VWC		SatVWC	0.2	

			VWC	0.2	
Ice	Thermal conductivity	constant	Unfrozen material	52,272	J/day-m-°C
			Frozen material	191,808	J/day-m-°C
	Heat capacity	constant	Unfrozen material	4,287,000	J/m^3-°C
			Frozen material	1,880,000	J/m^3-°C
	SFCC	Multi-linear estimation	Residual uvwc	0	
	VWC		SatVWC	0.99	
			VWC	0.99	
Sand Gravel	Thermal conductivity	Johansen	Material State	Nature	
			Material Type	Coarse	
			Solid conductivity	736,128	J/day-m-°C
			Dry density	1,600	kg/m^3
	Heat capacity	Jame-Newman	Dry density	1,600	kg/m^3
			Solid component	710	J/kg-°C
	SFCC		Estimated by SWCC (Fredlund and Xing)		
	VWC		satVWC	0.35	
			VWC	0.3	

Table 3 Parameters of thermal properties for the model with imperial units

Material name	Thermal Properties	Method	Parameters	Value	Units
Asphalt	Thermal conductivity	Constant		20.7	Btu/day-ft-°F
	Heat capacity	Constant		37.7	Btu/ft^3-°F
Embank Fill	SFCC	None			
	VWC		SatVWC	0.001	
			VWC	0.001	
	Thermal conductivity	Johansen-Lu et al	Material type	fine	
			Quartz content	60	
	Heat capacity	Jame-Newman	Soil dry density	140	lb/ft^3
			Heat capacity of solid component	0.170	Btu/lb-°F
	SFCC	Tice & Anderson	Tef	31.9	°F
			Tep	31.8	°F
Sand	VWC		SatVWC	0.15	
			VWC	0.15	
	Thermal conductivity	De Vries	Solid phase	118.4	Btu/day-ft-°F
	Heat capacity	Jame-Newman	Dry density	100	lb/ft^3
			Specific heat capacity	0.17	Btu/lb-°F
	SFCC	Exponential Function	Residual uvwc	0.025	
			Param W	3.6	
Ice	VWC		SatVWC	0.2	
			VWC	0.2	
	Thermal conductivity	constant	Unfrozen material	8.4	Btu/day-ft-°F
			Frozen material	30.9	Btu/day-ft-°F
	Heat capacity	constant	Unfrozen material	64.1	Btu/ft^3-°F
			Frozen material	28.1	Btu/ft^3-°F
Sand Gravel	SFCC	Multi-linear estimation	Residual uvwc	0	
	VWC		SatVWC	0.99	
			VWC	0.99	
	Thermal conductivity	Johansen	Material State	Nature	
			Material Type	Coarse	
			Solid conductivity	118.4	Btu/day-ft-°F
			Dry density	99.9	lb/ft^3
	Heat capacity	Jame-Newman	Dry density	99.9	lb/ft^3
			Solid component	0.17	Btu/lb-°F
	SFCC		Estimated by SWCC		
	VWC		SatVWC	0.35	
			VWC	0.3	

2.2.4 Results and Discussions

The temperature profiles simulated with the metric and imperial model are illustrated in Figure 8 and Figure 9, because each region in the model has different approaches to specify thermal conductivities, heat capacity, and SFCC. Figure 8 demonstrates the same temperature profiles are obtained from both metric and imperial models, which indicates that the unit conversion in the calculation of thermal conductivities, heat capacity, phase change, and temperature are correct in the SVHEAT software.

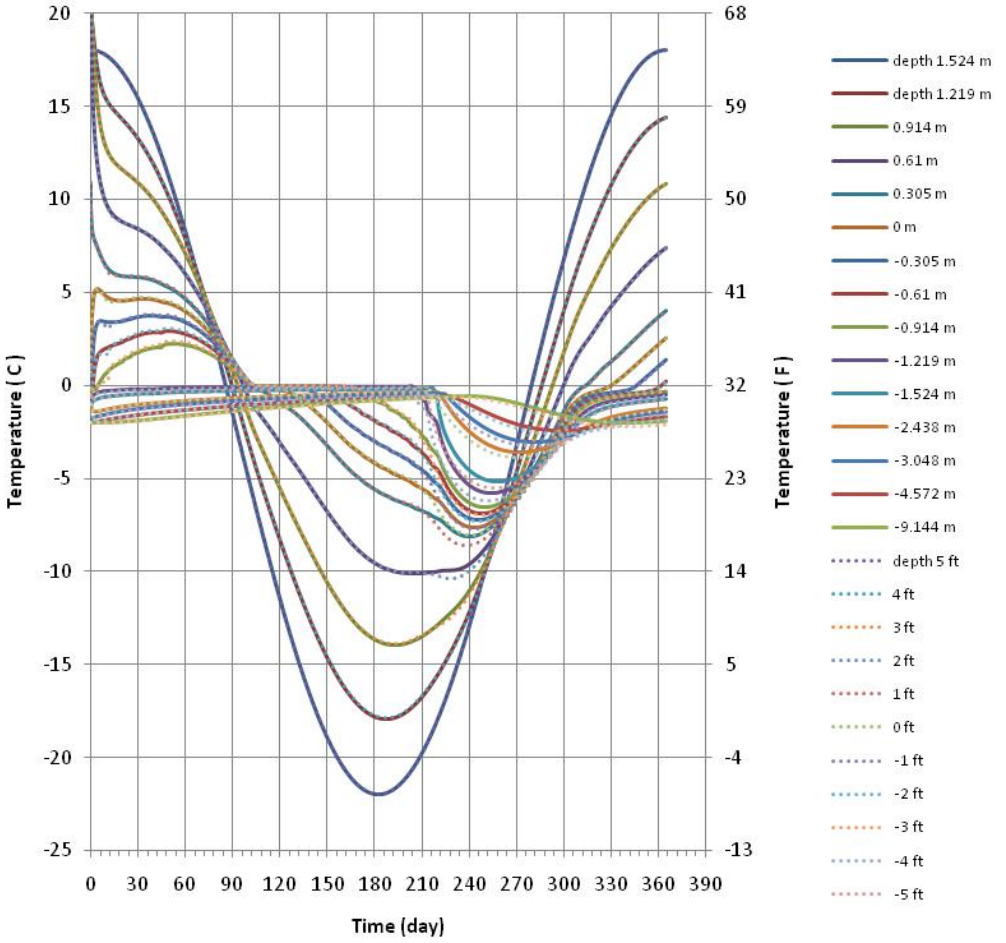

Figure 8 Temperature profiles obtained from the model with metric and imperial units

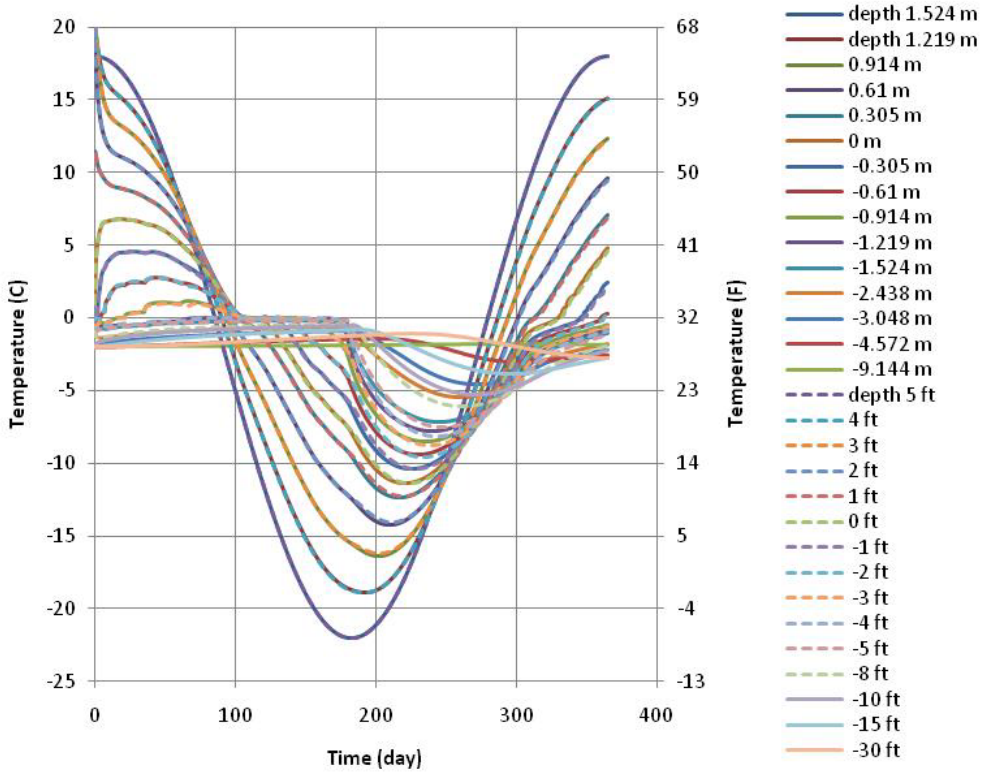

Figure 9 Temperature profiles obtained from the model with metric and imperial units used in verification of thermal conductivity

2.3 DISSANAYAKA ET AL. (2012): VERIFY THERMAL CONDUCTIVITY OF PEATS

Project: Geothermal
Model: ThermalConductivity_JohansenPeat

2.3.1 Purpose

In this section, calculated thermal conductivity curves of peats in SVHEAT were verified against measured data in Dissanayaka et al. (2012). SVHEAT uses Johansen's approach in calculating peat thermal conductivity in this example.

2.3.2 Material Properties

Peat physical properties used in this section are an average measured value from 9 samples in Dissanayaka et al. (2012), given in Table 4. These sample cores were collected using an undisturbed method at Bibai marsh, Hokkaido in Japan.

2.3.3 Results and Discussions

The calculated thermal conductivity was plotted in SVHEAT and checked against measured data in Dissanayaka et al. (2012).

Table 4. Physical properties of peat

Water content (%)	Specific Gravity	Dry Density (g/cm^3)	Saturated Hydraulic Conductivity (cm/s)	Porosity (cm^3/cm^3)	Dry Thermal Conductivity (W/m-°C)	Unfrozen Saturated Thermal Conductivity (W/m-°C)	Frozen Saturated Thermal Conductivity (W/m-°C)
828.4	1.55	0.123	2.67×10^{-3}	0.92	0.1	0.6	1.8

Figure 10 shows the relation between unfrozen thermal conductivity and volumetric water content. This figure shows an excellent agreement between the SVHEAT calculation and the measured thermal conductivity of peat. The measured dry thermal conductivity is on average around 0.1 W/m-°C and the saturated thermal conductivity is 0.6 W/m-°C.

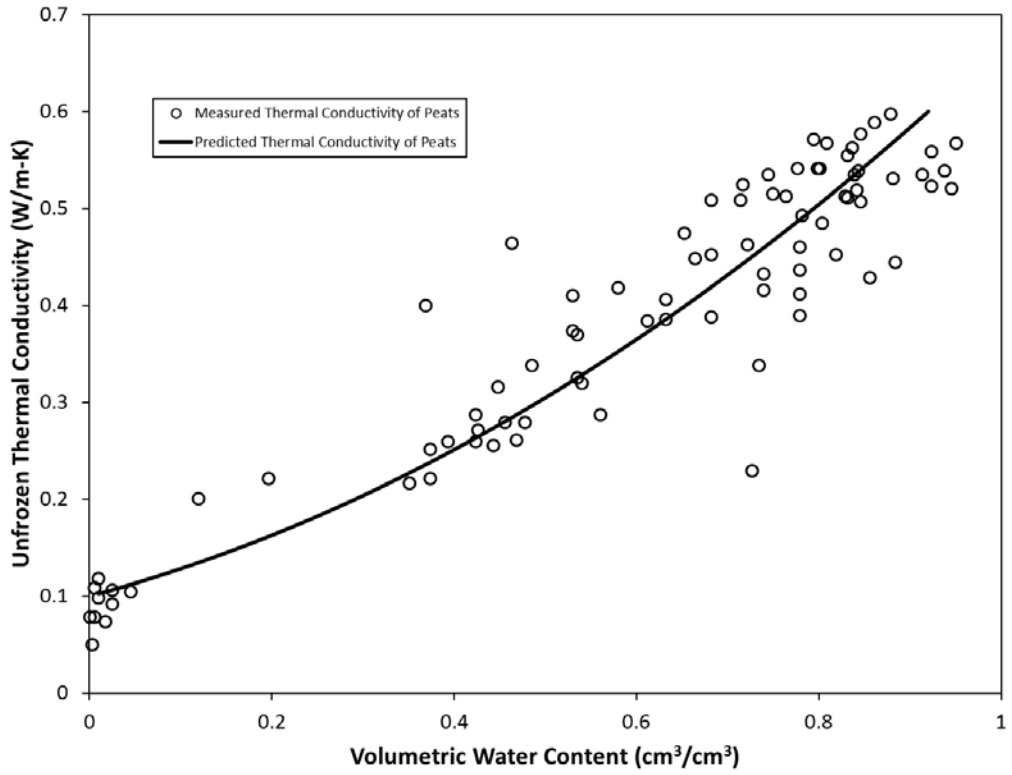

Figure 10. Comparison between measured and predicted unfrozen thermal conductivity

Figure 11 shows the effect of temperature on the thermal conductivity (J/day-m-°C) at various volumetric water contents. In this figure no SFCC curve was used, and this means that no unfrozen state at temperatures below the freezing temperature. Figure 12 and Figure 13 show the effect of dry density changes in thermal conductivity both in unfrozen (1 °C) and frozen (–5 °C) states. The dry density varies between 20 and 200 kg/m^3. At a given water content, the changes in thermal

conductivity in a thawed state are smaller than in a frozen state. This short verification example proves that the Johansen approach, implemented in SVHEAT, can accurately predict thermal conductivity of peat at various water contents.

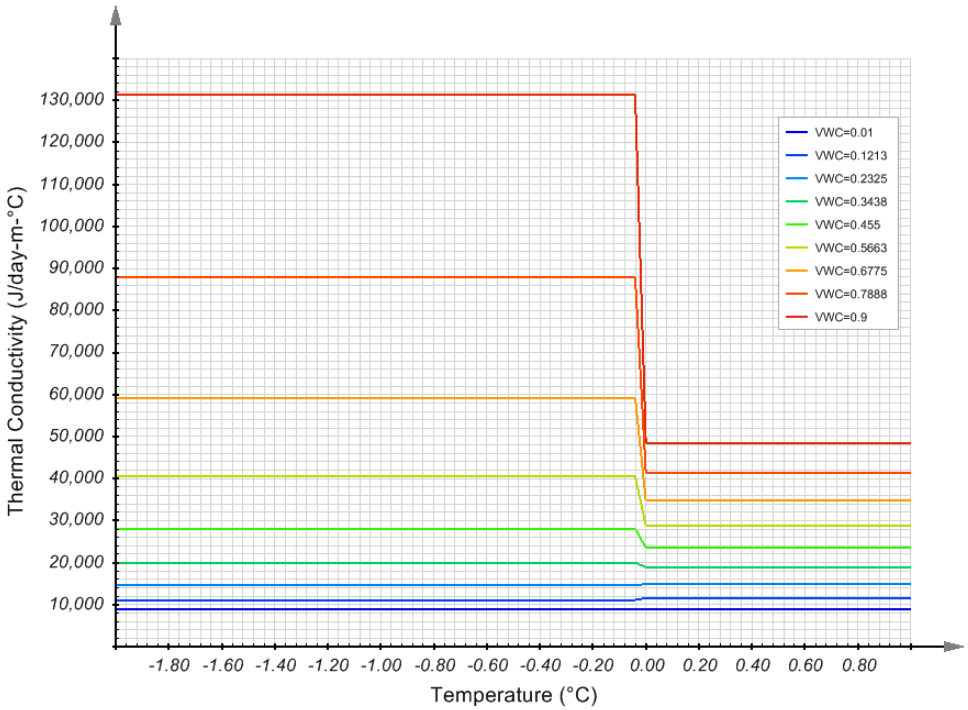

Figure 11. Temperature effect on thermal conductivity at various volumetric water contents

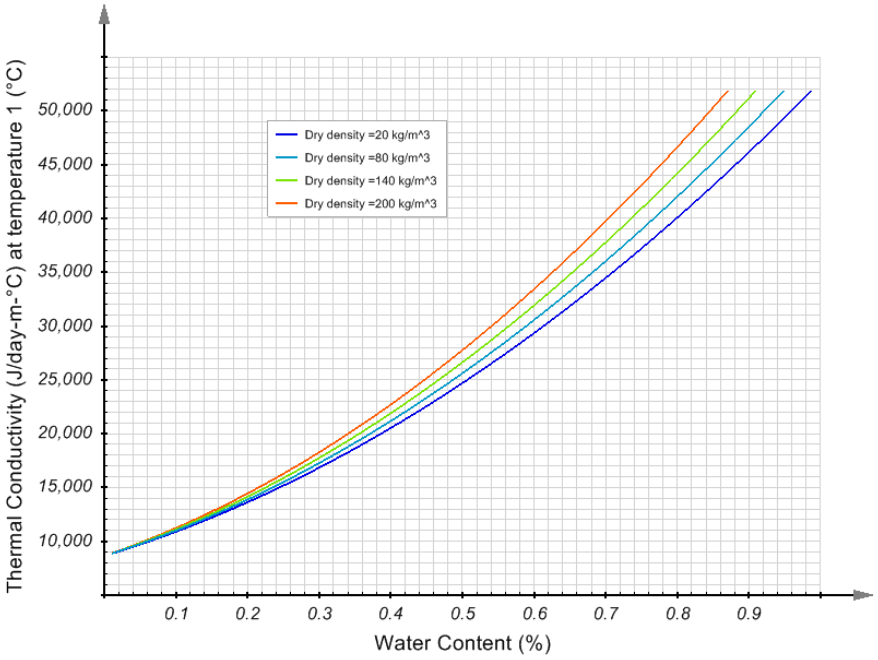

Figure 12. Dry density effect on thermal conductivity at various volumetric water contents at temperature of 1 °C

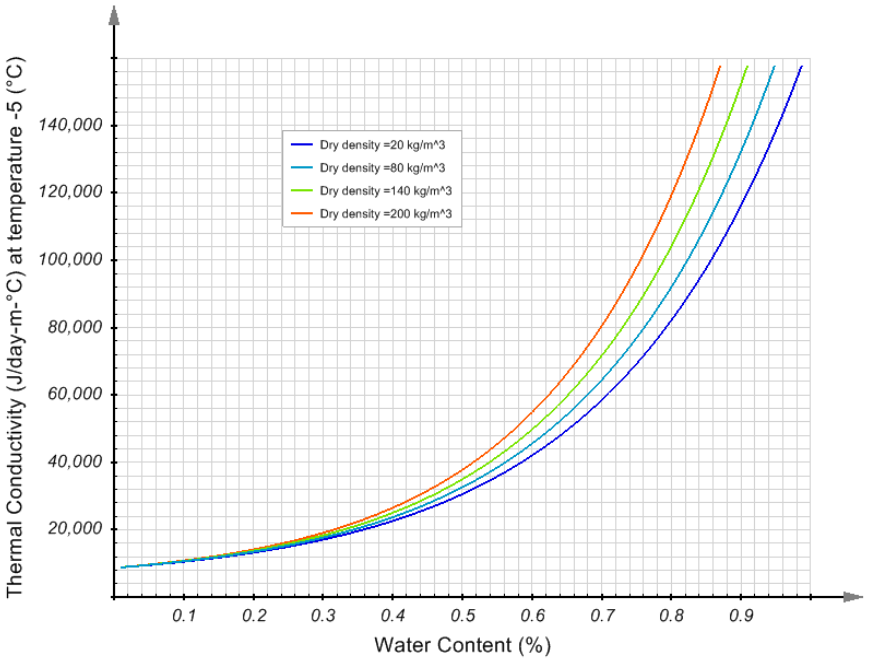

Figure 13. Dry density effect on thermal conductivity at various volumetric water contents at temperature of –5 °C

2.4 JAME (1997): HORIZONTAL SOIL FREEZING - UNCOUPLED

Project: GeoThermal
Model: JameData

This example illustrates the validity of SVHEAT calculations of soil temperature when compared with laboratory experimental data. The laboratory data for this experiment was originally collected by Jame (1977), and serves as the basis for a reasonable comparison to the SVHEAT software. There is no flow in this example model. A constant volumetric water content is assumed for the fluid phase.

2.4.1 Purpose

The purpose of this model is to compare the soil temperature calculated by SVHEAT with the laboratory experimental data using known material properties as collected by Jame (1977). It also shows how phase change plays a significant role in soil freezing.

2.4.2 Geometry and Boundary Conditions

The soil column has a length of 0.3 m. Cold temperature is applied to one end of the soil column, and warming temperature to another end, as shown in Figure 14.

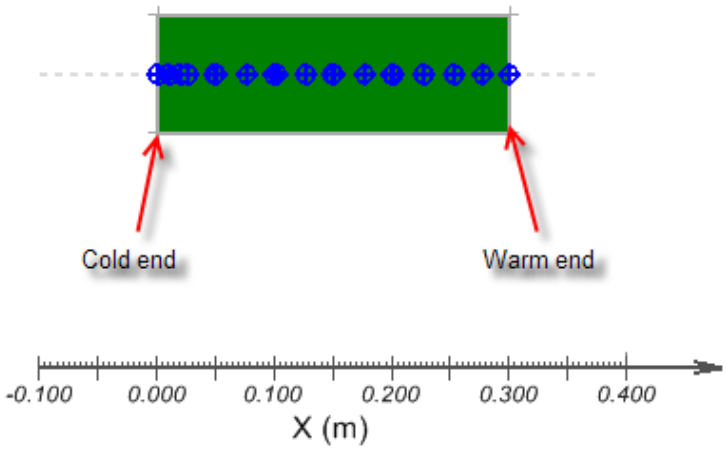

Figure 14 Geometry of 1-D horizontal column

No water flows in or out from both ends of the soil column. Therefore, it is a closed hydraulic system.

Initial temperature: 4.50 °C
Warm end temperature: 4.25 °C

The freezing rate at the cold end, temperature is given as following expression.

$$Te = -7.6t \quad if\ t < 0.5$$
$$Te = -3.8 - 2.1/3.5\ (t - 0.5) \quad if\ t < 4 \qquad [3]$$
$$Te = -5.9 \quad if\ t >= 4$$

where:

t = time, hr, and

Te = cold end temperature of soil column, °C.

2.4.3 Material Properties

The following material properties are used in this model.

Material name: Silica flour soil

Thermal conductivity

The thermal conductivity is calculated based on the Johansen method (Johansen, 1975). Parameters to determine the thermal conductivity are shown in Table 5.

Heat capacity

The soil heat capacity is calculated based on the heat capacity of solid component, water, ice, soil dry density, and their fractions (Jame, 1977; Newman, 1995). Only soil dry density and heat capacity of solid component are required to input, as shown in Table 5.

Soil Freezing Characteristic Curve (SFCC)

SFCC is estimated using Fredlund and Xing SWCC. The SWCC is fitted with laboratory data of unfrozen water content as a function of matric suction that is converted from temperature using the Clapeyron equation, as given in Figure 15.

Table 5 Parameters of material hydraulic and thermal properties

Hydraulic/Thermal Properties	Method	Parameters	Value	Units
Thermal conductivity	Johansen	Material state	crushed	
		Material type	fine	
		Thermal conductivity of solid component	29,700	(J/hr-m-°C)
		Porosity	0.49	
Heat capacity	Jame-Newman	Soil dry density	1,330	kg/m^3
		Heat capacity of solid component	837	J/kg-°C
SFCC	Estimated by SWCC	Phase change temperature from (Tef)	–0.1	°C
		Phase change temperature from (Tep)	–0.607	°C
SWCC	Fredlund and Xing	af	127.7	kPa
		nf	1.3	
		mf	2.0	
		hr	673.7	kPa
		Output curve type	data points	
VWC and water flux		VWC	0.18	

NOTE:

SWCC output curve type as data points can improve the performance of model running.

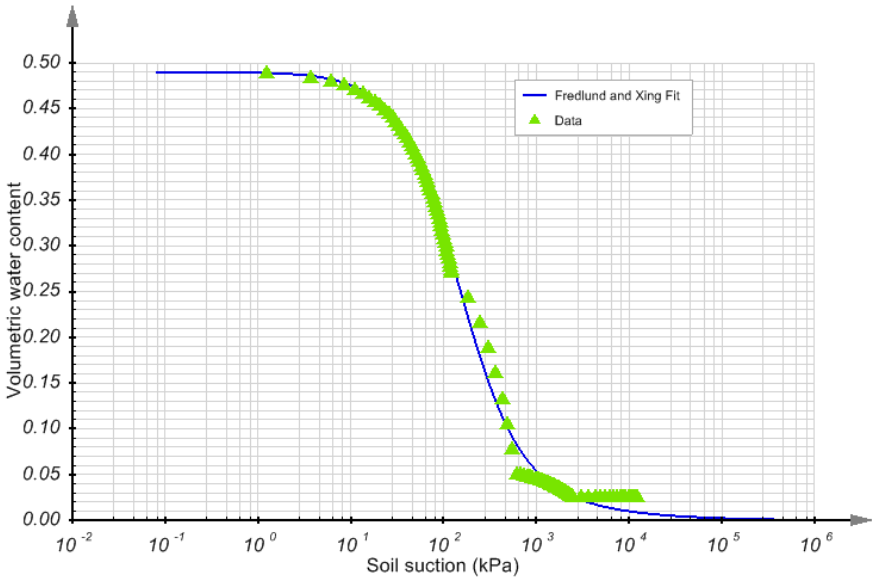

Figure 15 SWCC data fitting using unfrozen water content

2.4.4 Results and Discussions

The simulation results are illustrated in Figure 16 and Figure 17. In Figure 16, it can be seen that the calculated soil temperature has good agreement with the experimental data, although the predicted soil temperature after 48 hours is slightly higher than experimental data.

The difference may be due to the SFCC value not changing with temperature. As mentioned in the section of "Geometry and Boundary Conditions", the model is a closed hydraulic system, and moisture migration due to temperature gradient is not included. As a result, the water content does not change during simulation. That means the slope of SWCC does not change with time.

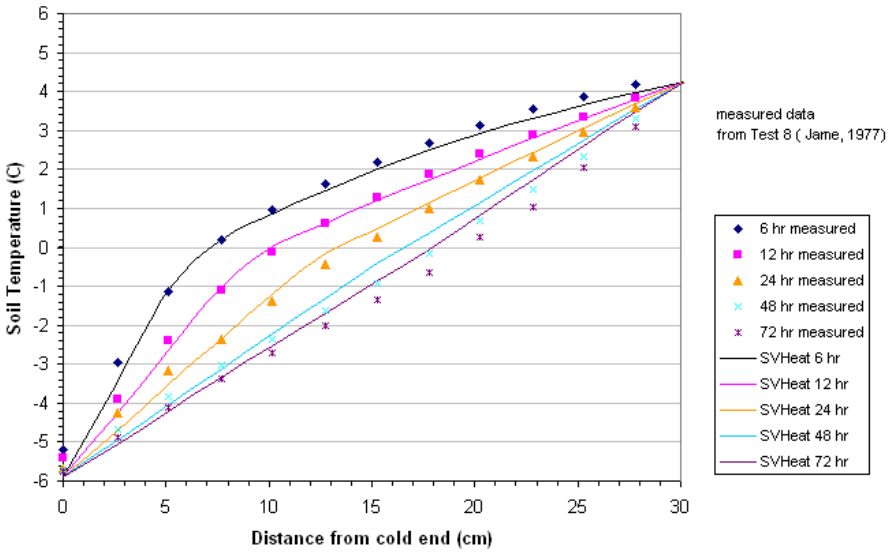

Figure 16 Comparison of calculation of SVHEAT model with Jame (1977) experimental data - phase change included

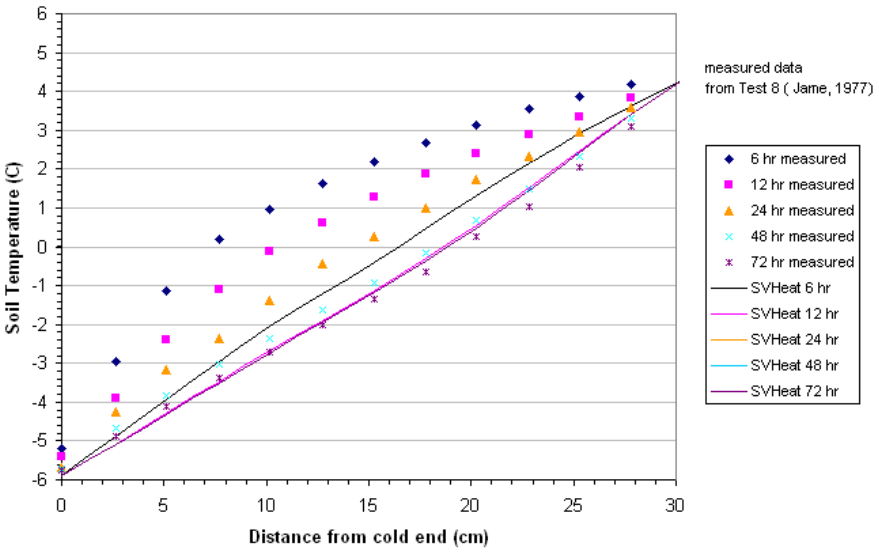

Figure 17 Comparison of simulation results without consideration of phase change

The value of m_2^i has a significant effect on the soil freezing process. To investigate this possibility, another model was created with the same material properties and boundary conditions, but without consideration of phase change, i.e., set m_2^i = 0. The result is given in Figure 17. Without phase change, thermal flux tends to steady-state after 12 hours. After that, the soil temperature profiles are almost the same. The results also indicate from Figure 17 that if phase change is not included, the result of simulation after 6 hours has good agreement with steady-state experimental data.

By the comparison of results in Figure 16 and Figure 17, the following conclusions can be reached:

- Phase change plays a significant role in soil freezing and thawing process. It is therefore very important to specify or estimate a proper SFCC if the soil freezing and thawing process are of more interest than frozen steady-state, and
- In some engineering applications, the steady-state of the frozen ground is of more interest than the freezing process. For example, in artificial ground freezing, the primary focus is on the soil temperature after a steady state is reached. In this case, simulation without considering phase change can be considered, which will be further illustrated in another example of ArtificialGroundFreezing in this document.

2.5 ALDRICH (1956): VERTICAL SOIL COLUMN - UNCOUPLED

Project: USMEP_Textbook
Model: Soil_Column_Aldrich

This model is designed to verify the SVHEAT results with the analytical solution proposed by Aldrich (1956), and Li and Koike (2001). Only conductive heat flows are modeled in this example.

2.5.1 Purpose

This model illustrates the accuracy of an SVHEAT simulation of the maximum frost depth compared with the analytical solution. The model also illustrates the distribution of soil temperature, unfrozen water content, and ice content during soil freezing and thawing.

2.5.2 Geometry and Boundary Conditions

The model is a 1-D homogenous vertical soil column with a 5 m depth, as shown in Figure 18.

Temperature Boundary Condition:
A temperature on the upper boundary condition is shown in Figure 19, and it is expressed as follows:

$$
\begin{aligned}
Te &= 5.0 && \text{if } t < 50 \\
Te &= 5.0 - 1.0 * (t - 50) && \text{if } 50 <= t < 60 \\
Te &= -5.0 && \text{if } 60 <= t < 180 \\
Te &= -5.0 + 1 * (t - 180) && \text{if } 180 <= t < 190 \\
Te &= 5.0 && \text{if } t > 190
\end{aligned}
\qquad [4]
$$

where:

t = time, hr, and

Te = cold end temperature of soil column, °C.

On the bottom of the soil column, the thermal flux is set to a unit gradient.
Initial temperature is 5 °C.

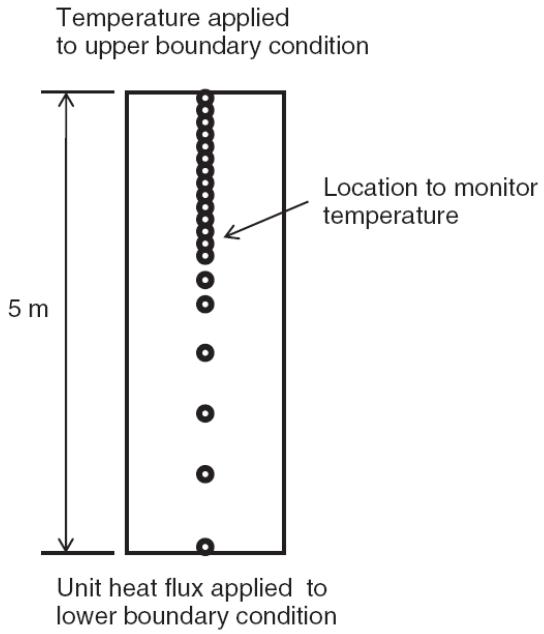

Figure 18 Aldrich Column Conceptual Model

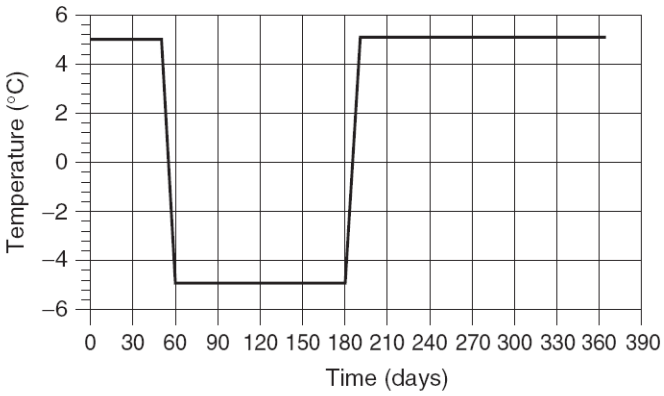

Figure 19 Aldrich Column Temperature Boundary Condition

2.5.3 Material Properties

The material properties are the same as used in the model JameData as described earlier in this manual. Any material properties can be used with the Aldrich solution. The material properties used in the model JameData were entered in the Aldrich closed-form solution as well as SVHEAT and the answers were compared.

2.5.4 Results and Discussions

The following is the result of the simulation. The results of the Aldrich solution were calculated with a brief JAVA software program.

2.5.4.1 Soil Temperature

Figure 20 illustrates the soil temperature changes during soil freezing and thawing. In the simulation, the temperature at depth 0 m is maintained at 5 °C in the first 50 days, and then it drops from 5 °C to –5 °C from day 50 to 60.

After that time, the temperature holds at –5 °C. From day 180 to 190, the temperature increases from –5 °C to 5 °C, and the soil column experiences a thawing period.

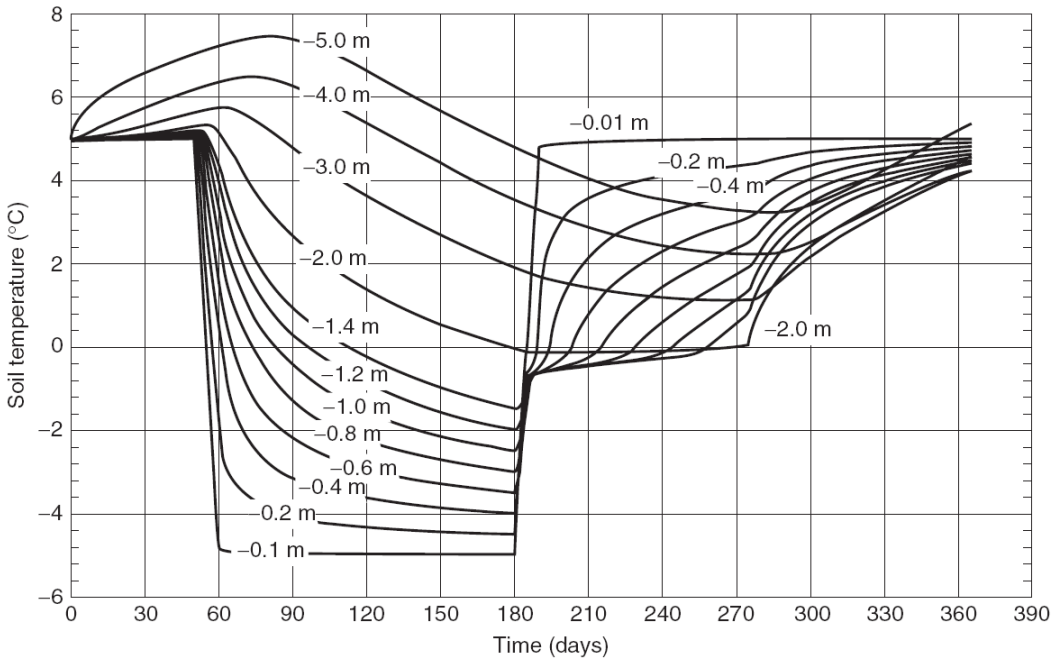

Figure 20 Soil temperatures change during soil freezing and thawing

2.5.4.2 Frost depth during soil freezing and thawing

The frost depth in soil freezing and thawing is given in Figure 21. In the figure, the maximum frost depth calculated with the analytical solution is based on the Aldrich (1956) equation:

$$D_m = 294\beta\sqrt{\frac{2\lambda\sum T_f}{L_f\Theta}} \qquad [5]$$

where:

D_m = Maximum frost depth, m,

β = a dimensionless correction parameter,

λ = thermal conductivity, W/(m-°C),

ΣT_f = cumulative temperature below the freezing point, °C-day,

L_f = latent heat of fusion of water, 3.34×10^8 J/m^3, and

Θ = volumetric water content, m^3/m^3.

In the analytical calculation, the thermal conductivity (λ = 2.9 W/m-°C) is averaged based on the thermal conductivity of frozen and unfrozen soil calculated with the Johansen approach in the simulation. Θ = 0.47, L_f = 3.34×10^8 J/m^3, and β = 1.

It can be seen from the Figure 21 that the frost depth obtained in simulation has very good match to the analytical value during the soil-freezing period.

After the day 180, analytical solution cannot predict the frost depth because soil column starts to thaw, but the simulation shows that some frost depth develops during the soil thawing period.

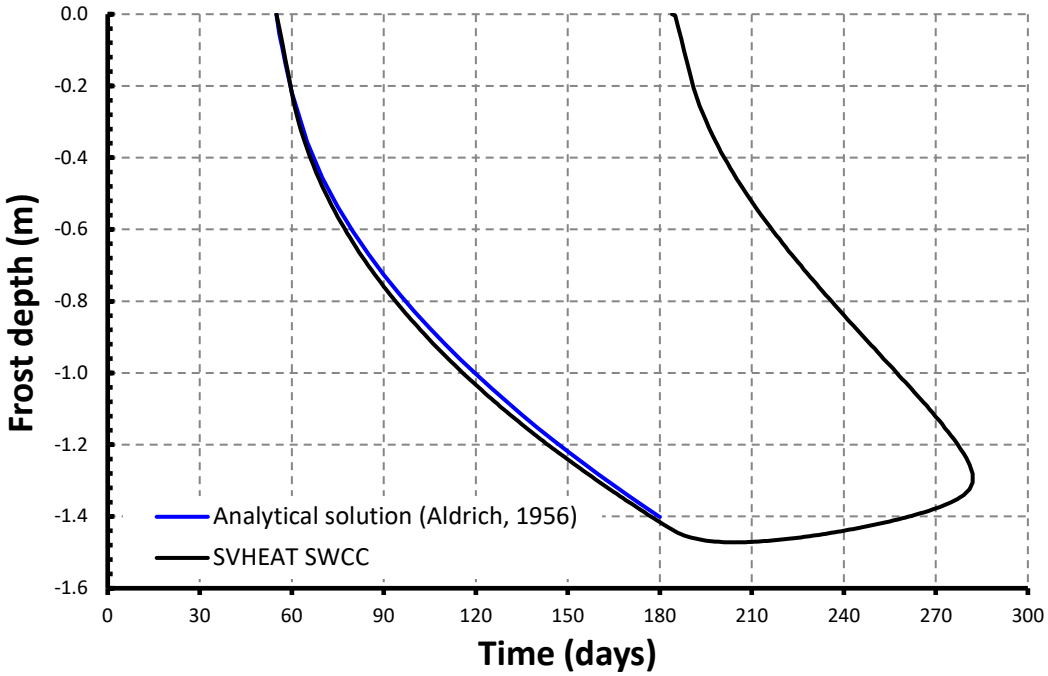

Figure 21 Frost depth during soil freezing and thawing

2.6 MASS CONSERVATION DURING FREEZE AND THAW - UNCOUPLED

Project: GeoThermal
Model: Freeze_Thaw_Check

This model is designed to verify the conservation of mass during the freeze/thaw cycle. In this model a simple soil column is first frozen and then allowed to thaw. If mass conservation is correct, then the final volumetric water contents will exactly match the initial volumetric water contents present before the freezing process is initiated.

2.6.1 Purpose

The purpose of this model is to illustrate that mass is conserved through the soil freezing and thawing process.

2.6.2 Geometry and Boundary Conditions

The geometry and boundary conditions are the same as used in model Soil_Column_Aldrich.

2.6.3 Material Properties

The material name and properties are the same as used in model JameData.

2.6.4 Results and Discussions

The distribution of unfrozen water content, and ice content is illustrated in Figure 22 and Figure 23. The value of unfrozen water content during soil freezing depends on soil temperature and the soil freezing characteristic curve. It should be noted that at the same depth, the water content is the same compared to the value before freezing and after thawing.

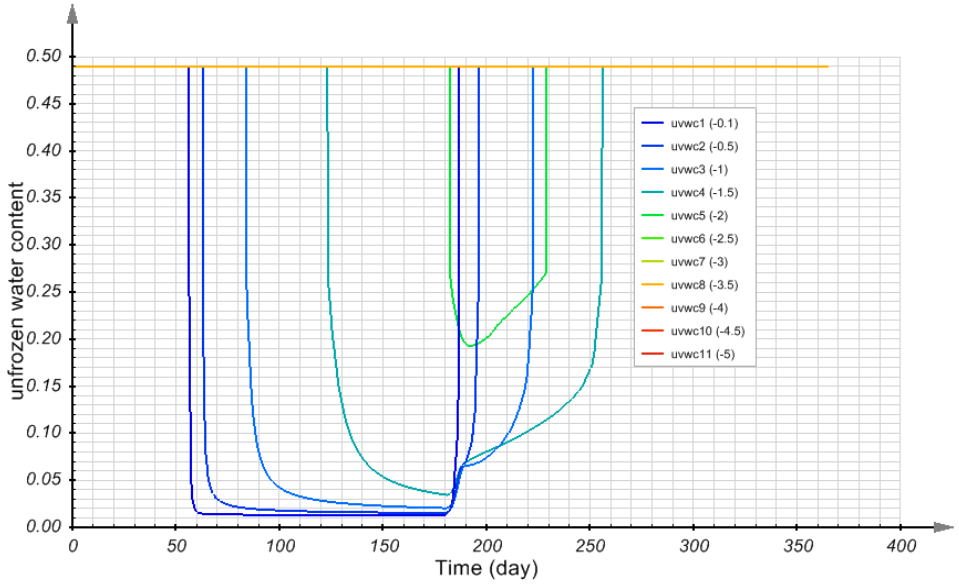

Figure 22 Volumetric unfrozen water content during soil freezing and thawing

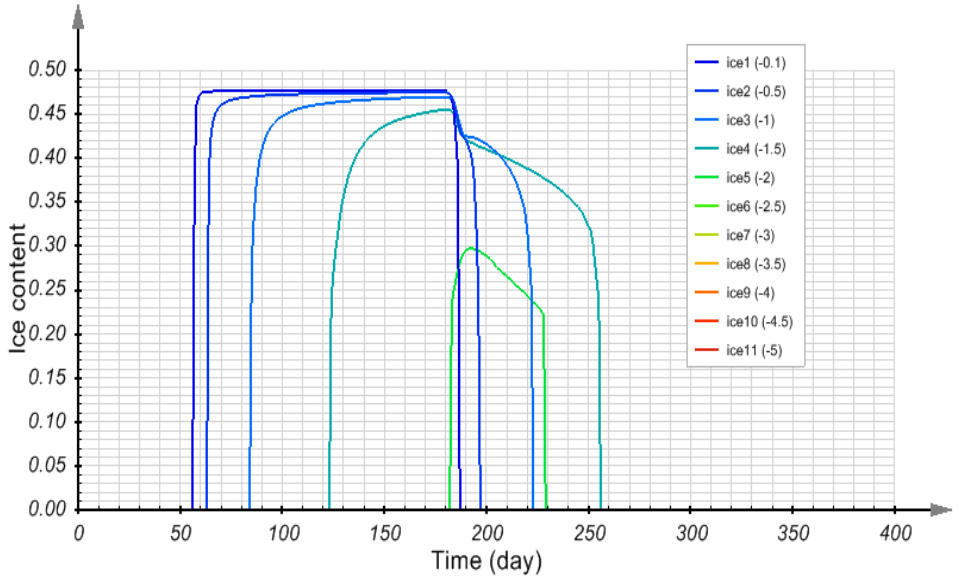

Figure 23 Volumetric ice content during soil freezing and thawing

2.7 TAILINGS FREEZE/THAW WITH SNOW COVER - UNCOUPLED

Project: MineTailings
Model: TailingsFreezeThawSnowCover

This benchmark presents a generic scenario of mine tailings freezing and thawing with a snow cover. The snow accumulation and melt is simulated according to the climate data including precipitation and air temperature. This benchmark demonstrates that SVHEAT can predict the temperature at the surface of tailings with snow cover included.

2.7.1 Purpose

The benchmark is to illustrate the validity using the SVHEAT software to simulate the freeze-thaw process for tailings that are covered with snow at the surface and consolidated with time. It is also demonstrated that the snow accumulation and melting process can be simulated with the snow climate boundary condition provided by SVHEAT and SVFLUX software.

2.7.2 Geometry and Boundary Conditions

The model domain is a 1D column representing generic tailings pit 9.6m in height. The climate boundary condition is applied at the tailings surface. Snow may be accumulated on the surface of tailings during the winter time, and melted during spring. The accumulation of snow is the result of snowfall events, which are calculated according to the precipitation climate data (Figure 25) and air temperature (Figure 26). In the calculation of the snow precipitation (see Figure 27) the minimum temperature of rain is assumed to be 2 °C, and the maximum temperature for snow is 0 °C. If the air temperature is above 2 °C, the precipitation is regarded as a rain event, while the air temperature is below 0 °C, the precipitation is considered to be snow event. The mixture of rain and snow happens in the range of air temperature from 0 °C to 2 °C.

The temperature-index approach (i.e. degree-Melt-Factor approach) is used to estimate snow melted daily. The snow melt factor is described by the sine function, as illustrated in Figure 28. Please see the SVHEAT and SVFLUX theory manual for details of the formulation of snow accumulation, melt, and thermal boundary with snow cover.

Boundary conditions:
Top: air temperature (see Figure 26),
Bottom: Geothermal flux = 0.036 W/m^2.

Initial conditions: 20 °C.

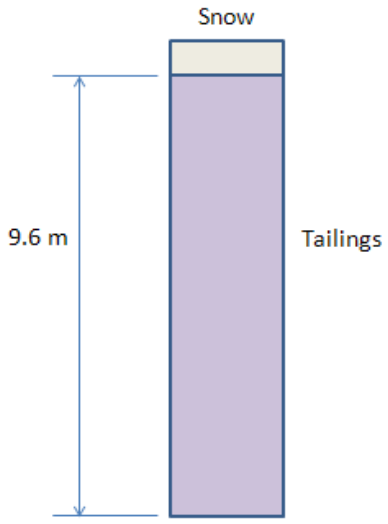

Figure 24 Model geometry for tailings freeze/thaw with snow cover

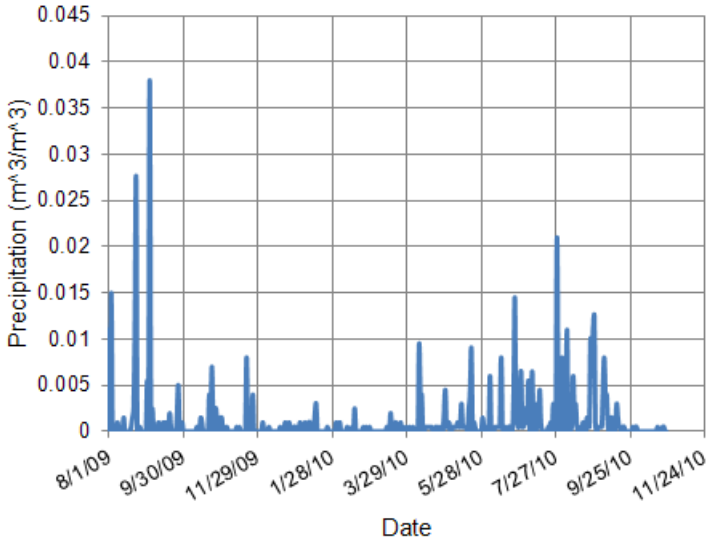

Figure 25 Precipitation data used to determine snow precipitation for tailings freeze/thaw

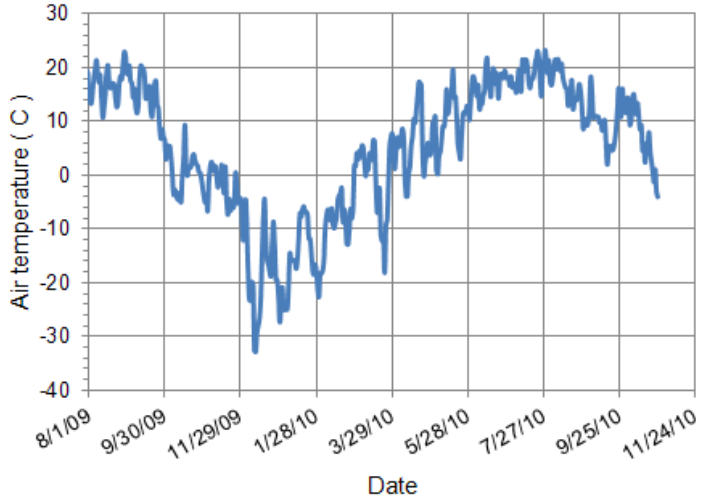

Figure 26 Air temperature used in the climate boundary for tailings freeze /thaw

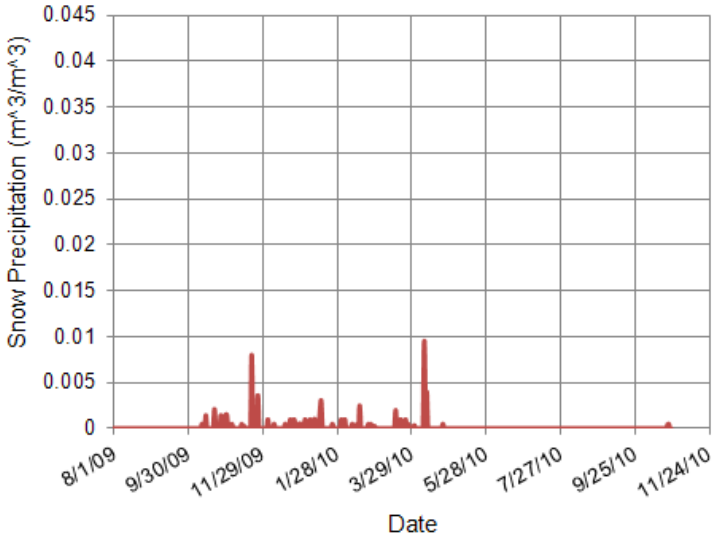

Figure 27 Snow precipitation calculated based on the precipitation and air temperature

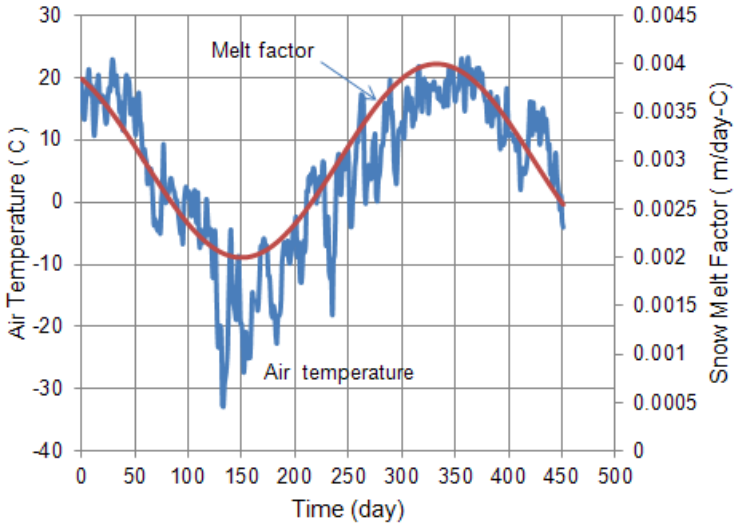

Figure 28 Snow melt factor changing seasonally for modeling tailings freeze/thaw with snow cover

2.7.3 Material Properties

The thermal properties of the tailings are estimated based on the relative reference (Dawson et al., 1999; Nixon, 1993), and are presented in the Table 6. The snow thermal conductivity is calculated based on the snow density (Yen, 1969). The mean snow density is estimated with the value of 300 kg/m^3. Please see SVHEAT theory manual for the detailed formulation of snow thermal conductivity. With the parameters as given in Table 6, the thermal conductivity, heat capacity, and unfrozen water content changing with the temperature are illustrated in Figure 29, Figure 30, and Figure 31.

Table 6 Material properties for modeling tailings freeze/thaw

Hydraulic/Thermal Properties	Method	Parameters	Value	Units
Tailings Thermal conductivity	Johansen	Material state	crushed	
		Material type	fine	
		Quartz content	28	%
Tailings heat capacity	Jame-Newman	Soil dry density	1,247.5	kg/m^3
		Heat capacity of solid component	660	J/kg-^{o}C
Tailings SFCC	Tice approach	Parameter A	0.051	
		Parameter B	0.4	
Tailings volumetric water content			0.85	m^3/m^3
Tailings bulk density			1,248	kg/m^3
Snow density			300	kg/m^3
Snow thermal conductivity			0.257	W/m-^{o}C

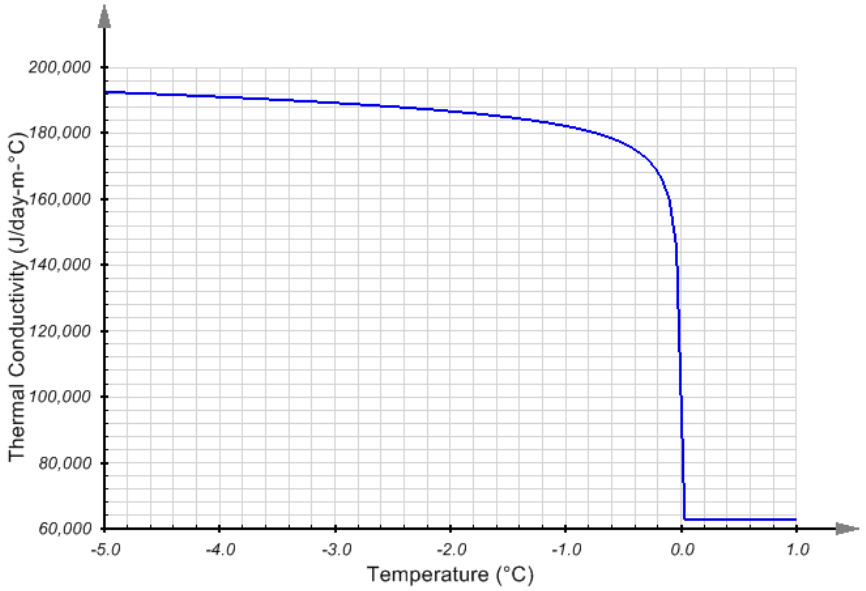

Figure 29 Thermal conductivity for tailings freeze/thaw model

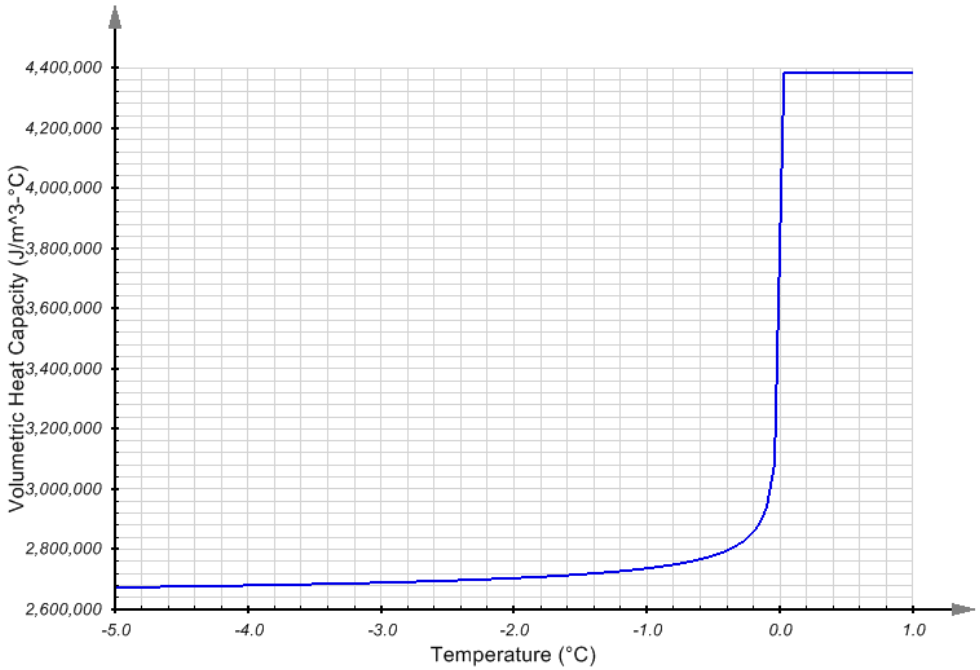

Figure 30 Heat capacity of tailings freeze/thaw model

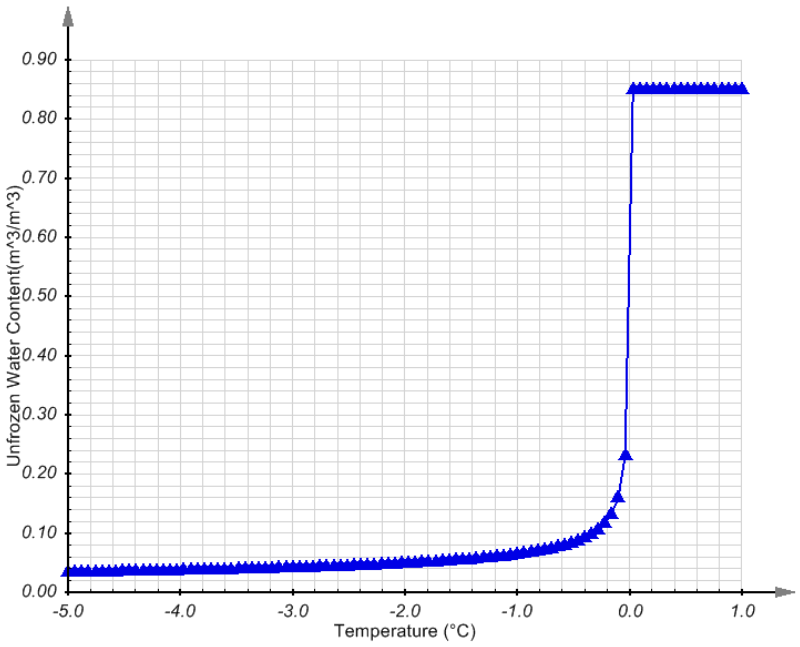

Figure 31 Volumetric unfrozen water content for tailings freeze/thaw model

2.7.4 Results and Discussions

The model is simulated for 451 days. The following sections summarize the results obtained through the modeling program.

2.7.4.1 Snow depth and snow water equivalent (SWE)

In the SVHEAT and SVFLUX software the snow accumulation is represented by the snow water equivalent (SWE) value, and the snow depth is calculated according to the SWE and snow density. Figure 32 illustrates the result of SWE and snow depth simulated with the SVHEAT software, where the accumulated SWE is determined with the snow precipitation and snow melt. Figure 32 indicates that the maximum snow depth is about 120 mm, and the snow was melted down in a few days during spring.

2.7.4.2 Temperature at the surface of tailings

It can be seen from Figure 33 that the calculation of the temperature at the surface of tailings matches the measured value very well. Due to the insulating effect of snow cover, the temperature at the surface of tailings fluctuates smoothly, and has a lower value in magnitude compared to the air temperature during the period of snow cover. It is also indicated that the temperature at the surface of the tailings is approximated by the air temperature if no snow exists at the tailings surface.

2.7.4.3 Conclusions and suggestions

This benchmark illustrates the validity of thermal modeling of snow cover. The model also demonstrates that it is feasible to model tailings freezing/thawing process with snow cover included using the SVHEAT software.

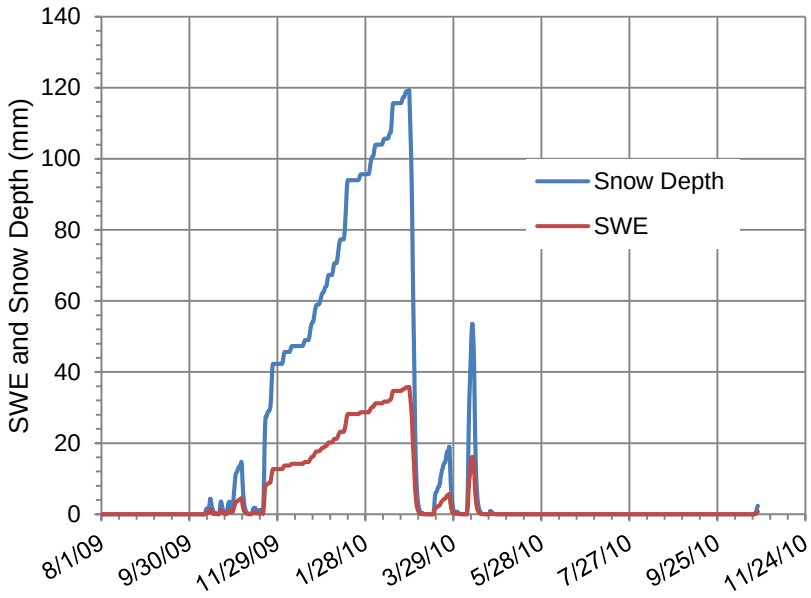

Figure 32 The simulated snow accumulation and melt at the surface of tailings

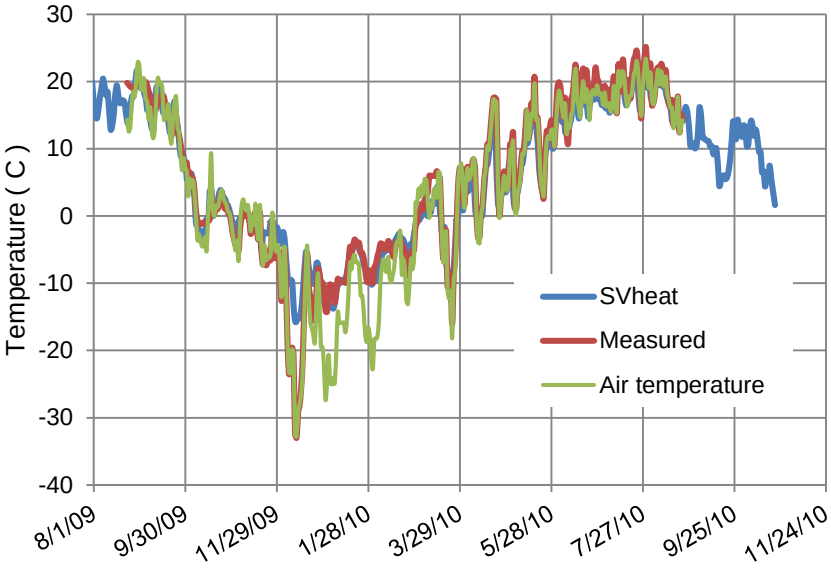

Figure 33 Comparison of temperatures at the surface of tailings (elevation = 9.6 m)

2.8 SOIL COLUMN FREEZING/THAWING UNDER CLIMATE CONDITIONS - COUPLED

Project: GeoThermal
Model: SoilFreezingThawing1Y

This example is to demonstrate hydrothermal coupling including seepage, evaporation, freezing, and thawing under climate conditions. The following features can be provided in this example.

- The change of soil temperature with climate condition,
- The Frost depth during soil freezing and thawing,
- Comparison of frost depth with the analytical solution,
- The change of pore water pressure or soil saturation in soil freezing and thawing, and
- The evaporation and runoff under climate condition.

The results of the SVHEAT software are compared to closed from calculations of frost depth as presented by Aldrich (1956).

2.8.1 Purpose

This model illustrates soil freezing and thawing process under climate boundary conditions, including precipitation, evaporation, and air temperature.

2.8.2 Geometry and Boundary Conditions

The model geometry is a 1-D vertical column with a 10 m depth as shown in Figure 34. The upper body of the soil column is applied to climate boundary conditions. The climate daily precipitation, air temperature, humidity, and potential evaporation are given in Figure 35, Figure 36, Figure 37, and Figure 38.

One year of climate data is used in this model starting from October 1 to September of the next year. The ground surface temperature is estimated based on n-factor and air temperature. The n-factor is set to 0.8 in this example.

Unit hydraulic and thermal gradient boundary conditions are used at the bottom of the column.

Initial pore water pressure: -100 kPa,
Initial temperature: 12 °C

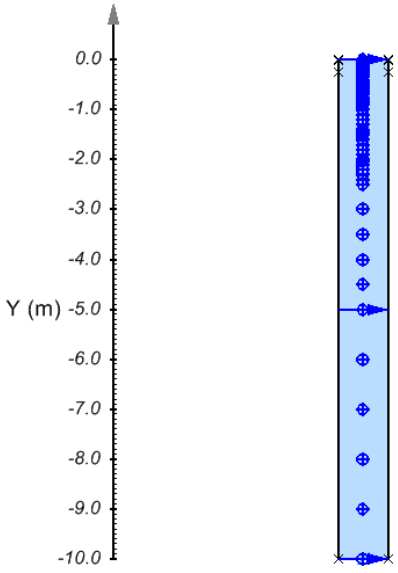

Figure 34 Geometry of the 1-D vertical soil column model applied to climate data

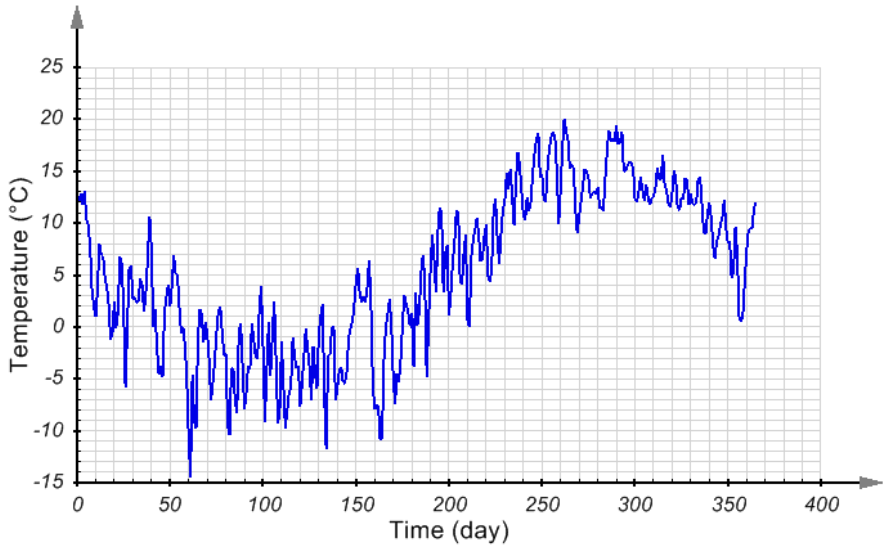

Figure 35 Daily air temperature of one-year climate from October 1

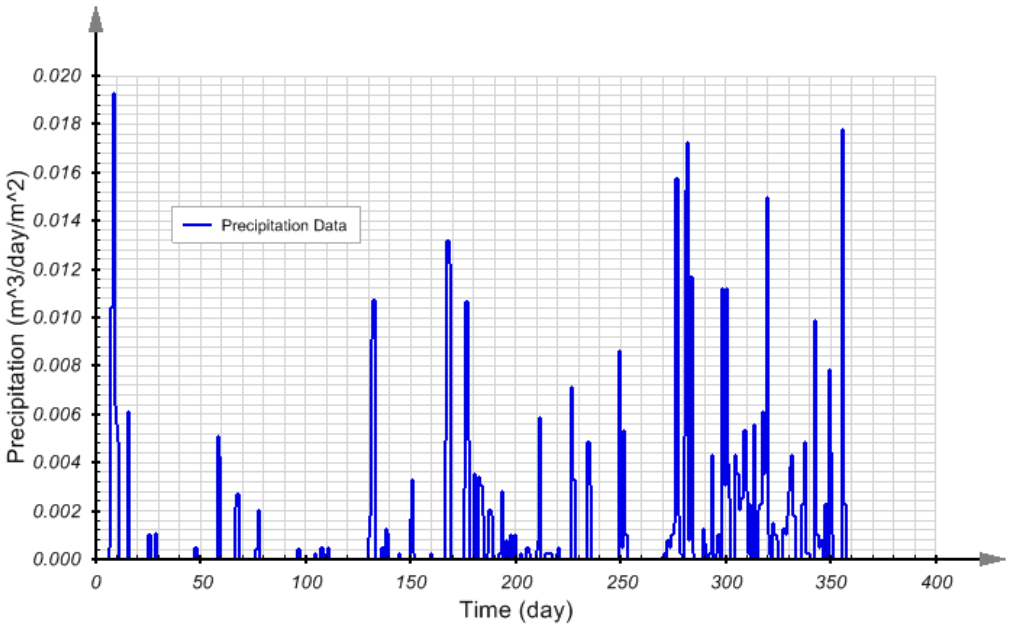

Figure 36 Daily precipitation of one-year climate from October 1

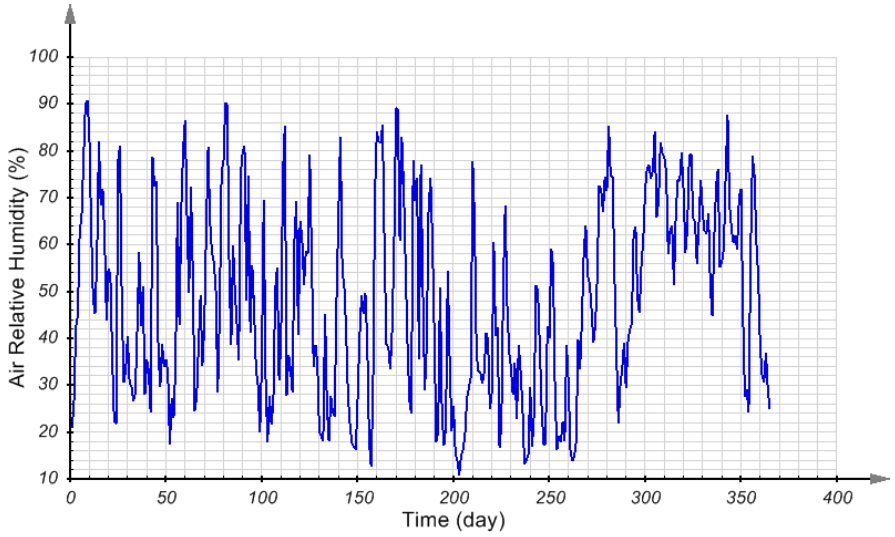

Figure 37 Daily humidity of one-year climate from October 1

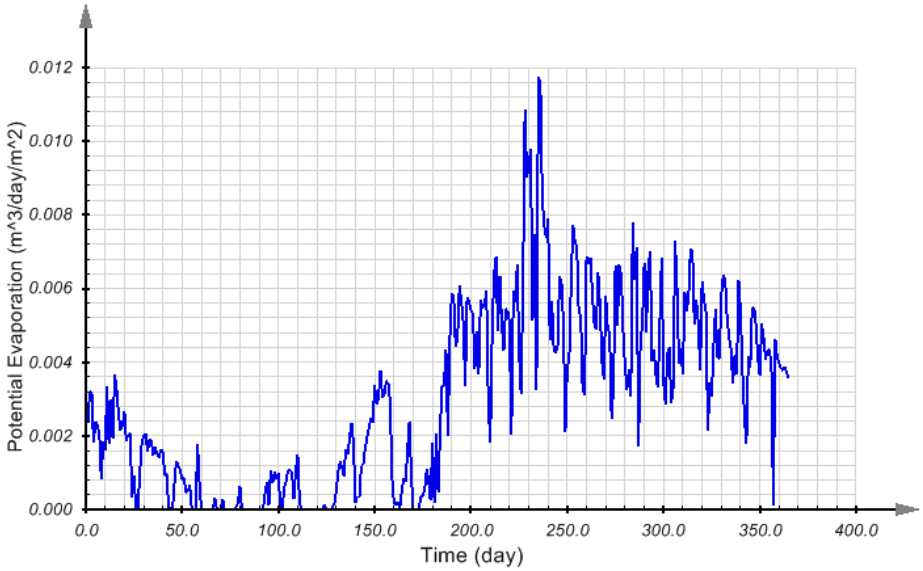

Figure 38 Daily potential evaporation of one-year climate from October 1

2.8.3 Material Properties

The soil column consists of only one sandy material. The hydraulic properties of the material were used in Molycorp seepage numerical modeling.

Soil Water Characteristic Curve (SWCC)
Saturated volumetric water content: 0.30 m^3/m^3
SWCC fitting equation and parameters are given in Figure 39 and

Table 7.

Hydraulic conductivity

Saturated hydraulic conductivity: 1.47 m/day

Unsaturated hydraulic conductivity fitting is shown in Figure 40, and its parameters are given in Table 2. Because of ice existence, the hydraulic conductivity in frozen soil is reduced, based on the temperature of frozen soil and Clapeyron equation.

Thermal conductivity

Thermal conductivity is calculated based on the Johansen method (Johansen, 1975) with the parameters as given in

Table 7. The thermal conductivity of solid component is determined according to the quartz content.

Heat capacity

The soil heat capacity is calculated based on the heat capacity of solid component, water, ice, soil dry density, and their fractions (Jame, 1977; Newman, 1995).

Table 7 is the parameters used in the calculation. The water and ice heat capacities are 4,184 J/kg-°C and 2,094 J/kg-°C, respectively.

Soil Freezing Characteristic Curve (SFCC)

SFCC is estimated with SWCC of Fredlund and Xing Fit as shown in Figure 39.

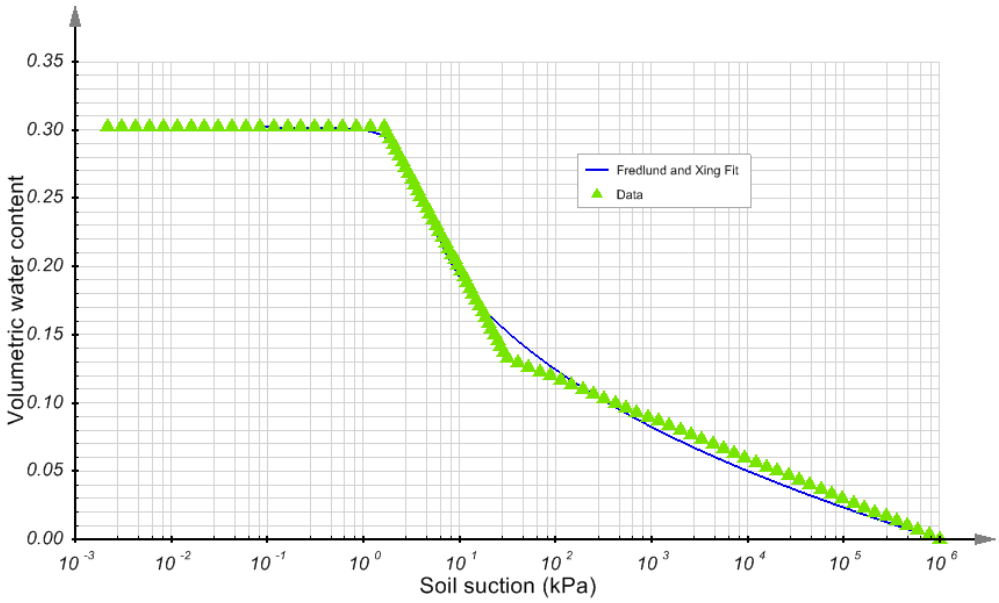

Figure 39 Soil Water Characteristic Curve for sandy material used in the model

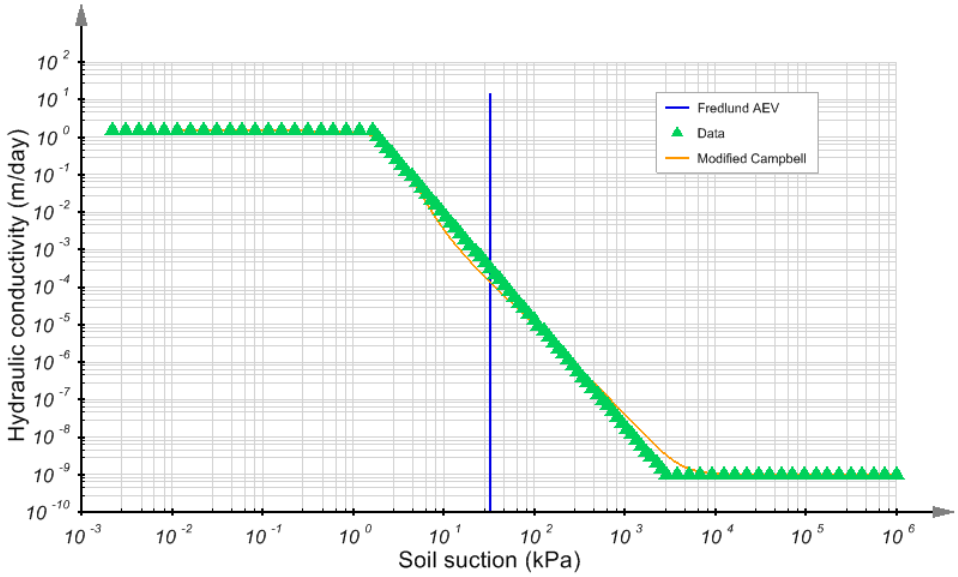

Figure 40 Unsaturated hydraulic conductivity for sandy material used in the model

Table 7 Parameters to determine material hydraulic and thermal properties used in 1-D vertical soil column with climate conditions

Hydraulic/Thermal Properties	Method	Parameters	Value	Units
SWCC	Fredlund and Xing	af	2.85	kPa
		nf	3.34	
		mf	0.289	
		hr	22.27	kPa
		Output curve type	Data points	
Hydraulic conductivity	Modified Campbell Estimation	K minimum	1×10^{-9}	m/day
		Mcampbell P	13.42	
		Output curve type	Data points	
Thermal conductivity	Johansen	Material state	crushed	
		Material type	fine	
		Quartz content	40	%
Heat capacity	Jame-Newman	Soil dry density	1,600	kg/m^3
		Heat capacity of solid component	750	J/kg-°C
SFCC	Estimated by SWCC			

NOTE:
SWCC output curve type as data points can improve the performance of model running.

2.8.4 Results and Discussions

The following sections discuss the results of modeling simulation.

2.8.4.1 Soil temperature

Figure 41 is soil temperature with time at different depths from 0 to 3 m during soil freezing and thawing. The lowest soil temperature on the ground surface is about –12 °C.

The soil temperature profile changing with depth is shown in Figure 42. It clearly shows from Figure 42 that the soil temperature increases dramatically from depth 0 to 1 m, in which temperature changes from –12 °C at depth 0 m to –8 °C at 0.15 m, and –1 °C at 1 m.

2.8.4.2 Comparison of frost depth with analytic calculation

The frost depth during ground freezing and thawing is given in Figure 43. The frost depth calculated with analytical solution (Aldrich, 1956) is provided in Figure 43. The Aldrich equation is expressed in equation [5]. It can be seen from Figure 43 that the model simulation has good agreement with the analytical calculation during the freezing period.

2.8.4.3 Soil saturation and pore water pressure change

Snow cover is not included in the model simulation. During wintertime, any precipitation event is regarded as rainfall. But because the ground is frozen, the precipitation cannot infiltrate into the ground, and exists on the ground surface as ice content.

As a result, the soil saturation at the ground surface is built up, as shown in Figure 44. This situation is particularly true during the period of soil thawing in spring.

It should be noted that all precipitation data in the software is applied to the upper body exactly at the time specified. Snowfall is applied in a separate dialog and its application to the numerical model happens in the springtime.

In contrast, soil saturation without considering soil freezing and thawing is illustrated in Figure 45. In this case, the precipitation can infiltrate into the ground in the wintertime. The pore water pressure change with time is given in Figure 46 in the case of soil freezing and thawing.

2.8.4.4 Cumulative summary change with time

As we have analyzed soil saturation in the case of soil freezing and thawing, runoff will happen due to over-saturation at the ground surface during the soil thawing period. Figure 47 illustrates this case at 180 days.

Figure 48 is the cumulative summary without considering soil freezing and thawing. It can be seen from Figure 47 that runoff happens at a time of about 180 days, but no runoff is observed in Figure 23.

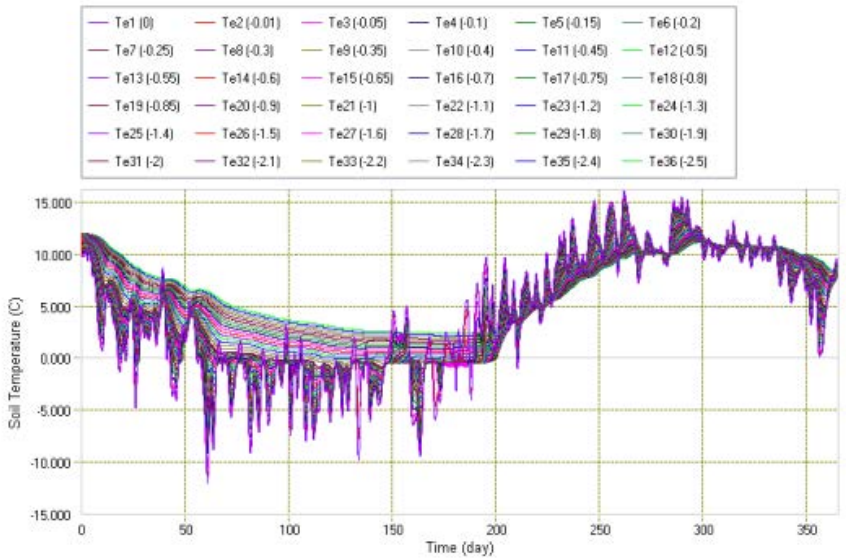

Figure 41 Soil temperature changing with time at different depth from 0 to 3 m

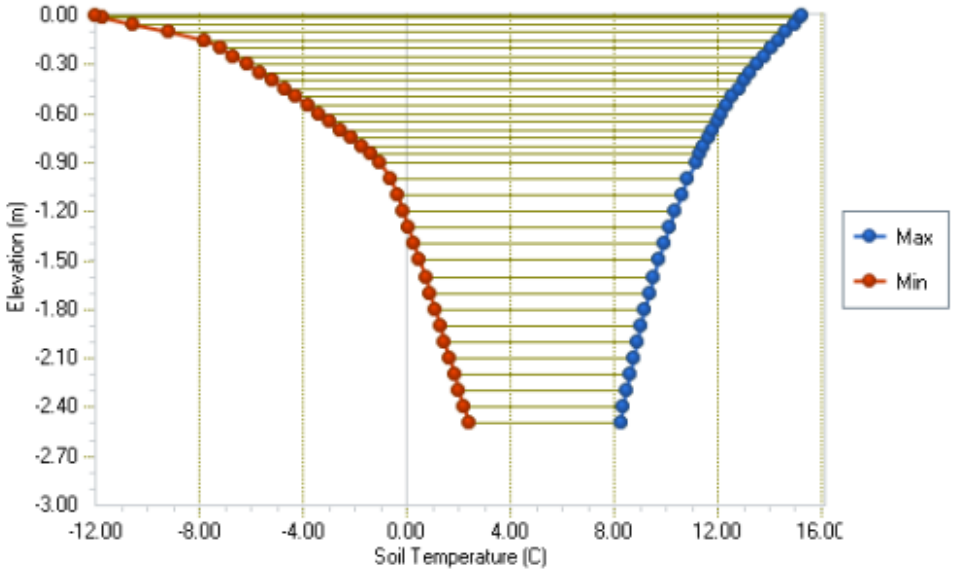

Figure 42 Max/Min Soil Temperature at different depths from 50 to 250 days of year with initial temperature of 16 °C

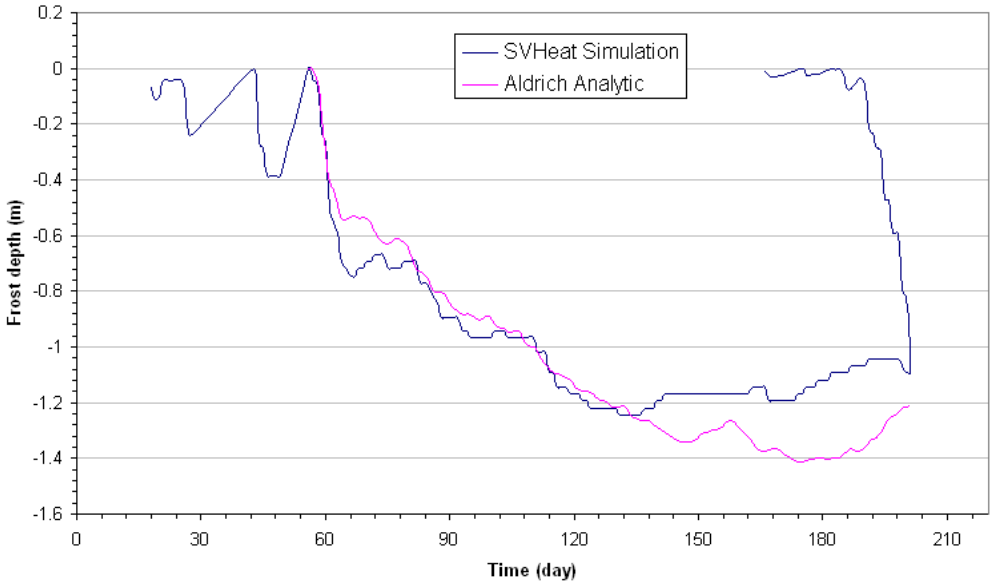

Figure 43 Comparison of simulated frost depth with analytical solution

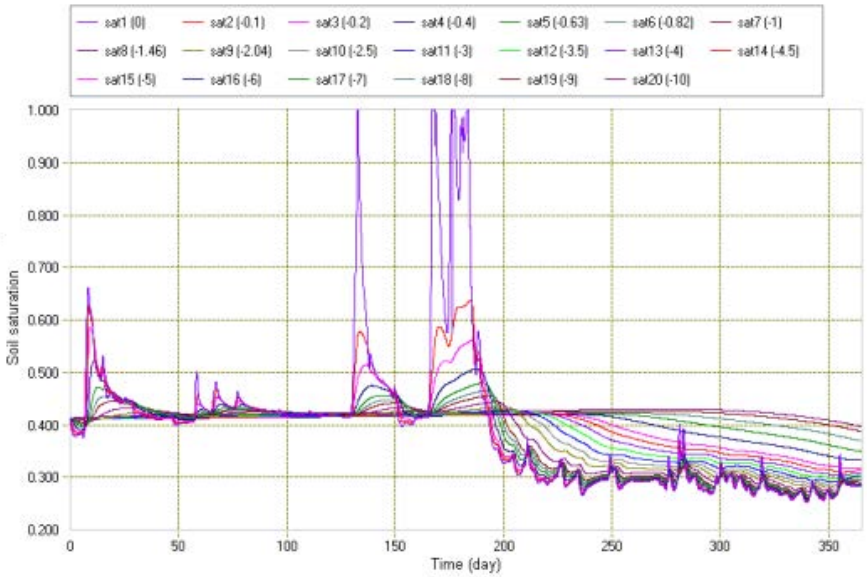

Figure 44 Soil saturation change with time in consideration of soil freezing and thawing

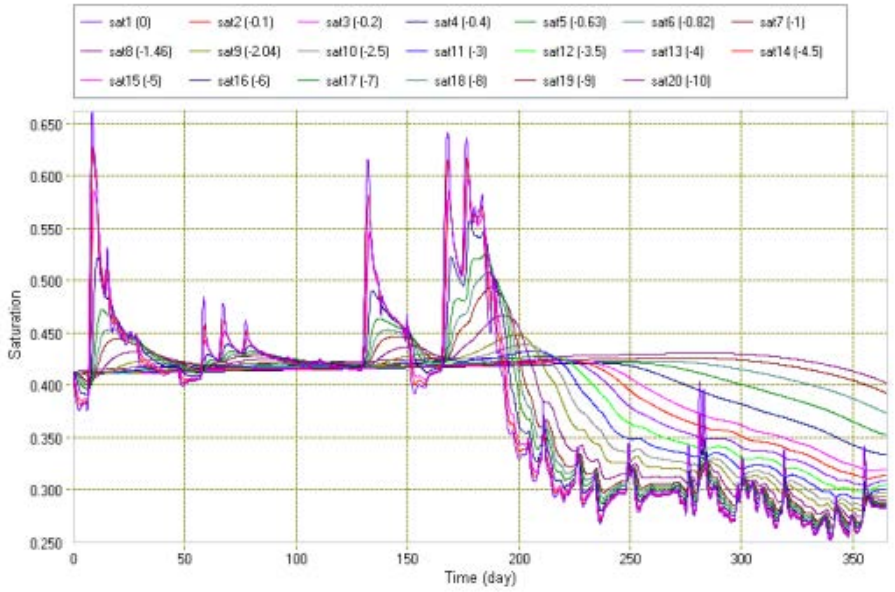

Figure 45 Soil saturation changes with time without considering soil freezing and thawing

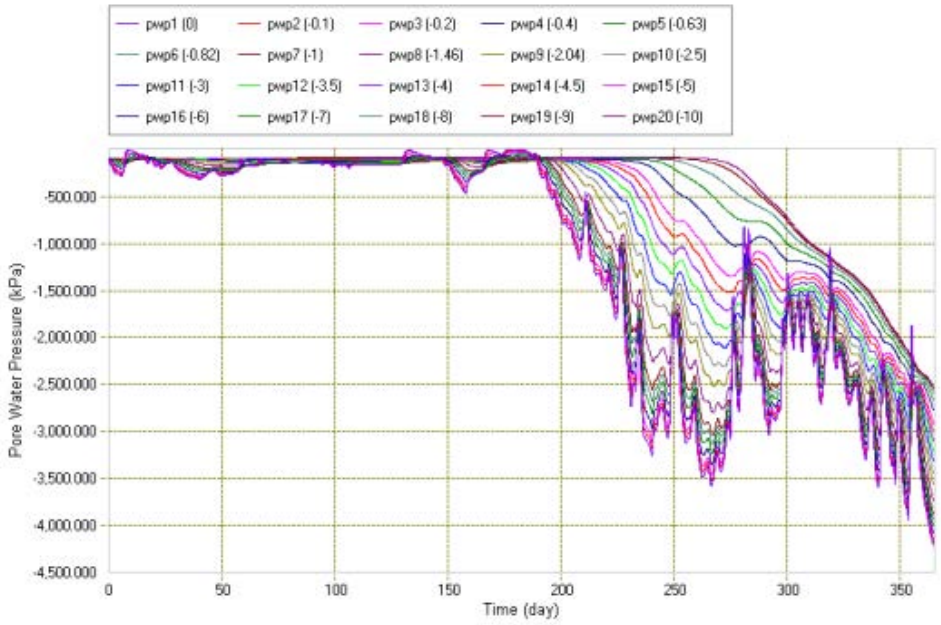

Figure 46 Soil pore water pressure changes with time in considering soil freezing and thawing

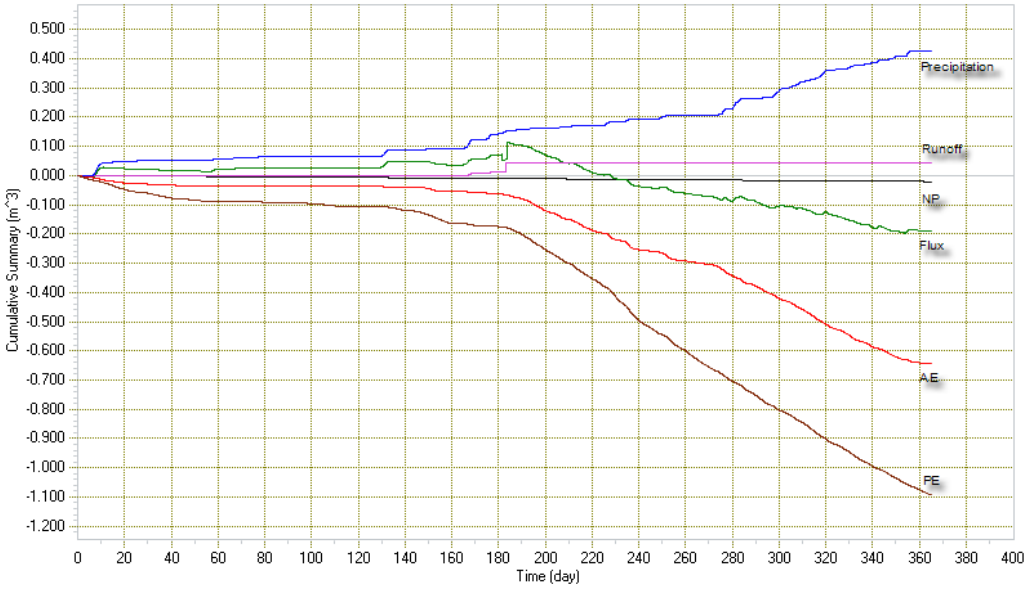

Figure 47 Cumulative summaries in the case considering soil freezing and thawing

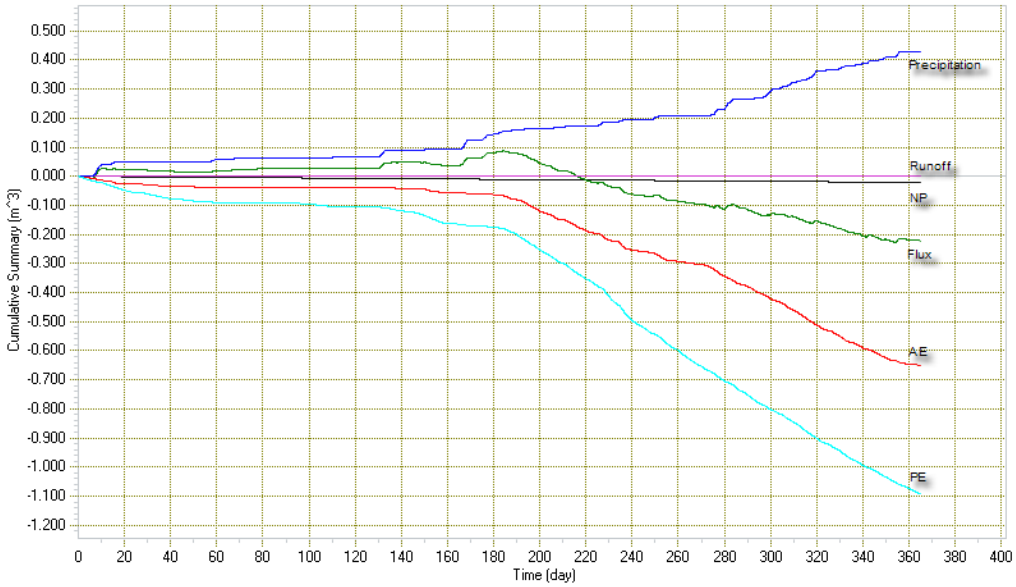

Figure 48 Cumulative summaries without considering soil freezing and thawing

2.9 SOIL COLUMN DRYING (WILSON, 1990) - COUPLED WITH WATER AND AIR FLOW

Project: Evapotranspiration, USMEP
Model: WilsonLimiting1997_THA, WilsonPenman1994_THA, WilsonEmpirical1997_THA, WilsonLimiting1997_TH, WilsonPenman1994_TH, WilsonEmpircalAE_TH

This benchmark is to use the SVFLUX, SVHEAT, and SVAIR software to verify the evaporative model coupled with water flow, vapor flow, air flow and heat flow using experimental data from a drying soil column that was presented in Wilson's PhD Thesis (Wilson, 1992).

2.9.1 Purpose

Prediction of soil evaporation, soil temperature profile, and water content profile are of interest to many applications such as cover design, agricultural soil science, and land surface parameterization in climate prediction, etc. The purpose of this model is to illustrate the prediction of soil surface temperature, and moisture evaporation calculated with the evaporative models of Wilson-Penman (Wilson, 1994), Wilson limiting-function and empirical expression (Wilson et al., 1997). The simulated results for the model coupled with moisture flow and heat (without air flow) are also discussed.

See SVHEAT theory manual for the governing equation of the coupled model.

2.9.2 Geometry and Boundary Conditions

The soil column drying test was presented in Wilson's Ph.D thesis within a laboratory environment which the air temperature and humidity are controlled. The depth of soil column is 0.3 m (see Figure 49). The upper end of the soil column was exposed to the air temperature, and the water can evaporate from the soil surface. The evaporative flux applied to the soil surface is the actual evaporation calculated using the Wilson's approach (Wilson-Penman, 1994, and Limiting function, 1997). The thermal boundary condition applied to the soil surface is based on the atmospheric thermal balance equation as given in equation [4]. At the bottom of the soil column, the flux of water-flow and air-flow is assumed to be zero, and a constant temperature of 37.7 °C is applied.

$$Q_g = Q_N - Q_L - Q_H \qquad [1]$$

where:

Q_g = Ground thermal flux, J/day-m^2,

Q_N = Net radiation, J/day-m^2, and

Q_L = Latent heat flux of water evaporation, J/s-m^2,

Q_H = Sensible heat transfer from the ground to the air, J/s-m^2.

Initial water head: 0.3 m,
Initial temperature: 38 °C,
Initial air pressure: 0 kPa.

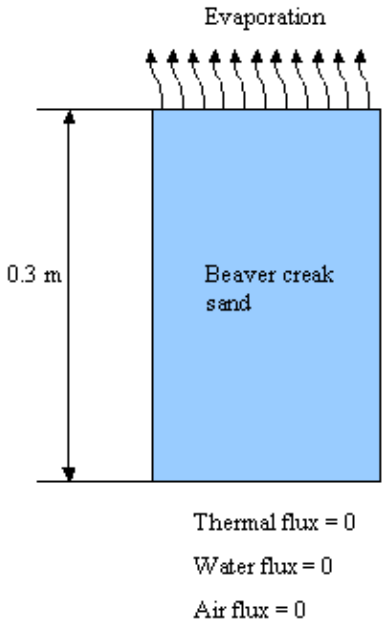

Figure 49 Model geometry of soil column drying

NOTE:

1. The model is required to set the "Apply Surface Suction Correction" option in the Suction tab of SVFLUX model settings dialog, and
2. The correction factor is set to be –1.8.

2.9.3 Material Properties

The material of the soil column is Beaver Creek Sand. The hydraulic, thermal, and air flow properties of the sand were presented as below.

Soil Water Characteristic Curve (SWCC)

Saturated volumetric water content: 0.41 m^3/m^3.
Unsaturated water content was approximated using the Fredlund and Xing fitting equation as shown in Figure 50. The curve fitting parameters are presented in Table 8.

Hydraulic conductivity

Saturated hydraulic conductivity: 2.57 m/day.
Unsaturated hydraulic conductivity fitting is shown in Figure 51, and its parameters are given in Table 8.

Thermal conductivity
Thermal conductivity is calculated using the Johansen method (Johansen, 1975) with the parameters listed in Table 8.

Heat capacity
The soil heat capacity is calculated based on the heat capacity of solid component, water, vapor, soil dry density, and their fractions (Table 8).

Soil Freezing Characteristic Curve (SFCC)
No soil freezing happens, so that SFCC method is specified as “None”.

Soil air conductivity
The air conductivity is calculated based on the air intrinsic permeability, and air relative permeability with van Genuchten-Mualem approach. Figure 52 shows air conductivity change with the water content.

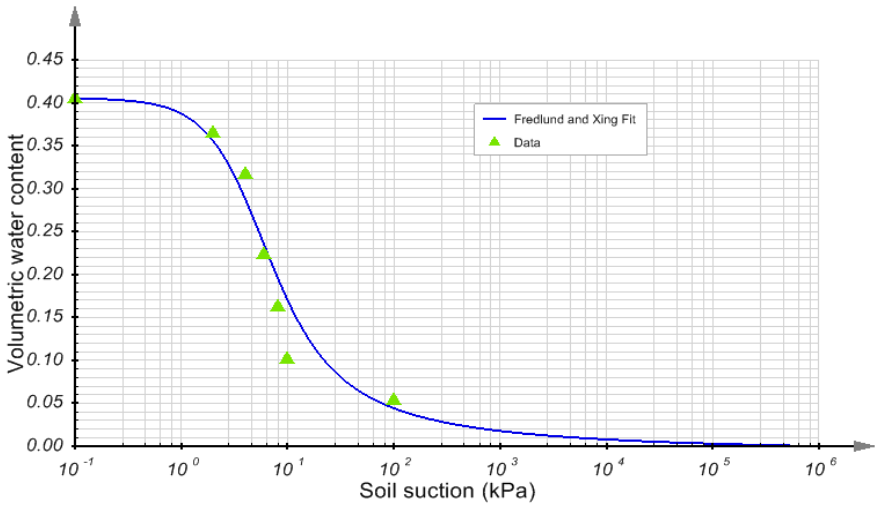

Figure 50 SWCC for Beaver Creek Sand

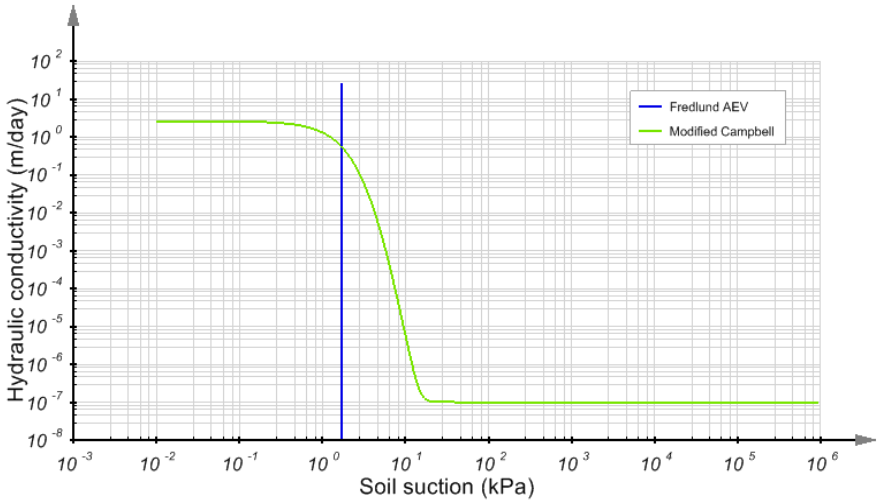

Figure 51 Hydraulic conductivity for unsaturated Beaver Creek Sand

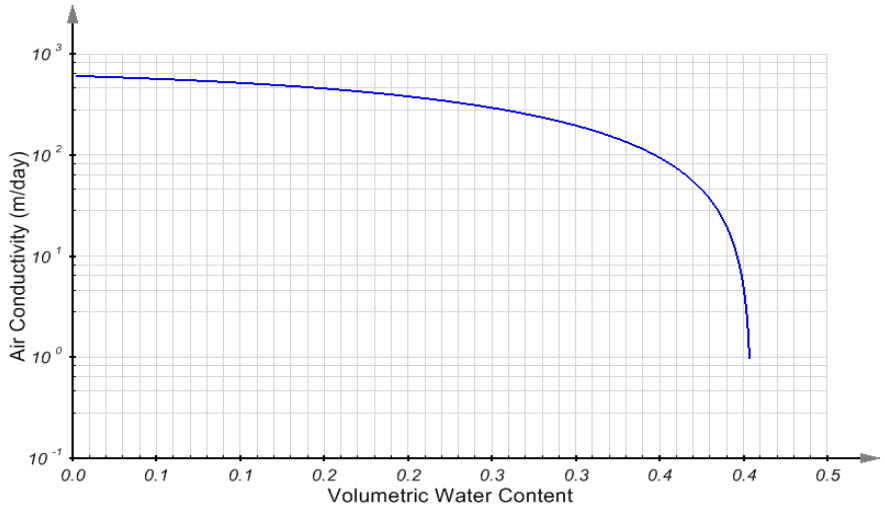

Figure 52 Air conductivity changes with volumetric water content for Beaver Creek Sand

Table 8 Hydraulic, thermal and air flow properties for Beaver Creek Sand

Hydraulic/Thermal /air flow Properties	Method	Parameters	Value	Units
SWCC	Fredlund and Xing	af	4.0458	kPa
		nf	1.6922	
		mf	1.1801	
		hr	12.415	kPa
Hydraulic conductivity	Modified Campbell Estimation	Output curve type	Data points	
		K minimum	1×10^{-7}	m/day
		Mcampbell P	15.0	
Thermal conductivity	Johansen	Output curve type	Data points	
		Material state	crushed	
		Material type	fine	
		Thermal conductivity of solid component	708,480	J/day-m-°C
Heat capacity	Jame-Newman	Soil dry density	1,577	kg/m^3
		Heat capacity of solid component	710	J/kg-°C
SFCC	None			
Air Conductivity	Estimated with air intrinsic permeability	air intrinsic permeability	3×10^{-9}	m^2
	relative air permeability	van Genuchten fitting parameter	0.38	
		Residual water content	0.002	m^3/m^3

2.9.4 Results and Discussions

The results for the model simulation coupled with water flow, vapor flow, air flow and heat flow are presented as follows:

2.9.4.1 Actual Evaporation

To calculate the actual evaporation using the equation of Wilson-Penman (1994), it is required to know the solar radiation. In this benchmark, the solar radiation is estimated by comparison of the calculated potential evaporation (PE) with the measured potential evaporation. It was found that there is a good agreement of measured PE (Wilson, 1992) with the calculated value based on the Penman equation (Penman, 1948) when the solar radiation is equal to 22 MJ/day-m^2, as shown in Figure 53. This value of solar radiation is used in the simulation.

The simulated results of actual evaporation using fully coupled model of SVFLUX and SVHEAT are shown in Figure 53. The numerical result presented in Wilson Ph.D. thesis is also illustrated in the figure. It can be seen from the Figure 53 that the simulated results for the different approaches of actual evaporation are a reasonable match to the laboratory data (Wilson, 1990). It is particularly noted that the actual evaporations calculated with Wilson-Penman approach and Limiting-Function approach are almost identical.

Please note that to improve the stability of evaporative model a correction factor is utilized to account for the steep suction gradient at the soil surface (see SVFLUX Theory manual for details). In this benchmark the correction factor = -1.8 is determined by trial and error.

To account for the air flow effect on the evaporation, a fully coupled model of SVFLUX, SVHEAT and SVAIR is simulated. The results of actual evaporation for different approaches are illustrated in Figure 54. The lower actual evaporations are predicted than the measured value. It is interesting to investigate for the difference of actual evaporation when the airflow is accounted for.

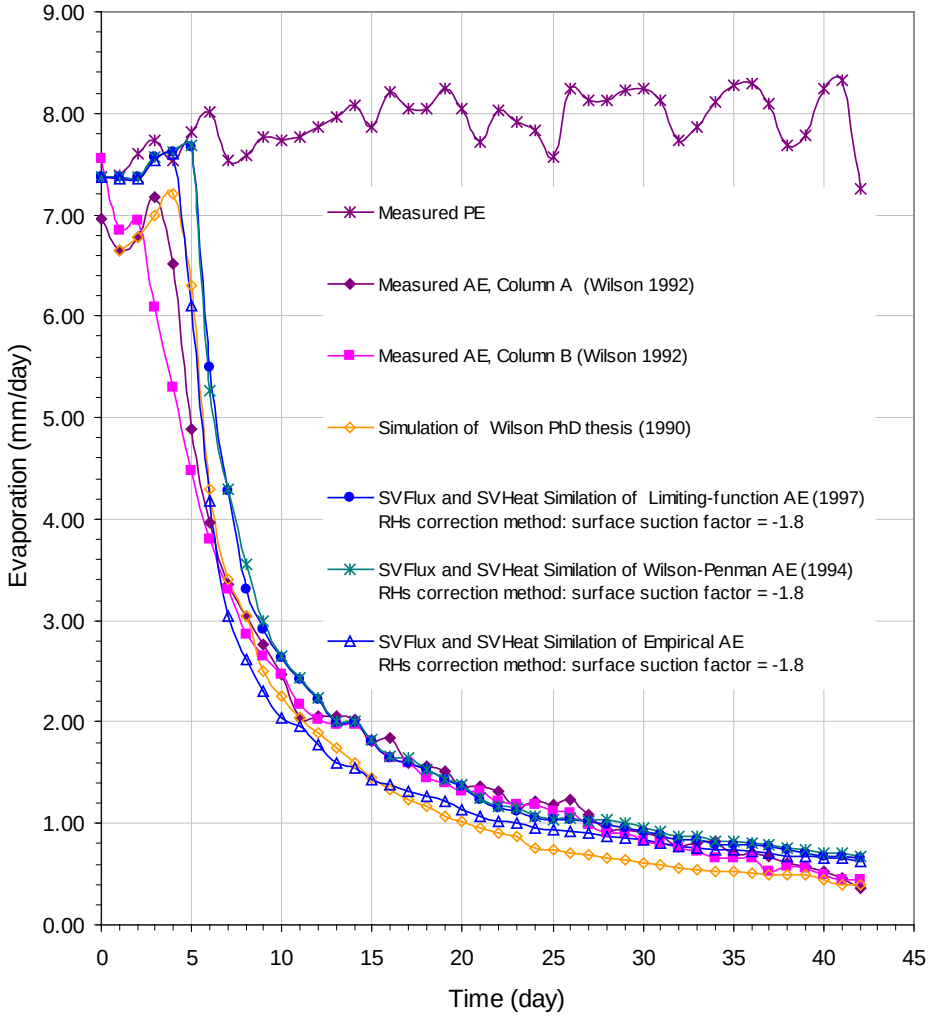

Figure 53 Comparison of the measured actual evaporation with the simulated result using the coupling model of SVFLUX and SVHEAT

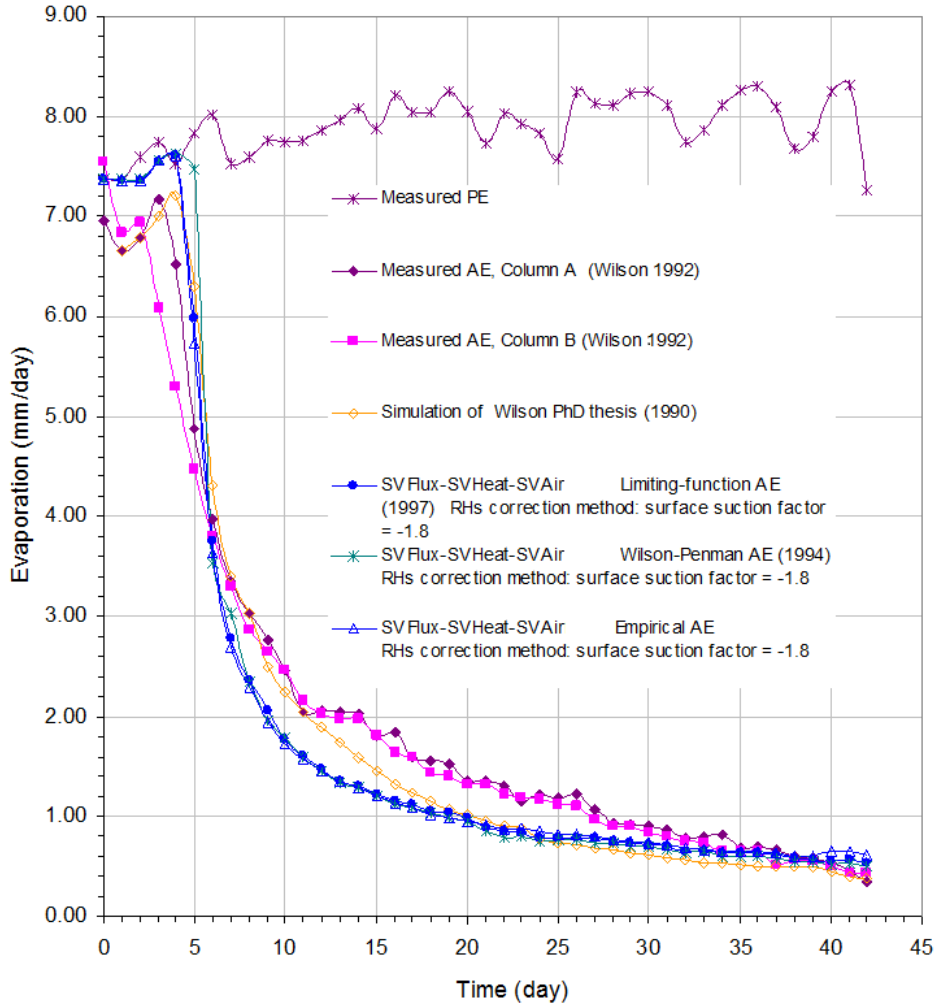

Figure 54 Comparison of the measure actual evaporation with the simulated results simulated using the fully coupled model of SVFLUX, SVHEAT, and SVAIR

2.9.4.2 Prediction of soil temperature at the soil surface and temperature profiles in the soil column

Figure 55 illustrates the comparison of the predicted soil surface temperature with the measured value during the soil column drying. Because of the heat absorption in the water evaporation, the soil temperature at the soil surface decreases with the water evaporative flux to air in the first four days. After that period the evaporative rate decreases with time (see Figure 53 and Figure 54), and the temperature at soil surface increases until it is close to the air temperature.

Figure 56 further shows the change of soil temperature at different depths with time, and Figure 57 compares the simulation of soil temperature profiles with the test results.

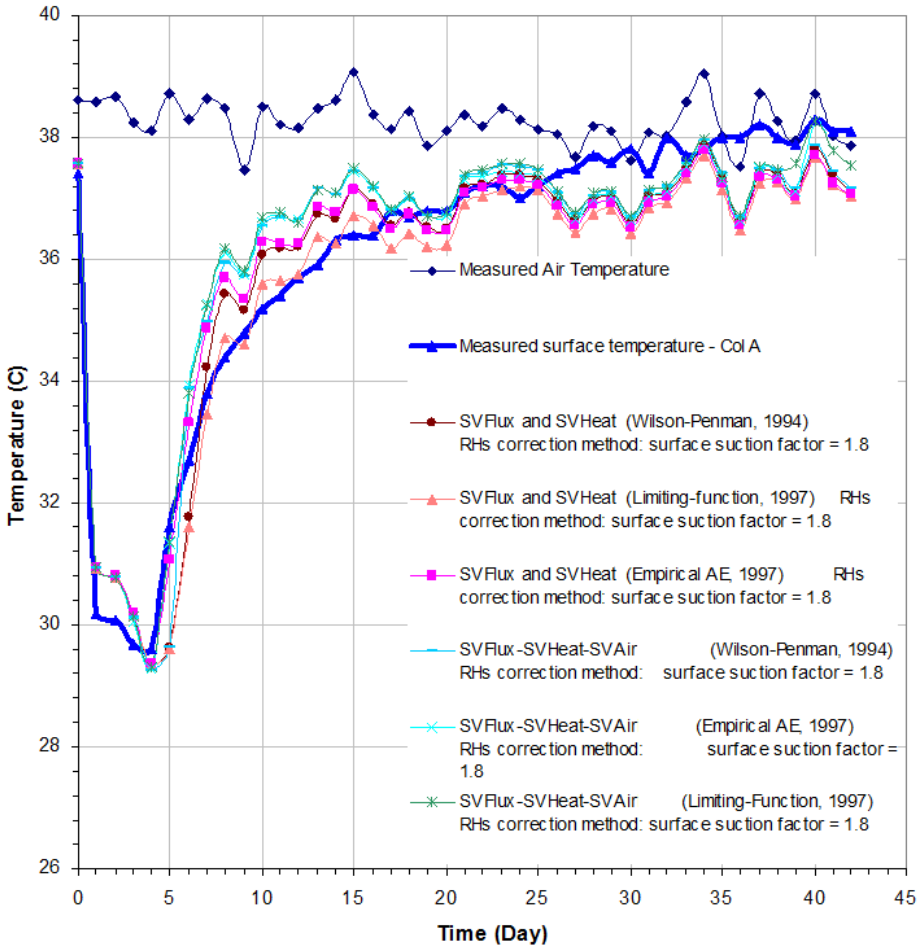

Figure 55 Comparison of the predicted soil surface temperature with the measured values

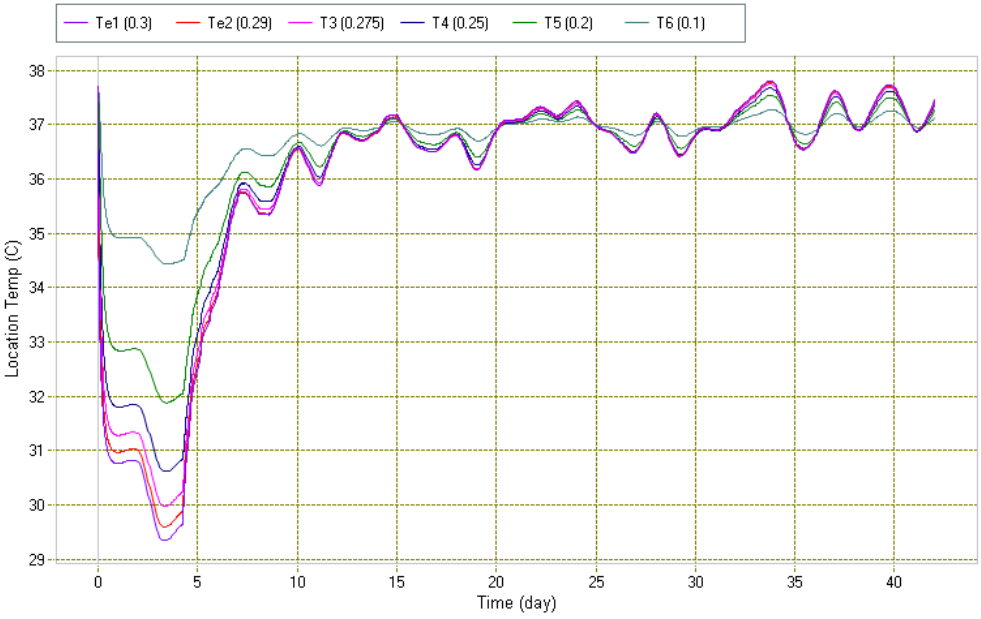

Figure 56 Soil temperature changes with time during the soil column drying with Limiting-Function AE

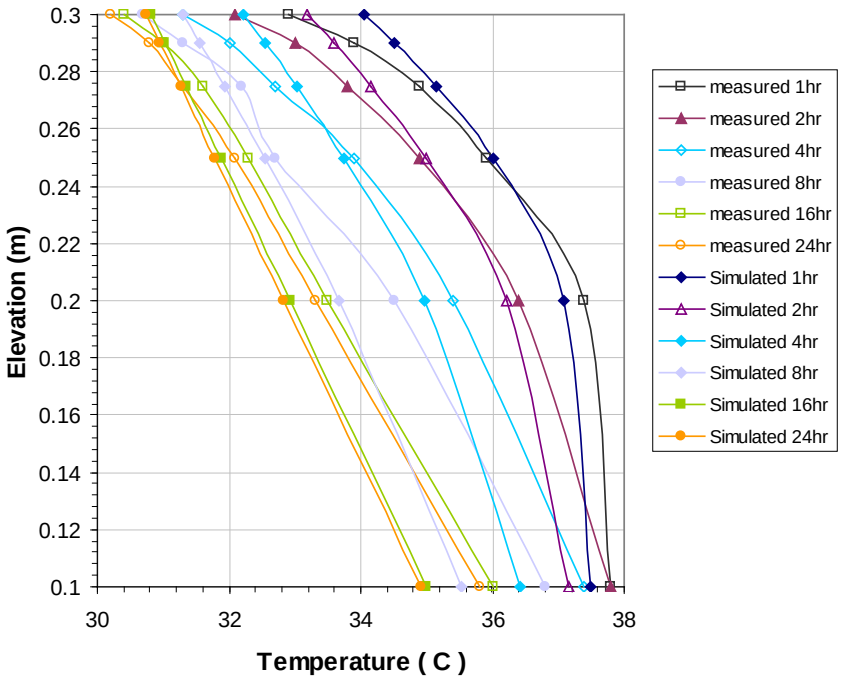

Figure 57 Predicted temperature profiles vs. the measured value in the first day of soil column drying

2.9.4.3 Pore Water Pressure, pore vapor partial pressure, and pore air pressure

The change of soil pore water pressure, pore vapor pressure and pore air pressure with time are shown in Figure 58, Figure 59, and Figure 60.

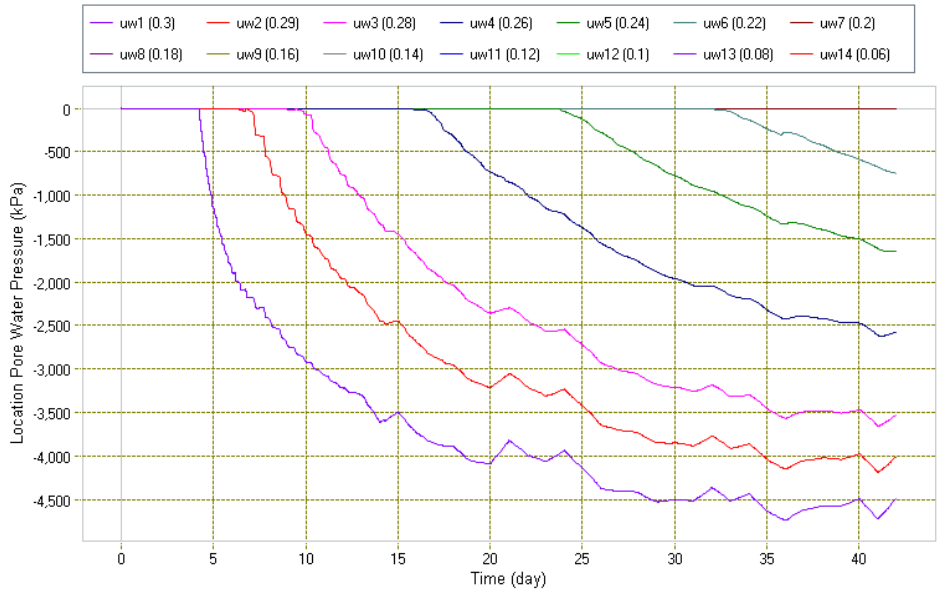

Figure 58 Pore water pressure changes with time during soil column drying for the coupling model of SVFLUX, SVHEAT and SVAIR

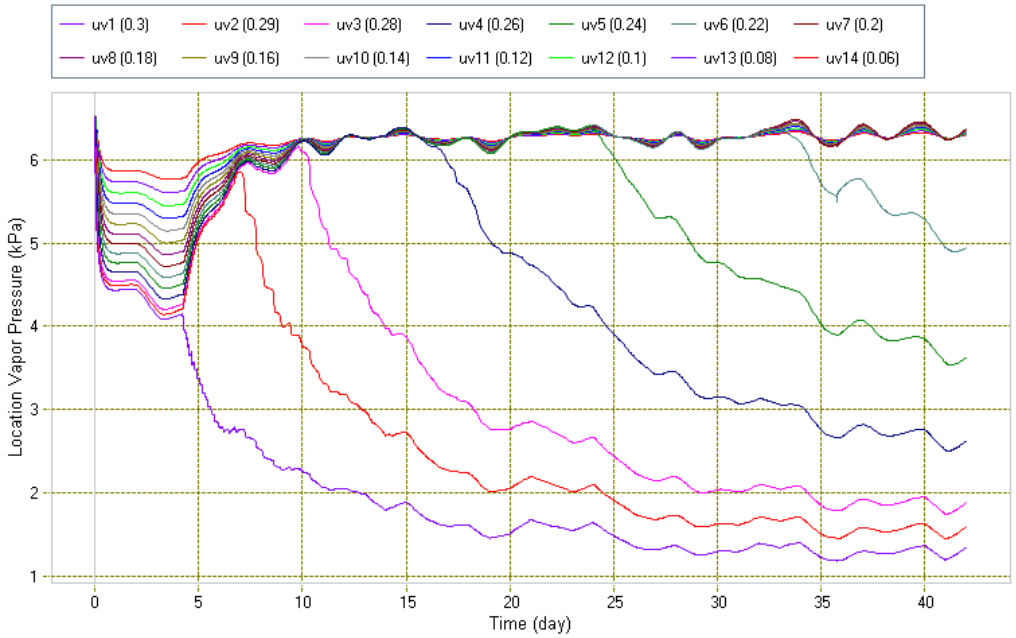

Figure 59 Pore vapor partial pressure changes with time during soil column drying for the coupling model of SVFLUX, SVHEAT and SVAIR

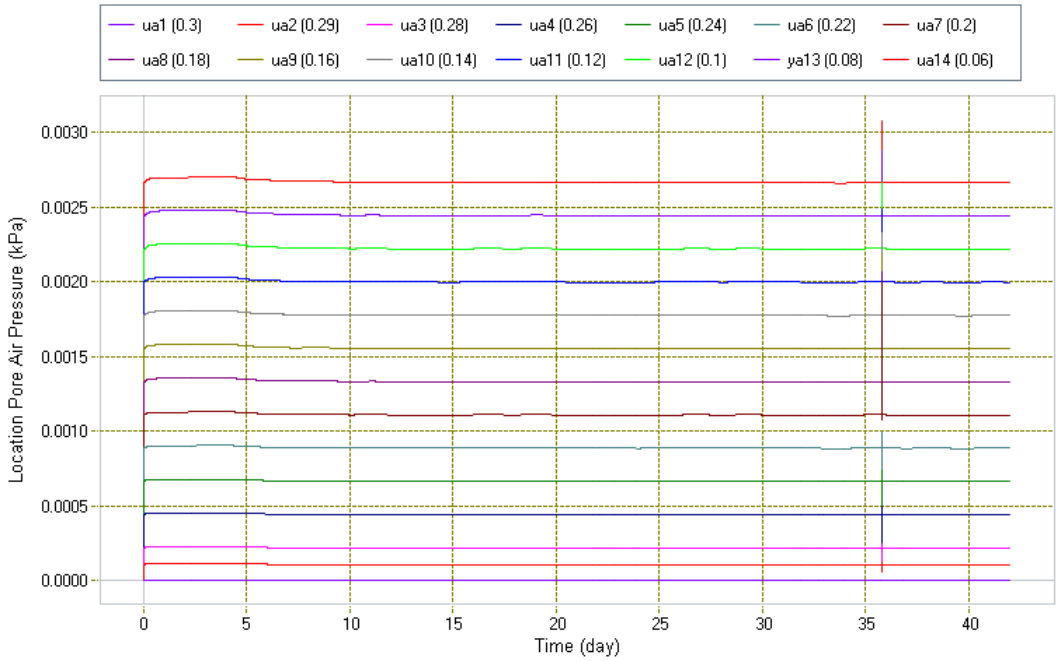

Figure 60 Soil pore air pressure changes with time during soil column drying for the coupling model of SVFLUX, SVHEAT and SVAIR

3 TWO-DIMENSIONAL HEAT TRANSFER

This chapter will verify the ability of SVHEAT to solve two dimensional steady-state and transient heat transfer models. The results from SVHEAT are compared to publish analytical results as well as other proven commercial software packages.

Each verification model will begin with a brief description of the model followed by the comparison of results, then conclusions about the model. All of the verification models presented in this document are included with the SVHEAT software.

3.1 HARLAN AND NIXON

Harlan and Nixon's work solves for the steady-state conditions between two adjacent areas with surface temperatures of +4 °C and −5 °C. The results from SVHEAT will be compared to the results of an analytical solution published by Harlan and Nixon (1978).

Project: USMEP_Textbook
Model: HarlanNixon1978

3.1.1 Model Description

In order to simulate the conditions proposed in Harlan and Nixon it was necessary to set the thermal conductivity of 1.0 W/m-°C for the range of temperatures expected in the model.

This is accomplished by entering at least two points on the thermal conductivity curve giving both points a thermal conductivity of 1.0.

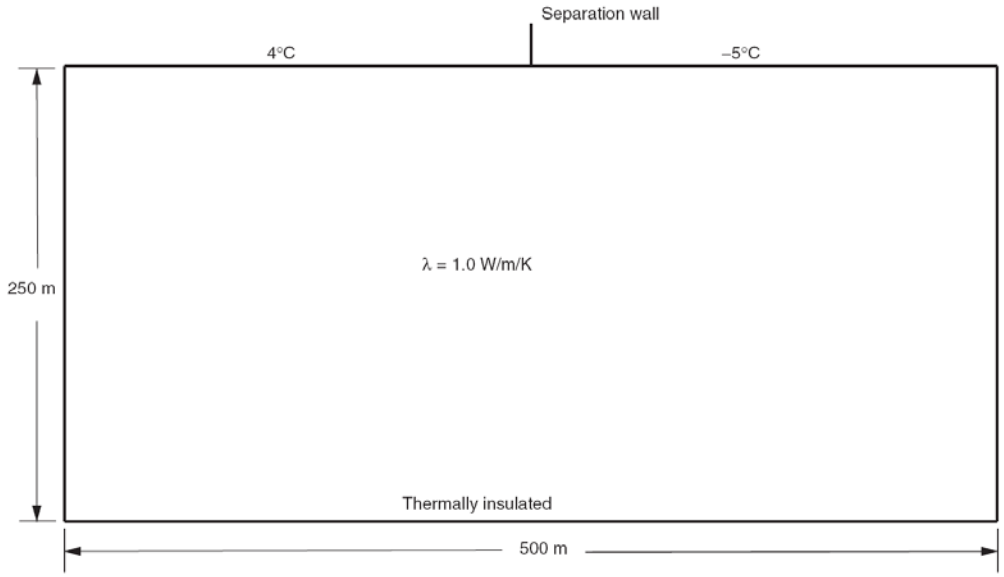

Figure 61 Harlan and Nixon Model Description

The model is setup to model two adjacent semi-infinite areas. One area with a surface temperature of +4 °C the other with a surface temperature of -5 °C. SVHEAT will solve for the resulting ground temperatures resulting from the applied boundary conditions.

3.1.2 Results and Discussions

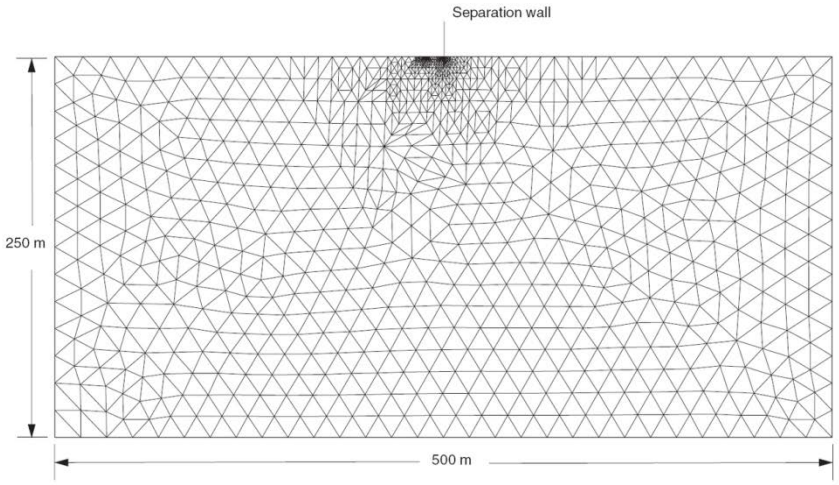

Figure 62 SVHEAT Solution Mesh

The ability of SVHEAT to provide automatic mesh generation and refinement simplifies the modeling process. This feature automatically creates a mesh within the boundaries of the model domain. The solution mesh for the model at hand may be seen in the above Figure 62.

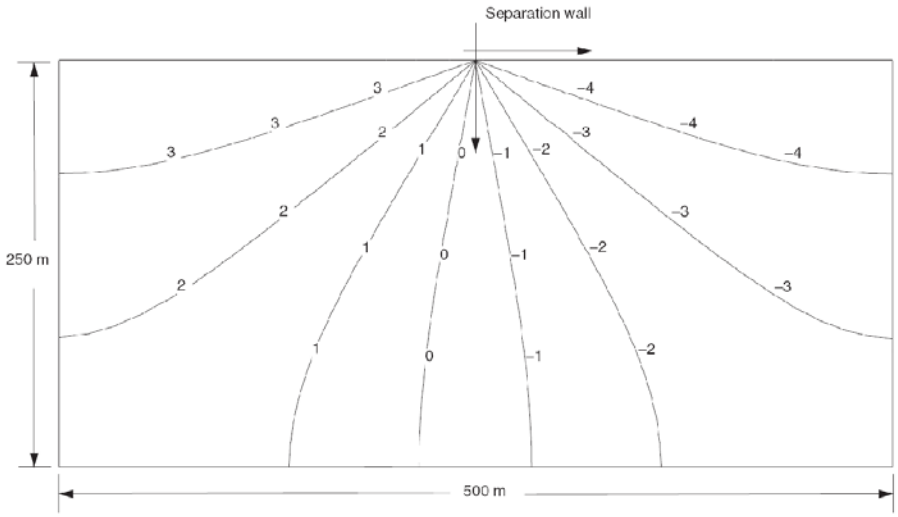

Figure 63 SVHEAT Temperature Contours

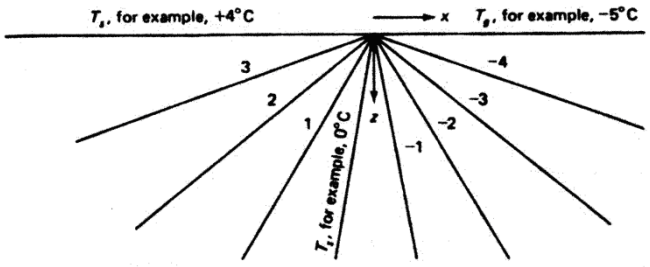

Figure 64 Analytical Results (Harlan and Nixon, 1978)

Comparing the above contour plots of temperature SVHEAT and the analytical solution published in Harlan and Nixon (1978) one can see that there is a good agreement. Both solutions show an agreement in the location of the freezing front as well as the remaining temperature contours in both the frozen and thawed regions.

3.2 HEATED STRIP

This verification model will be used to compare SVHEAT to the TEMP/W software package. This steady-state model will consider a heated strip extending across permafrost conditions.

Project: USMEP_Textbook
Model: HeatedStrip

3.2.1 Model Description

The presented example illustrates the effect of a warm building on the subsurface during sub-zero conditions outside.

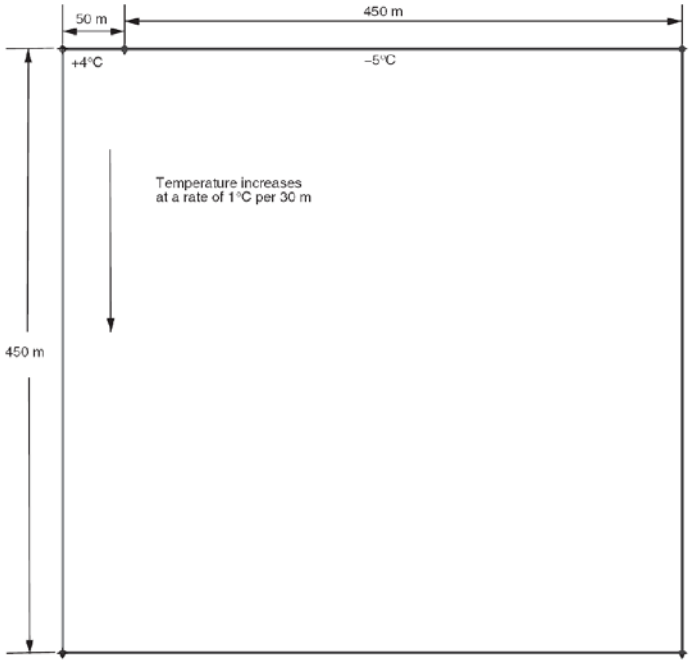

Figure 65 Heated Strip Model Description and Geometry

This model is designed to simulate a heated strip extending across permafrost conditions. The initial surface temperature is -5 °C and increases with depth at a rate of 1 °C/30 m.

The heated strip remains at a constant temperature of +4 °C. Due to the symmetry that exists, only half of the model will be considered.

3.2.2 Results and Discussions

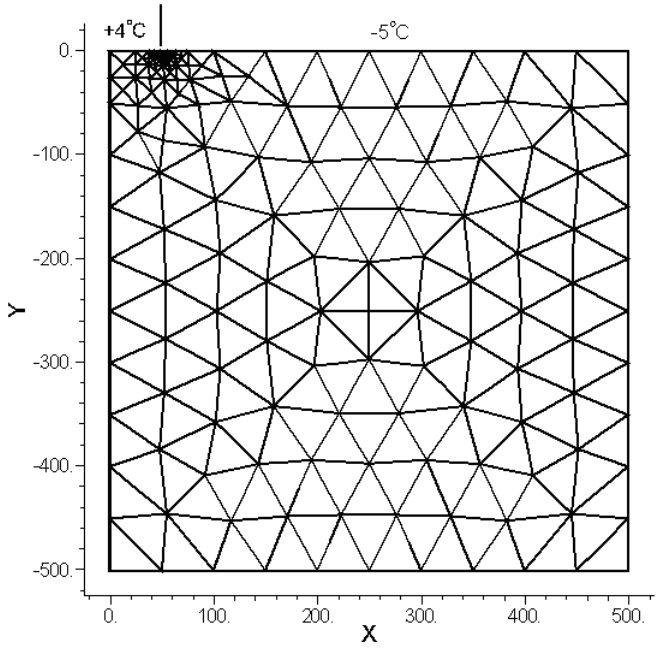

Figure 66 Heated Strip SVHEAT Solution Mesh (Error = 0.01 °C)

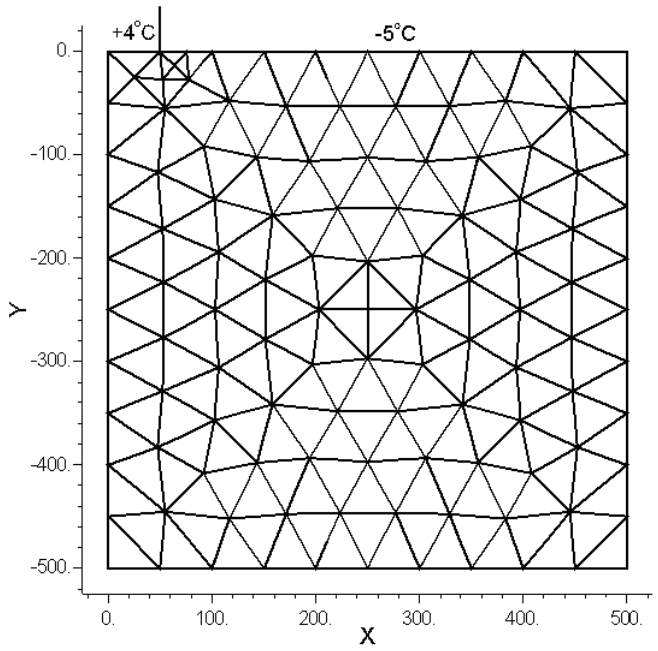

Figure 67 Heated Strip SVHEAT Solution Mesh (Error = 0.015 °C)

A refined mesh is necessary around areas where errors are expected to be high to ensure convergence and solution accuracy. How much resolution is required to achieve the proper balance between solution accuracy and efficiency? If the mesh has too much resolution the modeler sacrifices efficiency while not enough resolution will sacrifice solution accuracy. In fixed mesh software, it is left up to the user to determine where in the model this error is most likely to occur.

SVHEAT allows the user to set the error for each model by entering a global error limit, which is to be achieved. The mesh is subsequently refined until this error limit is achieved. The three figures above illustrate how the solution mesh will change depending on the error limit set in the model SVHEAT can generate meshes that would be impossible to create by hand and therefore provides an increased level of accuracy and convergence ability.

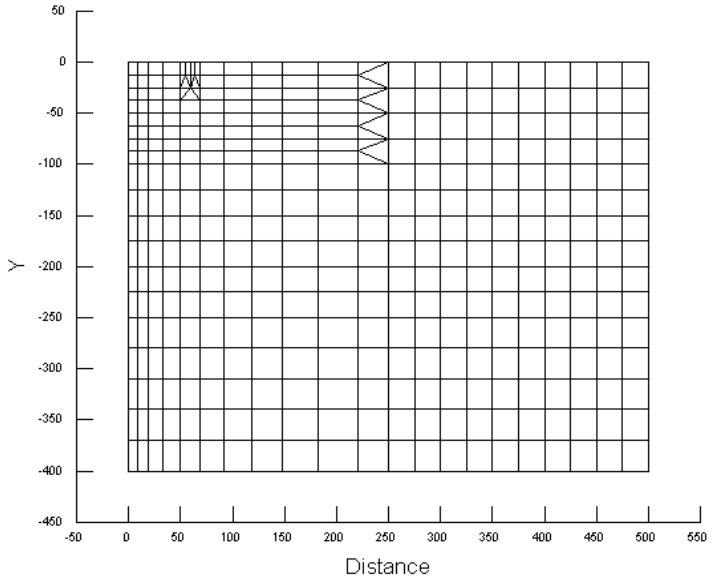

Figure 68 Verification #2 TEMP/W Solution Mesh

An experienced engineer understands that a refined mesh is necessary around areas where errors are expected to be high to ensure convergence and solution accuracy. However, even the most experienced engineers may question how much resolution to achieve the balance between solution accuracy and efficiency they are looking for.

If the mesh has too much resolution the modeler sacrifices efficiency while not enough resolution will sacrifice solution accuracy. Most software packages today do not supply the user with a way to quantify how much error they are allowing in their solution. In addition, it is left up to the user to determine where in the model this error is most likely to occur. SVHEAT allows the user to set the error for each model by typing in a single number and automatically refines the mesh in model areas resulting in significant time-savings.

A comparison between error limits can be generated as easily as saving the model under a new name using *Save As*, setting a new error limit, and running the model to see the results. The three figures above illustrate how the solution mesh will change depending on the error limit set in the model. SVHEAT can generate meshes that would be impossible to create by hand and therefore provides a level of accuracy and convergence ability that far surpasses current software.

The results in the subsequent figures show good agreement between the two software packages. The two figures also illustrate how easy it is to determine the solution accuracy using SVHEAT.

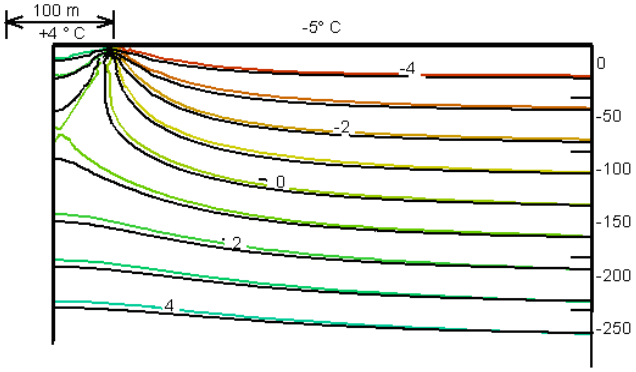

Figure 69 SVHEAT colors (printed light) versus TEMP/W (Error = 0.015 °C)

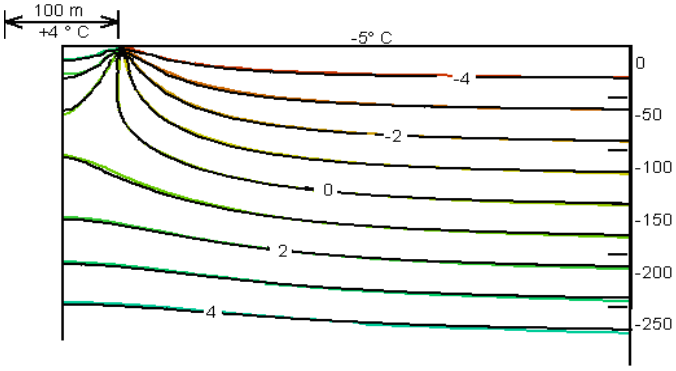

Figure 70 SVHEAT colors (printed light) versus TEMP/W (Error = 0.01)

3.3 COUTTS AND KONRAD (1994)

This verification model was originally published by Coutts and Konrad (1994) to look at the case of chilled pipelines stretching across areas of discontinuous permafrost. TEMP/W uses this model as verification therefore the results obtained from SVHEAT will be compared to those found in the TEMP/W User's Manual.

Project: USMEP_Textbook
Model: CouttsKonrad

3.3.1 Model Description

The material properties that were used in the model are presented below:

Table 9 Thermal properties for Coutts and Konrad (1994) model

Material Name	Thermal Properties	Method	Parameters	Value	Unit
Frozen soil	Thermal conductivity	constant	λ	1.8	W/m-°C
Unfrozen soil	Thermal conductivity	constant	λ	1.5	W/m-°C
Frozen soil	Heat capacity	Constant	C	2.1×10^6	J/m^3
Unfrozen soil	Heat capacity	constant	C	2.5×10^6	J/m^3

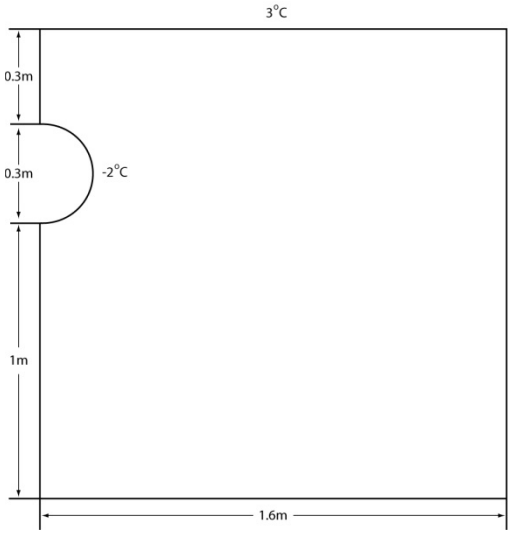

Figure 71 2D Pipe Geometry and Boundary Conditions

A chilled pipeline with an outside temperature of –2 °C is buried in material with an initial temperature of 3 °C. The results will show the condition of the material after a time period of 730 days. The ground surface temperature is kept constant at 3 °C.

3.3.2 Results and Discussions

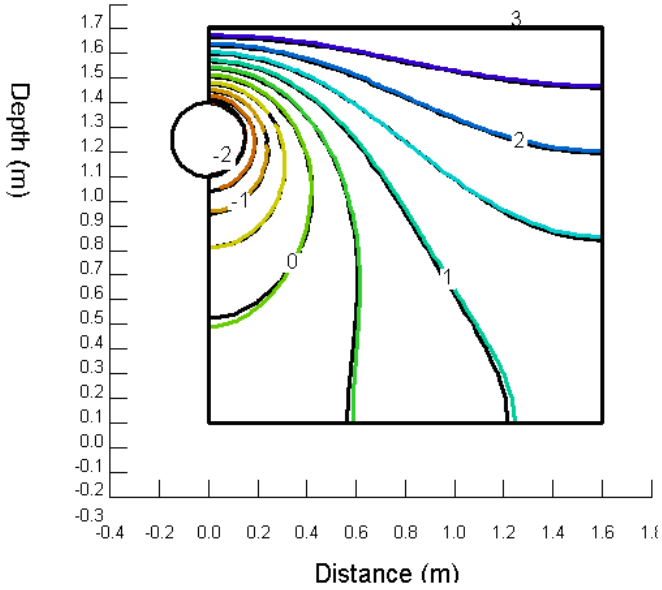

Figure 72 SVHEAT (color or light) versus TEMP/W (black) 730 days

From the above figure, it can be seen that there is good agreement between the two software packages on the location of the freezing front as well as the condition of the material in both the frozen and unfrozen areas.

3.4 GROUND FREEZING - COUPLED

Project: GeoThermal
Model: ArtificialGroundFreezing_no_convect

The example is to simulate artificial ground freezing. To simplify the problem, only one freeze pipe is installed. A similar example is provided in another software package (Vadose/W, 2008).

The following features are illustrated in this example.

- Frozen ground developed during ground freezing process,
- Water flow around frozen ground, and
- Thermal convection effect on temperature distribution and finally effect on frozen ground regime.

3.4.1 Purpose

This model is designed to demonstrate the water flow and heat flow during artificial ground freezing.

3.4.2 Geometry and Boundary Conditions

The example is a 2-D model. The model geometry consists of two regions, as shown in Figure 73. Region 1 is the soil ground with a length of 4 m, and a height of 3.02 m. Region 2 is a circular freeze pipe of 0.4 m in diameter. The freeze pipe is centered at the coordinate of (2, 1.5).

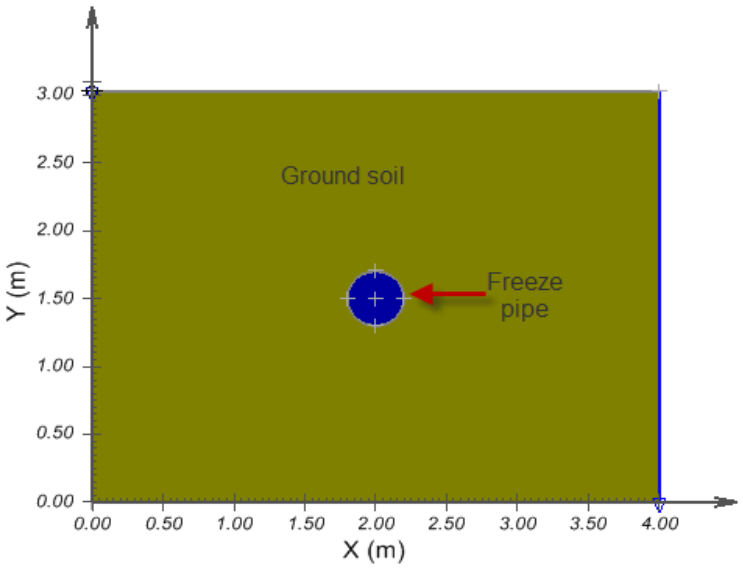

Figure 73 Geometry of artificial ground freezing model

Hydraulic boundary conditions

On the right side of the rectangle ground, a 3.02 m water head is applied, and on the left, a 3 m water head is set. The head gradient from right to left side will be (3.02 – 3.0)/4.0 = 0.005 m/m. No boundary is set on the top and bottom of the rectangle. The hydraulic flux is set zero for freeze pipe.

Thermal boundary conditions

No thermal boundary condition is applied to rectangle ground. The freezing rate of pipe is set using temperature expression as "if t < 1 then 3 –5*t else –2". The expression means pipe temperature will drop to –2 °C from the initial temperature 3 °C in one day, and it keeps –2 °C after.

Initial head is transferred from a steady state model. Therefore, before running the model, a steady state SVFLUX model was created, and it was run with the same the soil properties as described in section 2.1.3. Initial temperature is set to 3 °C.

3.4.3 Material Properties

The material in Region 1 is a coarse soil. The following hydraulic properties are assumed.

Soil Water Characteristic Curve (SWCC)

Figure 74 is the soil water characteristic curve for the ground soil material used in this example. The parameters for SWCC fitting equations are estimated as given in

Table 10 for ground soil and freeze pipe. A steel material contains no moisture in reality, but a low hydraulic value is specified as a special material involved in seepage modeling.

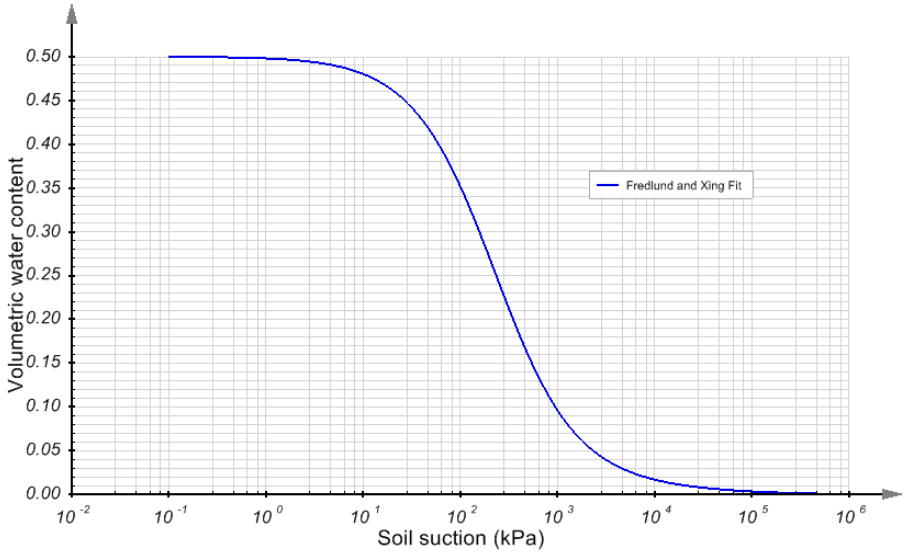

Figure 74 Soil Water Characteristic Curve for the soil material used in the ground freezing model

Hydraulic conductivity

The unsaturated hydraulic conductivity is calculated as shown in Figure 75 with parameters given in

Table 10.

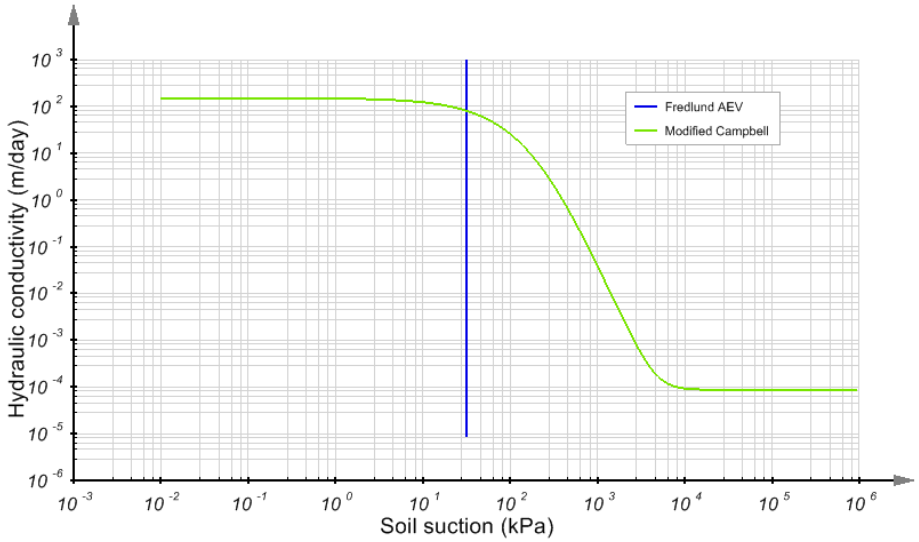

Figure 75 Unsaturated hydraulic conductivity for soil material used in ground freezing model

Thermal conductivity

The thermal conductivity of ground soil is calculated with Johansen approach, and for freeze pipe, it is set with a constant value as given in

Table 10.

Heat capacity
The heat capacity of ground soil is estimated with values given in

Table 10.

Soil Freezing Characteristic Curve (SFCC)

For ground freezing, the interest is focused on the final state of frozen ground, so that the phase change can be neglected in this example, as shown in

Table 10. The “None” method of SFCC means unfrozen water content is set to zero, and slope of SFCC is also zero, i.e., $m_2^i = 0$.

Table 10 Material properties of ground soil and freeze pipe used in ground freezing model

Material Name	Hydraulic/Thermal Properties	Method	Parameters	Value	Unit
Ground soil	SWCC	Fredlund and Xing	Saturated VWC	0.5	m^3/m^3
			af	200	kPa
			nf	1	
			mf	2	
			hr	1,500	kPa
			Output curve type	Data points	
	Hydraulic conductivity	Modified Campbell Estimation	Saturated K	150	m/day
			K minimum	8.6×10^{-5}	m/day
			Mcampbell P	5	
	Thermal conductivity	Johansen	Output curve type	Data points	
			Material State	Natural	
			Material Type	Coarse	
			Dry density	1,400	kg/m^3
			Thermal conductivity of solid component	501,568	J/day-m-°C
	Heat Capacity	Constant	Unfrozen heat capacity	2,900,000	J/m^3-°C
			Frozen heat capacity	1,450,000	J/m^3-°C
	SFCC	None			
Freeze pipe	SWCC	Fredlund and Xing	Saturated VWC	0.0001	m^3/m^3
			af	5,000	kPa
			nf	1	
			mf	2	
			hr	500,000	kPa
			Output curve type	Data points	
	Hydraulic conductivity	Modified Campbell Estimation	Saturated K	0.0001	m/day
			K minimum	1×10^{-8}	m/day
			Output curve type	Data points	
	Thermal conductivity	Constant	ktu	3,715,200	J/day-m-°C
	Heat Capacity	Constant	Unfrozen heat capacity	3,890,000	J/m^3-°C
			Frozen heat capacity	3,890,000	J/m^3-°C
	SFCC	None			

NOTE:
SWCC output curve type as data points can improve the performance of model running.

3.4.4 Results and Discussions

The following is the simulation results related to water flow, temperature contour, and thermal convection on the freezing process.

3.4.4.1 Water flow contour

Figure 76 and Figure 77 show water flow during the ground freezing process. At the beginning, water is surrounding the freezing pipe (see Figure 76). With the development of frozen ground, and due to the significant reduction of hydraulic conduction in frozen ground, water must flow around the frozen ground regime, as shown in Figure 77, and Figure 79.

Figure 78 further demonstrates the water flow velocity change in the frozen and unfrozen area. It clearly shows that water flow velocity from 1.05 m/day at the bottom of the unfrozen soil is reduced to 0 m/day in the frozen soil.

Because water phase change is not included in this example, the frozen ground is developed very fast. After 10 hours, ground freezing tends to steady state.

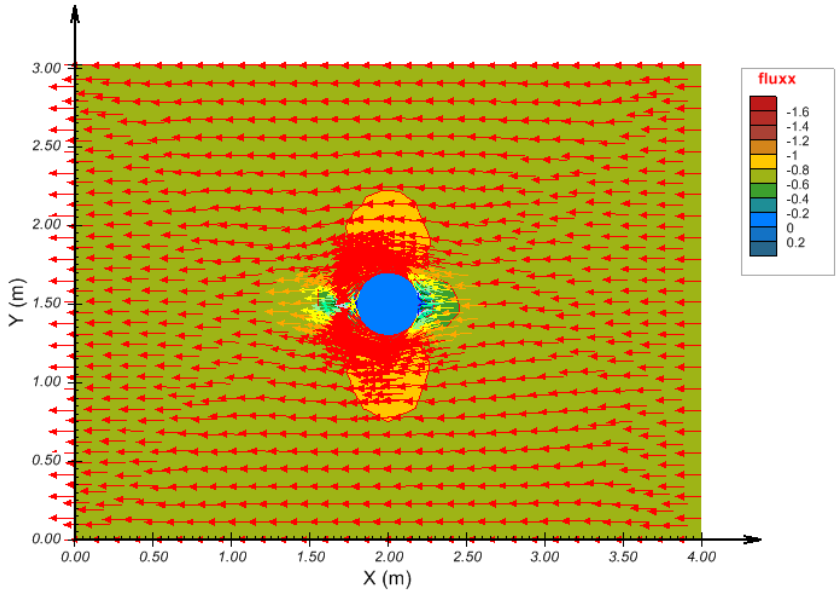

Figure 76 Water flow at a simulation time of 0.2 hour in the case of freeze pile temperature = –2 °C and without thermal convection being applied

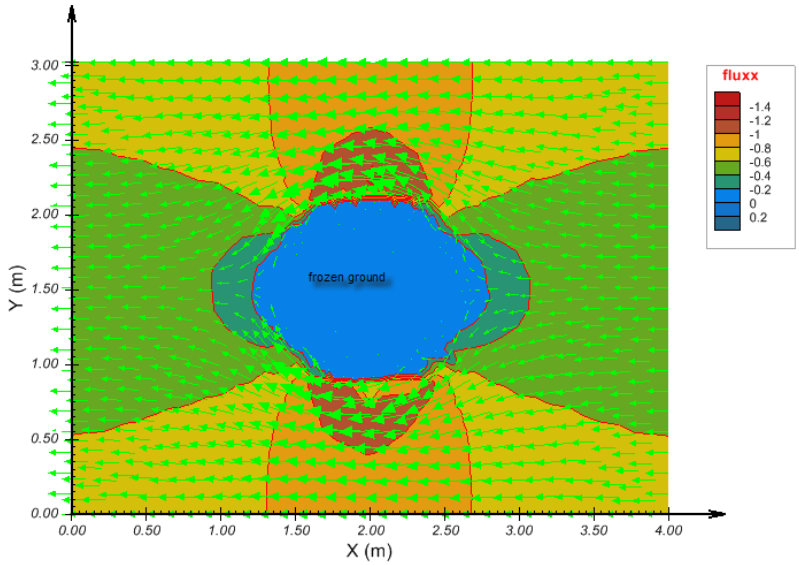

Figure 77 Water flow at a simulation time of 14 hours hour in the case of freeze pile temperature = –2 °C and without thermal convection being applied

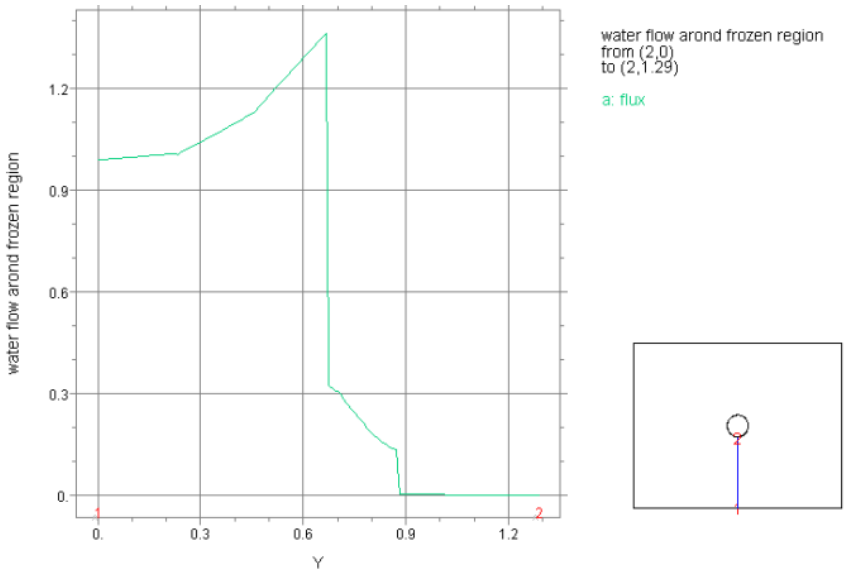

Figure 78 Change of water flow velocity through the unfrozen and frozen section

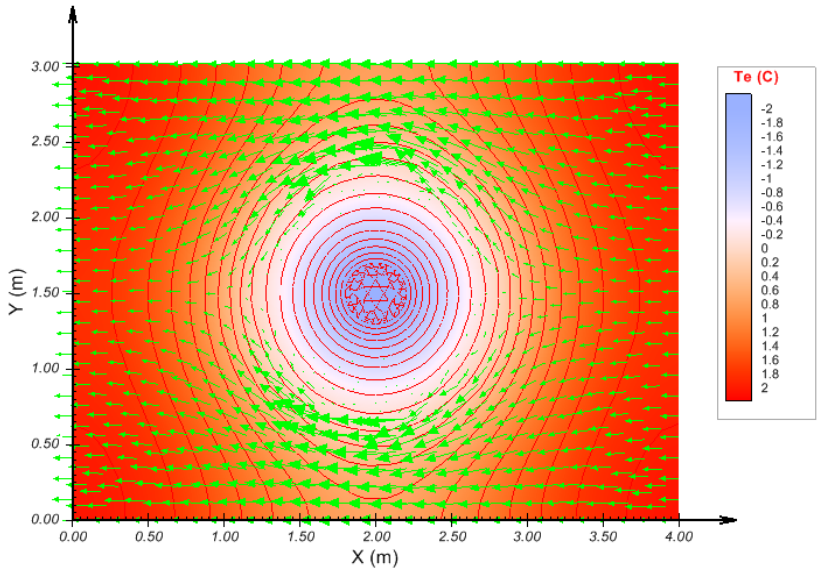

Figure 79a Temperature contour and water flow in the case of freeze pile temperature = –2 °C and without thermal convection being applied

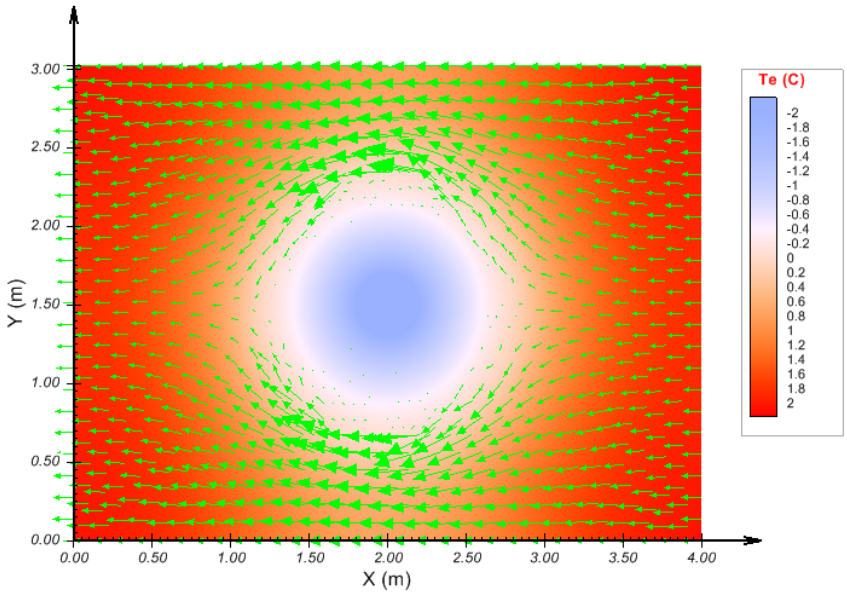

Figure 42b Temperature contour and water flow with freeze pile temperature = –2 °C and without thermal convection being applied

3.5 GROUND FREEZING WITH THERMAL CONVECTION - COUPLED

Project: GeoThermal
Model: ArtificialGroundFreezing_convect

The example is to simulate thermal convection effect on artificial ground freezing.

3.5.1 Purpose

This model is designed to demonstrate the water flow and heat flow, including thermal conduction and convection during artificial ground freezing.

3.5.2 Geometry and Boundary Conditions

The model geometry is the same as the model ArtificialGroundFreezing_no_convect. However to include the thermal convection, it is required to check “Convection” in SVHEAT model settings, as illustrated in Figure 80.

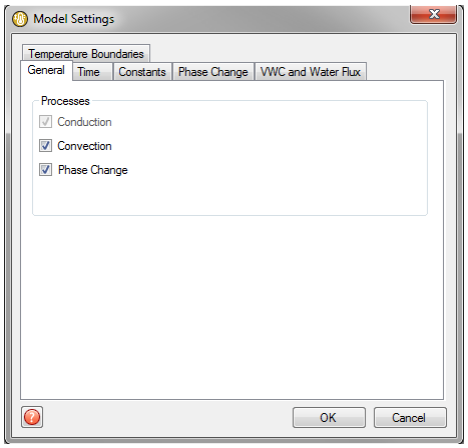

Figure 80 Illustration of model setting to include thermal convection

3.5.3 Material Properties

The material properties are the same as specified in model of ArtificialGroundFreezing_no_convect

3.5.4 Results and Discussions

Figure 81 and Figure 82 are the case after which the thermal convection is applied to chilled pipe temperature of –2 °C. Heat is lost due to larger water flux (see Figure 82), and consequently, the ground freezing is much slower. To cause faster freezing, one approach is to reduce the temperature of freeze pipe.

To test this case, the temperature expression for the freeze pipe is adjusted to “if t < 1 then 3 –8*t else –5”. In other words, the pipe temperature is changed from 3 °C to –5 °C. The results of the simulation are given in Figure 83 for water flow contours and Figure 84 for temperature contours.

The water flow obtained in this example is very similar to the result obtained by Vadose/W software package, as shown in Figure 85 and Figure 86.

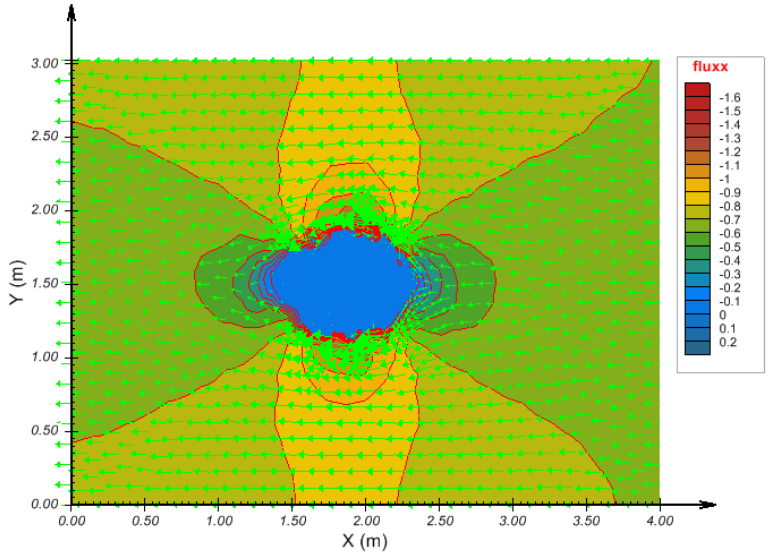

Figure 81 Water flow around frozen ground at a simulation time of 50 hours in the case of thermal convection applied and freeze pipe temperature = –2 °C

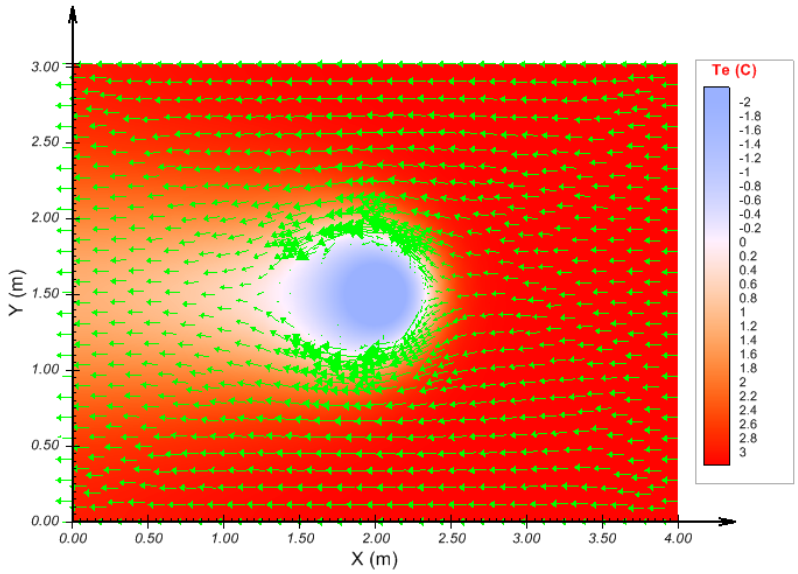

Figure 82 Temperature contour and water flow at a simulation time of 50 hour in the case of thermal convection applied and freeze pipe temperature = –2 °C

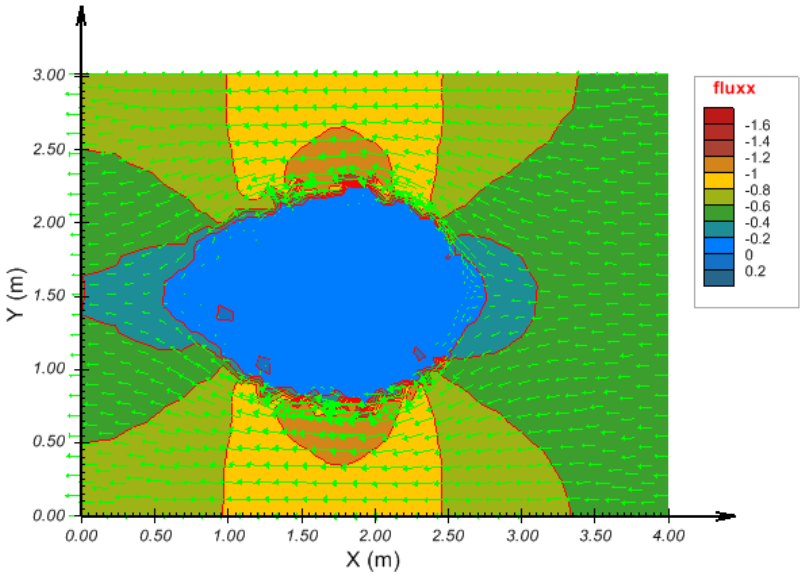

Figure 83 Water flow at a time of 40 hours in the case of thermal convection applied and pipe temperature is changed to –5 °C

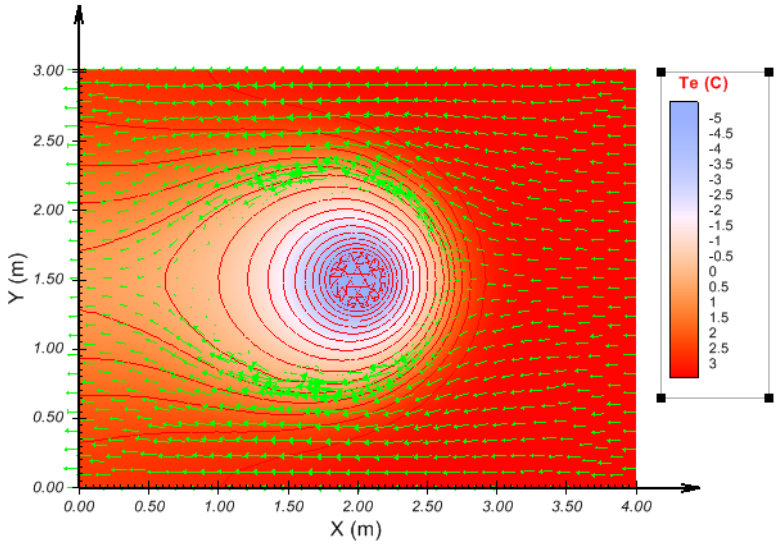

Figure 84 Water flow (green arrow) and temperature contour at a time of 40 hours in the case convection applied and pipe temperature is changed to –5 °C

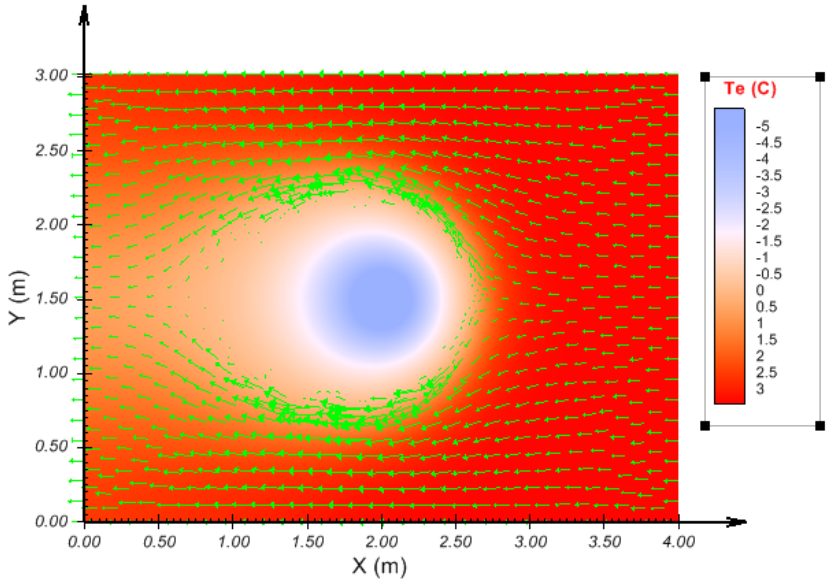

Figure 85 Water flow (green arrow) at a time of 40 hours in the case of thermal convection applied and pipe temperature = –5 °C

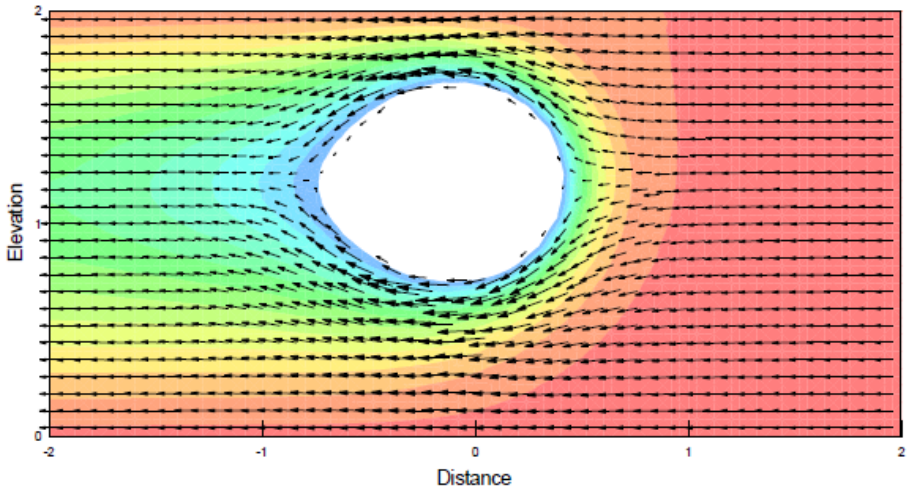

Figure 86 Water flow showing in Vadose/W software package

3.6 ERH HEAT CONVECTION WITH STEADY-STATE WATER FLOW (ERH, 1971)

Project:	Geothermal	
Model:	ErhHeatConvection_AikenV11,	ErhHeatConvection_AikenV14,
	ErhHeatConvection_AikenV16,	ErhHeatConvection_AikenV19,
	ErhHeatConvection_HanfordV03,	ErhHeatConvection_HanfordV09,
	ErhHeatConvection_HanfordV11,	ErhHeatConvection_HanfordV15,
	ErhHeatConvection_HanfordV24,	ErhHeatConvection_HanfordV35

Erh et al. (1971) presented experiments and an analytical solution to the heat convection problem under constant water flow. SVFLUX is not required for this analysis as the water flow is constant.

3.6.1 Purpose

Erh's experimental data and the analytical result are used as the benchmark of steady-state heat convection with constant water flow for simulation with the SVHEAT software.

3.6.2 Geometry and Boundary Conditions

The schematic of the model configuration is illustrated in Figure 87. The water flows at a constant rate, v, from the bottom to the top of the cylindrical soil column. The temperature of flowing water, T_w, is applied to the lower end of the soil column, and the temperature at the upper end of the soil column is equal to ambient temperature, T_{amb}. The thermal flux on the lateral surface of the cylindrical soil column is calculated based on the thermal convection coefficient, h_c. To simulate the water flow velocity effect on the heat convective transfer, 10 models were created. The parameters for each model are specified in Table 11.

Please note that the height of soil column is extended from 0.3 m to 0.6 m to approximate the boundary condition of $T = T_{amb}$ when $z = \infty$ in original Erh's analytical solution. However, only the temperatures from the elevation of 0 to 0.3 m are recorded during the simulation. No initial condition is required for the steady-state problem in this benchmark.

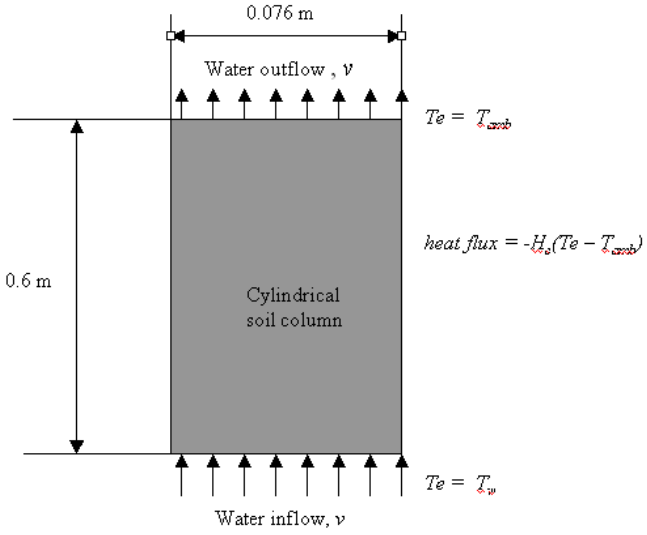

Figure 87 Model geometry of Erh et al. (1971) convection problem with steady-state water flow

Table 11 Parameters used in Erh et al. (1971) heat convection problem

Model name	Ambient temperature, T_{amb}, (ºC)	Water temperature, T_w, (ºC)	Water flow velocity, v, (m/min)
HanfordV03	21.5	30	3×10^{-4}
HanfordV09			9×10^{-4}
HanfordV11			1.1×10^{-3}
HanfordV15			1.5×10^{-3}
HanfordV24			2.4×10^{-3}
HanfordV35			3.5×10^{-3}
AikenV11	21.5	10	1.1×10^{-3}
AikenV14			1.4×10^{-3}
AikenV16			1.6×10^{-3}
AikenV19			1.9×10^{-3}

NOTE:

3. The model is required to set the "convection" option in the SVHEAT model settings dialog.
4. Select the "Per Material" radio button for "VWC and Flux" option in SVHEAT settings dialog.

3.6.3 Material Properties

The material properties are illustrated in
Table 14. Soil freezing and thawing are not considered in the benchmark.

Table 12 Material properties Erh et al. (1971) problem

Material name	Material properties	Symbols	value	unit
Hanford sandy loam	Thermal conductivity	λ	1.47	W/m-°C
	Thermal convection coefficient	h_c	10.47	W/m^2-ºC
Aiken clay	Thermal conductivity	λ	1.47	W/m-ºC
	Water thermal expansion	h_c	10.47	W/m^2-ºC

3.6.4 Discussion of Results

The dimensionless temperature *T1* and elevation *Z1* were employed in the analytic solution (Erh et al., 1971), and are defined as follows:

$$T1 = \frac{T - T_{amb}}{T_w - T_{amb}} \qquad [2]$$

$$Z1 = \frac{z}{L} \qquad [3]$$

where:

T1 = dimensionless temperature,

Z1 = dimensionless elevation,

T = soil temperature, °C,

T_{amb} = ambient temperature, °C,

T_w = temperature of water inflow, °C, and

L = a reference length, *L* = 0.03 m.

Figure 88 is the result simulated with SVHEAT vs. the analytical result presented by Erh et al. (1971), in which the temperature and elevation are represented by the dimensionless value as defined in equation [2] and [3]. Figure 89 is the comparison of the simulation with experimental results for Hanford sandy loam. It can be seen from both figures that the simulation agrees well with the analytical and experimental result.

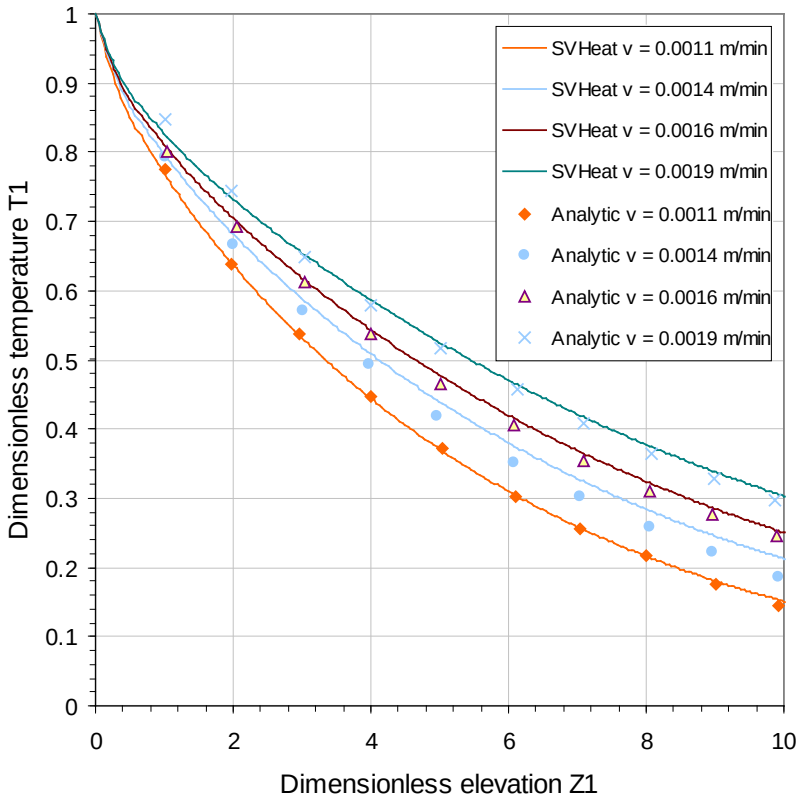

Figure 88 Comparison of SVHEAT simulation with the analytic result (Erh et al., 1971) for the temperature at the lateral surface of the cylindrical soil column of Aiken clay in the case of interflow water temperature = 10 °C,

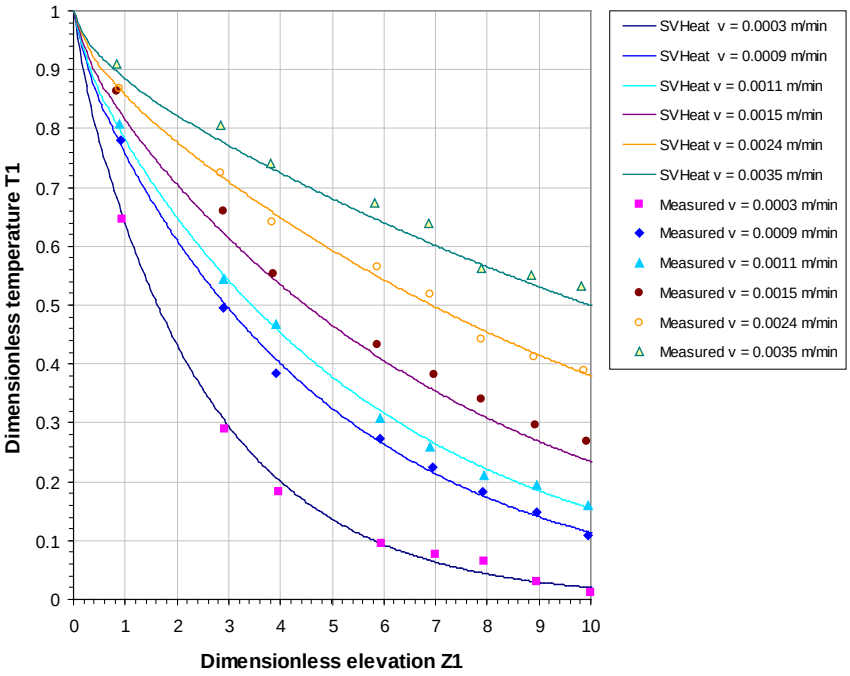

Figure 89 Comparison of SVHEAT simulation with the experimental result (Erh et al., 1971) for the temperature at the lateral surface of cylindrical surface of Hanford sandy loam in the case of inflow water temperature = 30 ºC

3.7 ELDER PROBLEM WITH HOT WATER BLOB RISING (COUPLED WITH SVFLUX)

Project: Geothermal
Model: ElderHotBlobRising

Elder (1967) illustrated the rise of a hot blob problem in the numerical analysis of transient convection in a porous medium.

3.7.1 Purpose

This benchmark presents the scenario of thermal convection and density-dependent flow in the numerical analysis of a hot blob rising using the SVHEAT software coupled with SVFLUX.

3.7.2 Geometry and Boundary Conditions

The model geometry and configuration is illustrated in Figure 90. A heat source is suddenly produced for a certain time, *t1*, at a narrow portion F-G at the bottom of the model. After the time, *t1*, the heat source is turned off. The density-dependent buoyant force causes the hot blob to rise from the bottom of the model domain.

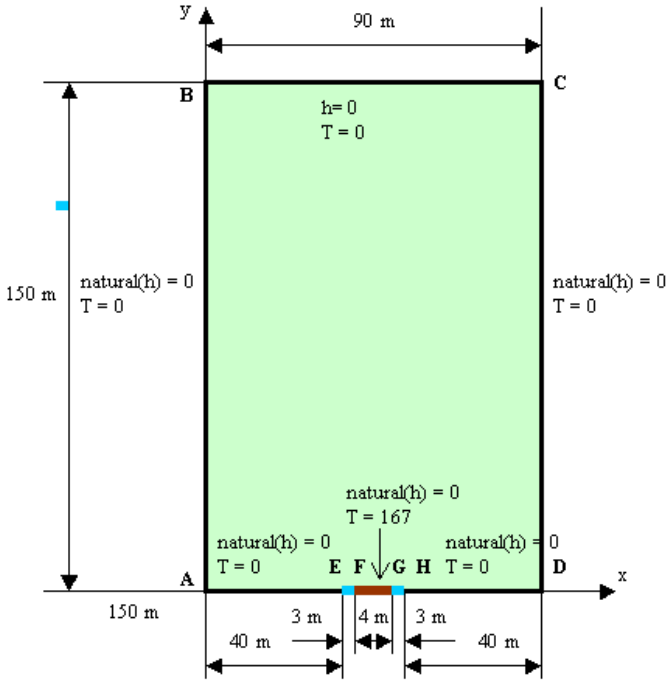

Figure 90 The model geometry and configuration for Elder hot blob rising problem

The thermal and hydraulic boundary conditions are specified, as shown in Figure 90. A constant temperature of 0 ºC is maintained at the sides of E-A-B-C-D-H. The heat source at the boundary F-G is described by the expression below:

$$Te = 167 \quad if \quad t < 183$$
$$Te = 0 \quad if \quad t >= 183 \qquad [4]$$

where:

t = time, day, and

Te = temperature, ºC.

For the consideration of numerical convergence, the margin of E-F and G-H are regarded as the thermal insulation. At the top of the model, water head is set to 0 m, and no water flow occurs at the other sides (B-A-D-C).

Initial Conditions:
Initial temperature: 0 °C
Initial water head: 150 m

NOTE:
To consider the effect of thermal convection and water flow due to the thermal-dependent density, the model is required to set the “convection” option in the SVHEAT model settings dialog, and check the “density flow” option in the SVFLUX model settings dialog.

3.7.3 Material Properties

The soil material is saturated, and soil freezing and thawing are not considered in the model. The material properties are illustrated in Table 13.

Table 13 Material properties for Elder hot blob rising problem

Material properties	Symbols	Value	Unit
Sat hydraulic conductivity	ksat	4.7×10^{-6}	m/s
Saturated water content	satVWC	0.1	m^3/m^3
Thermal conductivity	λ	1.52	W/m-ºC
Soil heat capacity	C	418,700	J/m^3-ºC
Water heat capacity	Cw	4,187,000	J/m^3-ºC
Water thermal expansion	betaT	4.1×10^{-3}	1/ ºC

It is noted that the above material properties and model configuration are designed to meet the Rayleigh number, Ra = 800, that is used in the Elder hot blob rising problem (Elder, 1967).

3.7.4 Discussion of Results

Figure 91 shows the hot blob expansion when the heat source is applied in the case of *Ra* = 800. After a heat region is reached, the hot blob is released at the time of the 183rd day. Under the influence of the buoyant force, the hot blob rises with time (Figure 92). At the same time, the temperature decreases with the rise of blob, as shown in Figure 93. In the figure, the temperature is the maximum temperature of the blob at the given time, and the blob elevation is the location at which the maximum temperature is located. Figure 94 demonstrates the water flow patterns of buoyant convection.

Figure 95 and Figure 96 are the comparison of temperature and convective flow simulated with SVHEAT and SVFLUX vs. the Elder's numerical result.

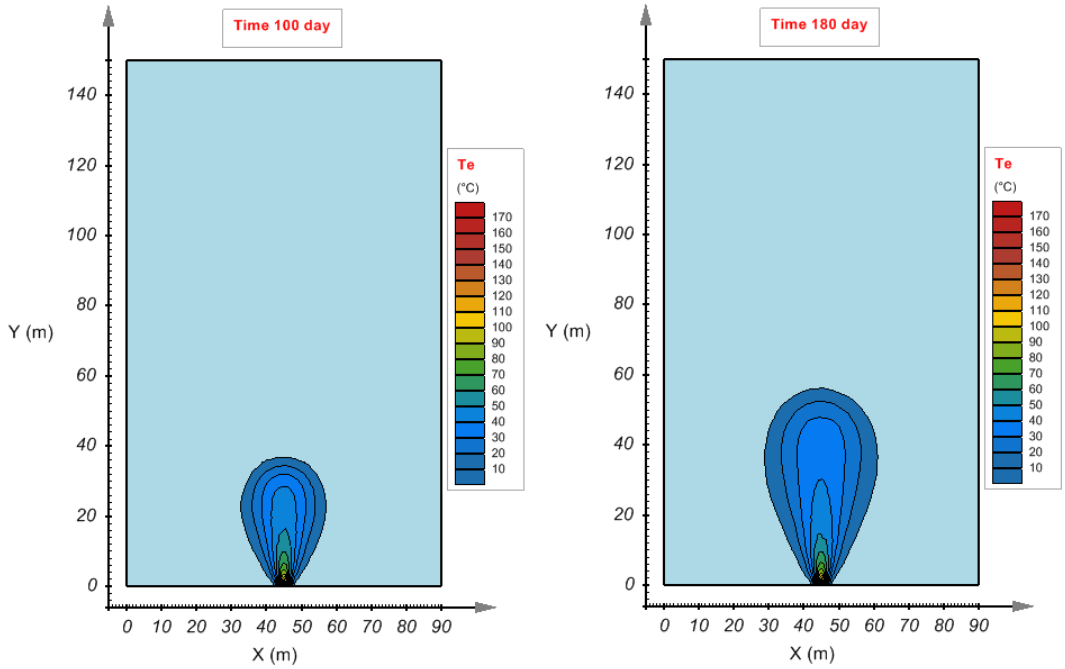

Figure 91 The temperature contour of hot blob expansion during heating period

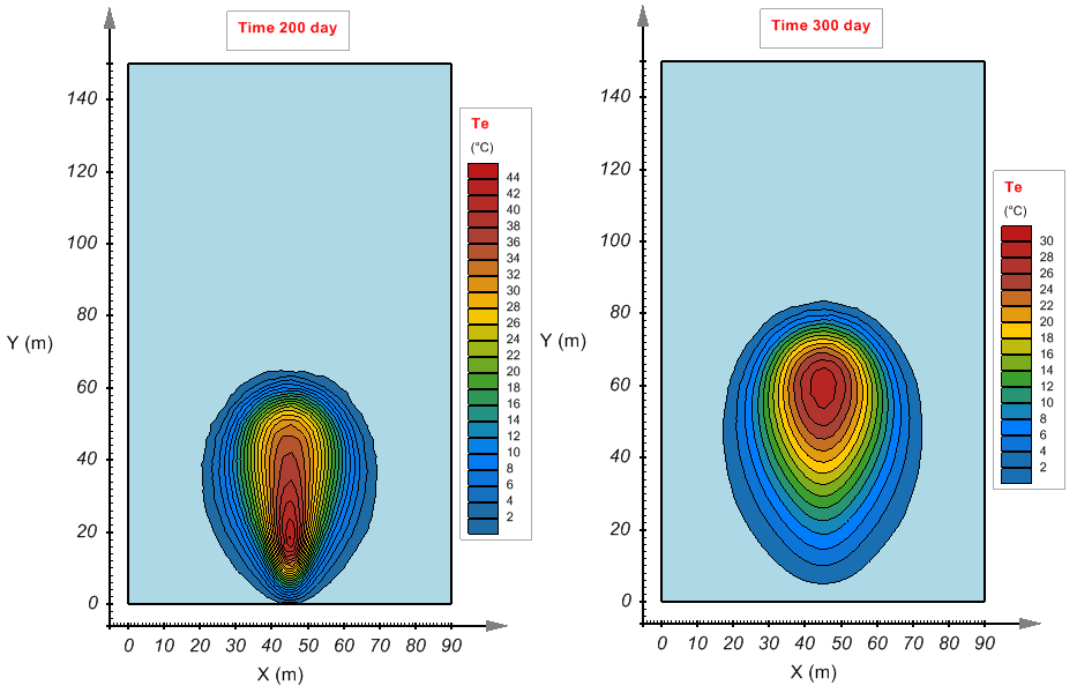

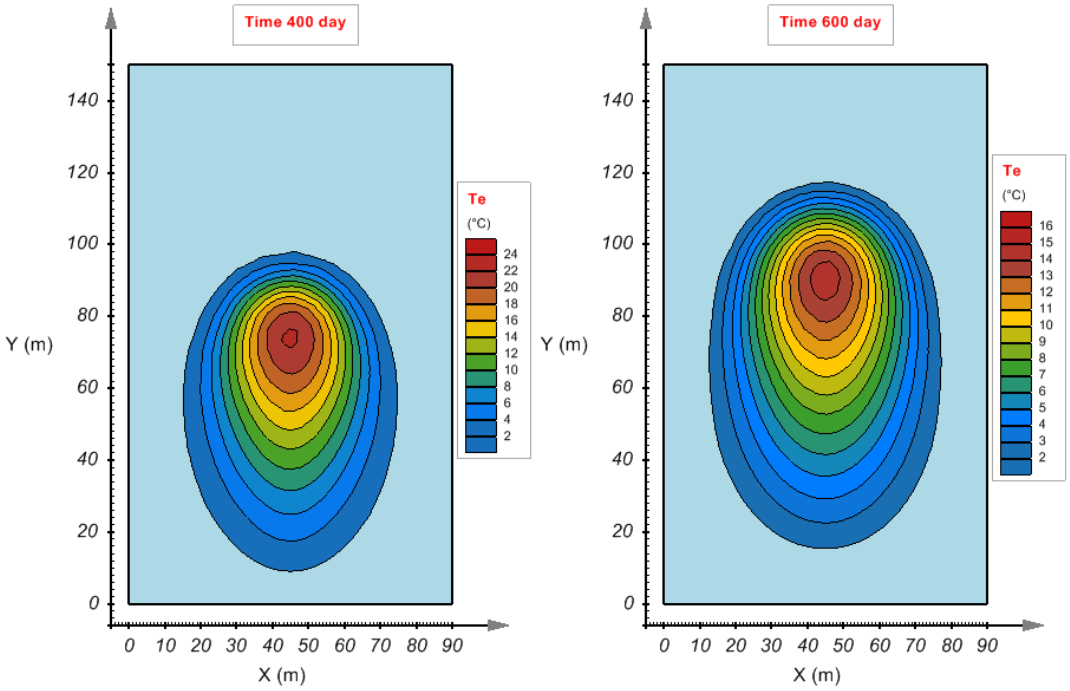

Figure 92 The hot blob rising with time due to the buoyant force after the heat source is turned off

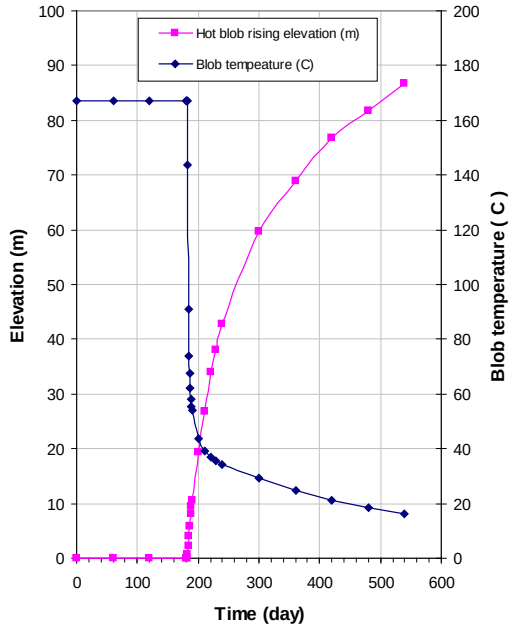

Figure 93 The elevation and temperature of hot blob vs. time

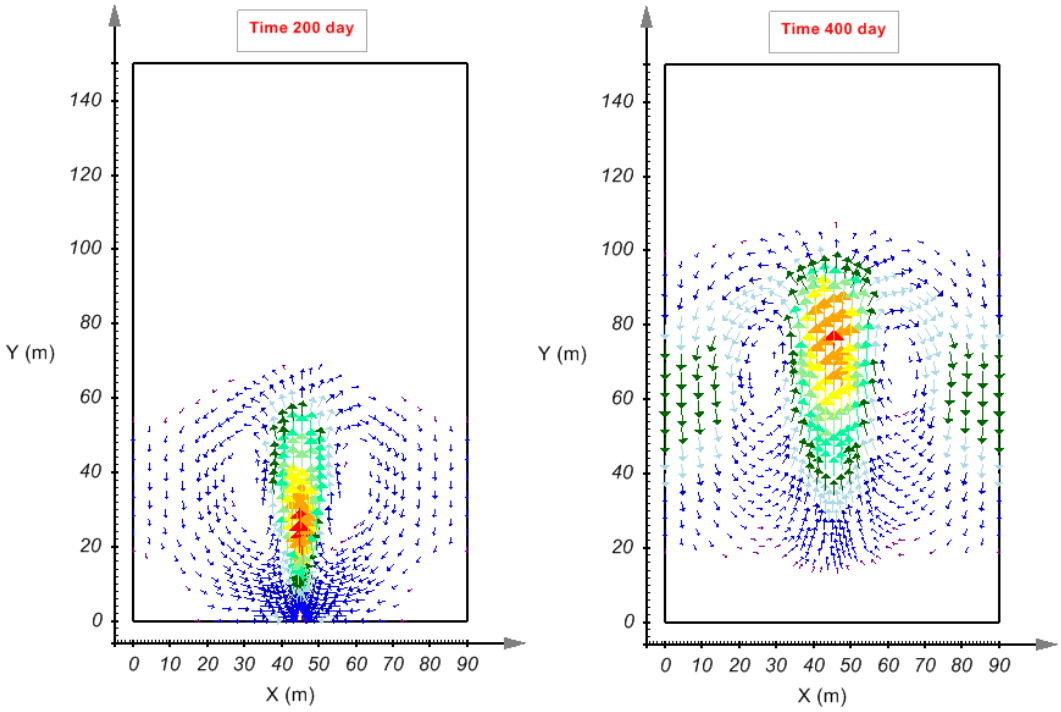

Figure 94 Water flow during the hot blob rising

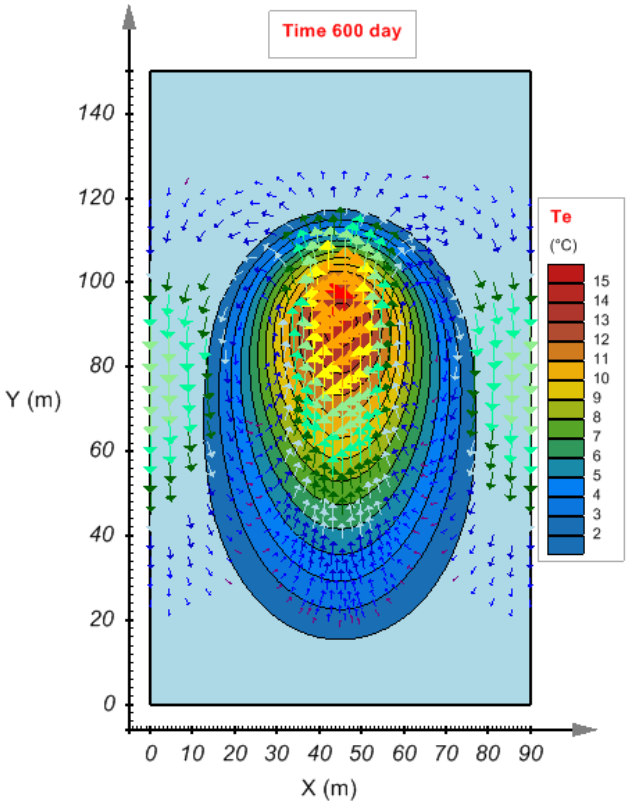

Figure 95 Hot blob and water flow simulated with SVHEAT coupled with SVFLUX

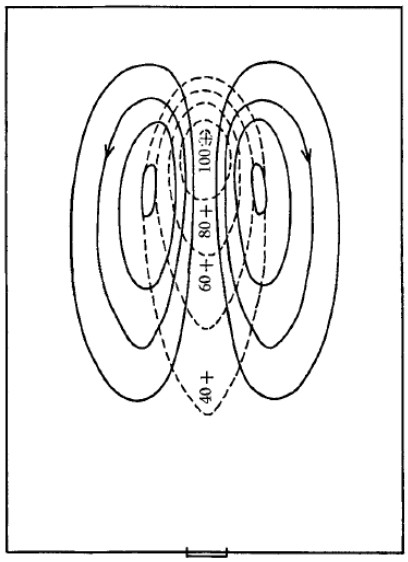

Figure 96 Hot blob and water flow of Elder's result (Elder 1967)

3.8 ELDER CONVECTION PROBLEM HEATED BELOW (COUPLED WITH SVFLUX)

Project: Geothermal
Model: ElderConvectionHeatedBelow

Elder (1967) presented a numerical analysis of convective heat flow when a slab is heated from below. The analysis has been regarded as a standard benchmark of buoyant convection.

3.8.1 Purpose

The Elder problem is used as the benchmark of buoyant convection problem for the numerical analysis with the coupled model of SVHEAT and SVFLUX.

3.8.2 Geometry and Boundary Conditions

The model made up of rectangular geometry with a length of 600 m, and a height of 150 m (see Figure 97). The continuous heating source is applied along the segment of the model bottom. At the top of the model domain, the temperature is maintained at 0 °C. Other sides are thermally insulated. At the top-left corner B-E and top-right corner F-C, a constant value of water head, h = 0 m, is maintained. No water flow is allowed on any of the other sides of the model domain.

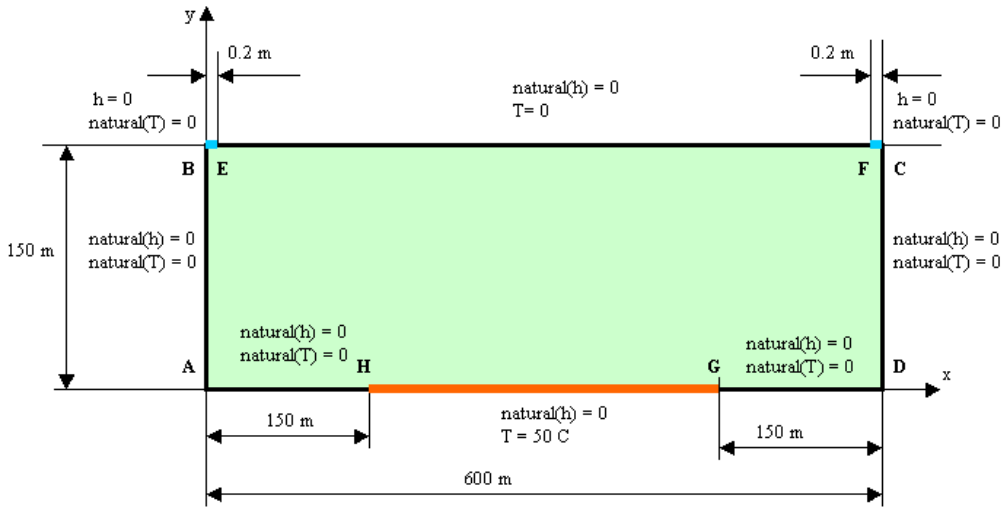

Figure 97 Model geometry of Elder convection heated below

Initial conditions:
Initial water head: 150 m
Initial temperature: 0 °C

NOTE:

To consider the effect of thermal convection and water flow due to the thermal-dependent density, it is necessary to set the "convection" option in the SVHEAT model settings dialog, and to set the "density flow" option in the SVFLUX model settings dialog.

3.8.3 Material Properties

The material of the model is saturated, and soil freezing and thawing are not considered in the model. The material properties are illustrated in
Table 14.

Table 14 Material properties for Elder hot blob rising problem

Material properties	Symbols	Value	Unit
Sat hydraulic conductivity	ksat	4.7×10^{-6}	m/s
Saturated water content	satVWC	0.1	m^3/m^3
Thermal conductivity	λ	1.52	W/m-°C
Soil heat capacity	C	418,700	J/m^3-°C
Water heat capacity	Cw	4,187,000	J/m^3-°C
Water thermal expansion	betaT	4.1×10^{-3}	1/ °C

It is noted that the above material properties together with model configuration settings are required to meet the Rayleigh number, Ra = 400, that is used for the Elder problem.

3.8.4 Discussion of Results

The temperature patterns simulated with SVHEAT and SVFLUX are shown in Figure 98. The simulation time is set to 10 years. The pattern of temperature distribution for the Elder problem is sensitive to the mesh spacing (Boufadel et al., 1999). Figure 99 illustrates the effect of different mesh spacing on the symmetry of contour, indicating that when the mesh spacing is less than 3 m, the distribution of temperature trends to be symmetric.

Figure 100 is the comparison of the result simulated from SVHEAT with the Elder's numerical analysis (1967) in the case of 20% and 60% isotherm. It is noted that the 20% isotherm is equivalent to 10 °C (0.2 x 50 = 10), and the 60% isotherm = 30 °C in the temperature contour as shown in Figure 99a.

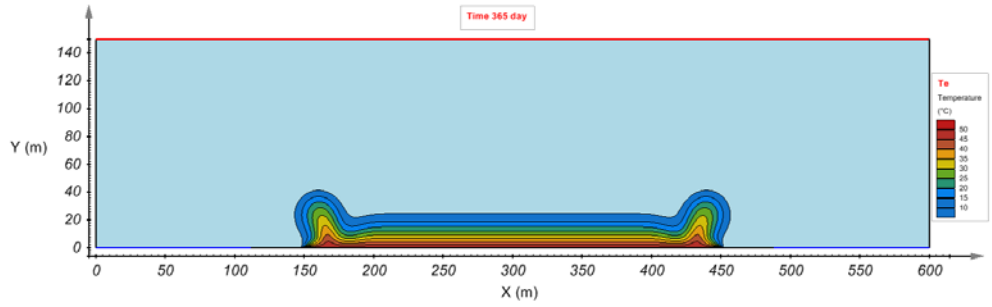

a. Temperature pattern after the 1st year

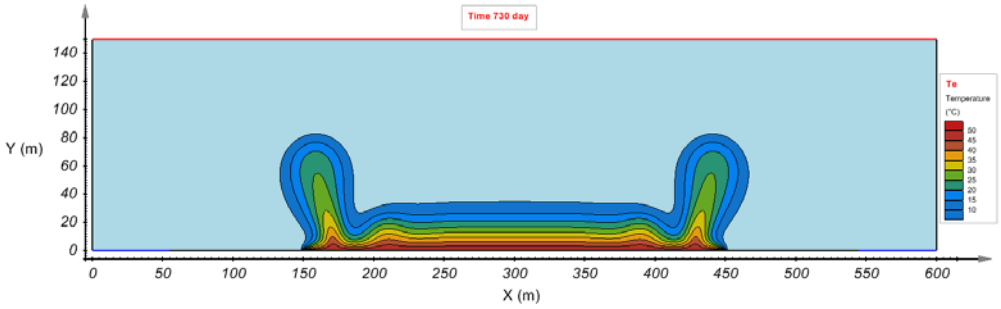

b. Temperature pattern after the 2nd year

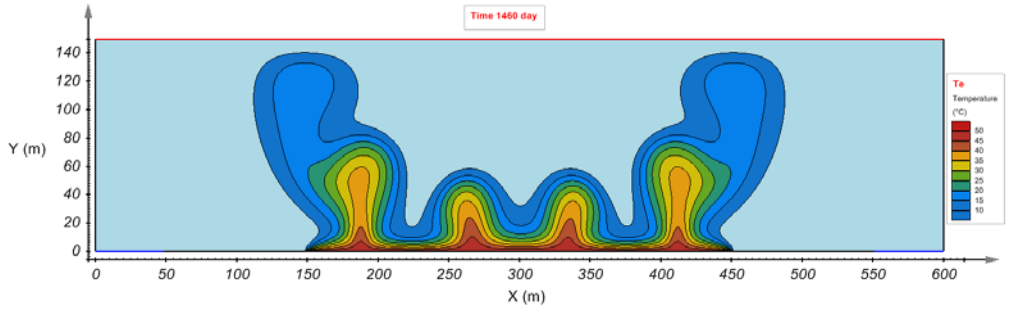

c. Temperature pattern after the 4th year

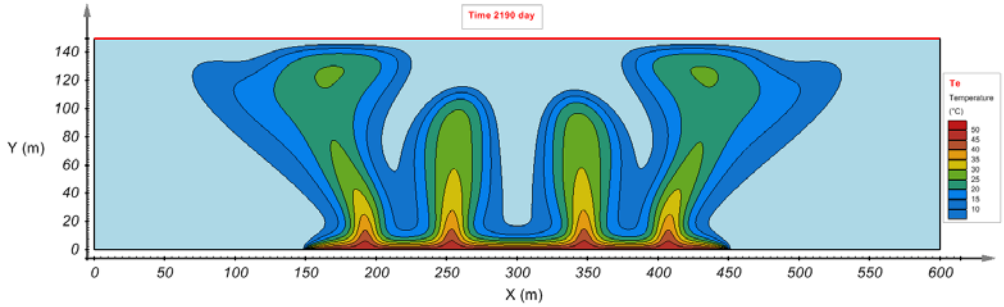

d. Temperature pattern after the 6th year

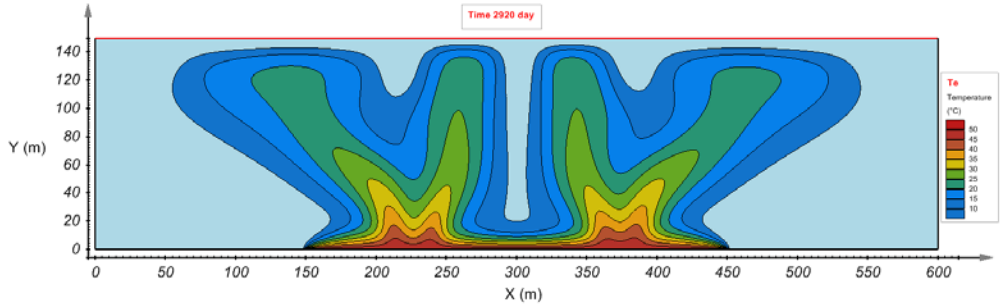

e. Temperature pattern after the 8th year

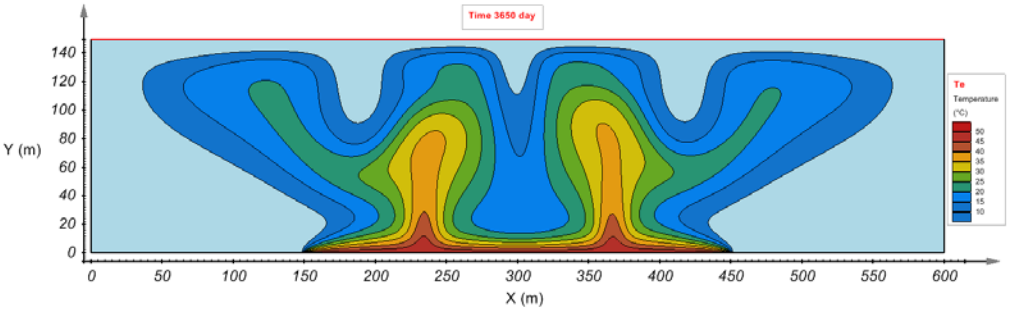

f. Temperature pattern after the 10th year

Figure 98 Temperature patterns of Elder convection problem simulated with SVHEAT and SVFLUX

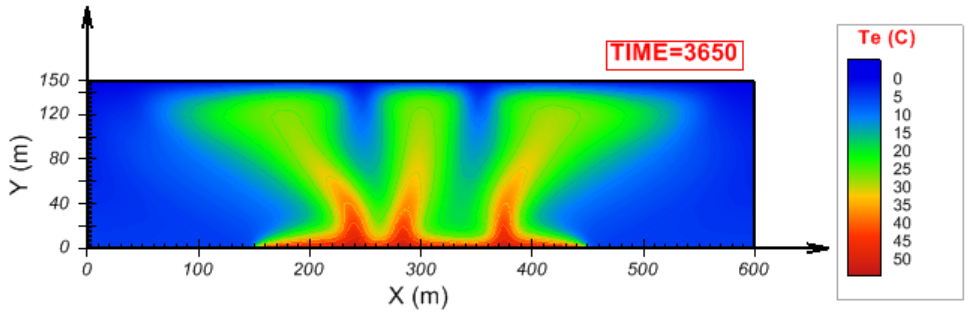

a. Implicit mesh spacing, nodes = 4787

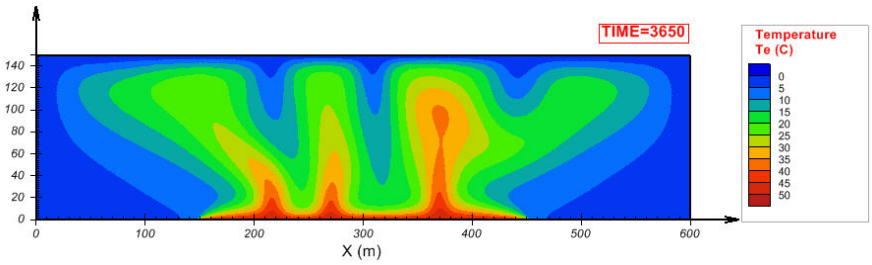

b. Mesh spacing = 5 m, nodes = 17250

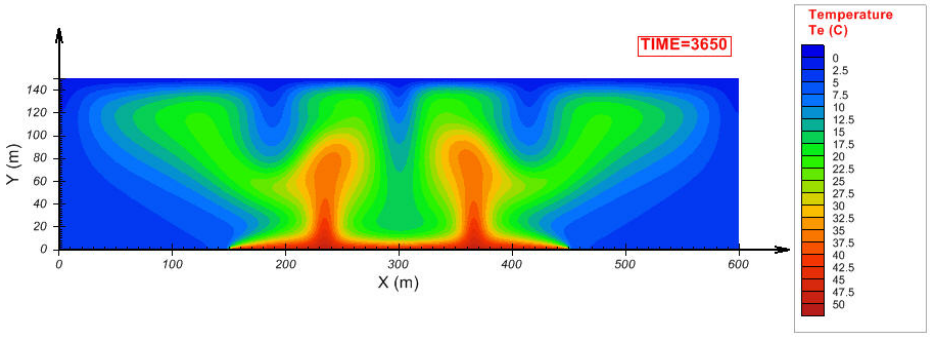

c. Mesh spacing = 3 m, nodes = 45383

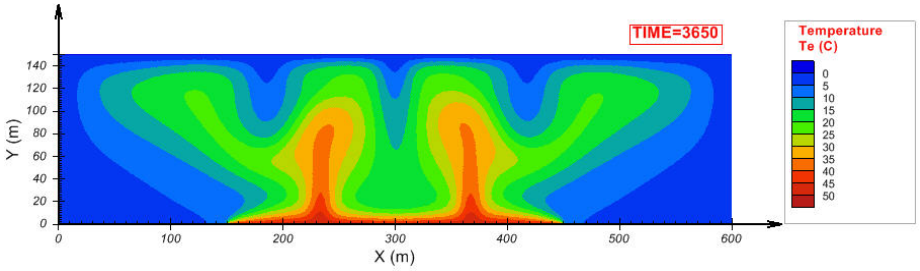

d. Mesh pacing = 2 m, nodes = 99606

Figure 99 Mesh spacing effect on the temperature contours of Elder problem

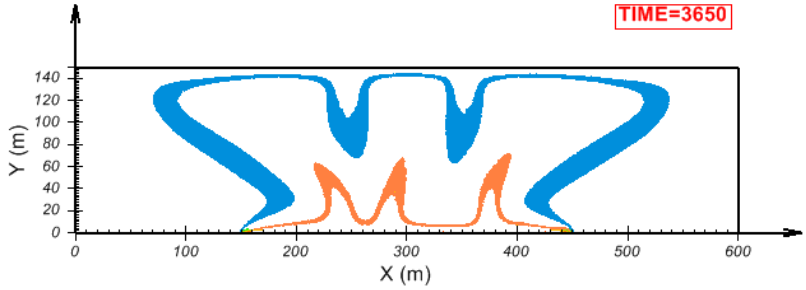

a. SVHEAT and SVFLUX numerical result of 20% and 60% isothermal patterns in the case of implicit mesh spacing and nodes = 4787

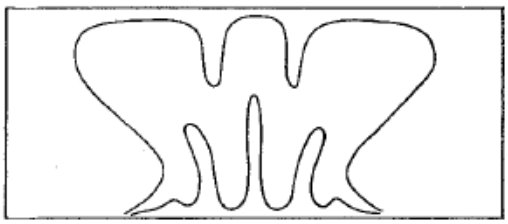

b. Elder numerical result (1967) of 20% and 60% isothermal patterns

Figure 100 Comparison of numerical result with Elder's result

3.9 WELL OBJECT VS. GEOMETRY DEFINED WELL

Project: GeoThermal
Models: SVHEAT_WellObject_SS,
SVHEAT_WellObject_T,
SVHEAT_WellGeometry_SS,
SVHEAT_WellGeometry_T

3.9.1 Purpose

In this verification, two approaches are taken to simulate a geothermal well. One approach is to simulate the well by using region geometry to provide the well dimensions. Another approach is to use the Wells function provided by SVHEAT.

The goal of this verification is twofold:

1. Verify that the results of the Well Object method match the results of the Geometry-Defined Well
2. To determine if the transient state models will reach steady state after a reasonable period of time.

3.9.2 Geometry and Boundary Conditions

The geometry of the geometry-defined approach is 40 m × 20 m. The well is 10 m deep and 0.5 m wide, as shown in Figure 101.

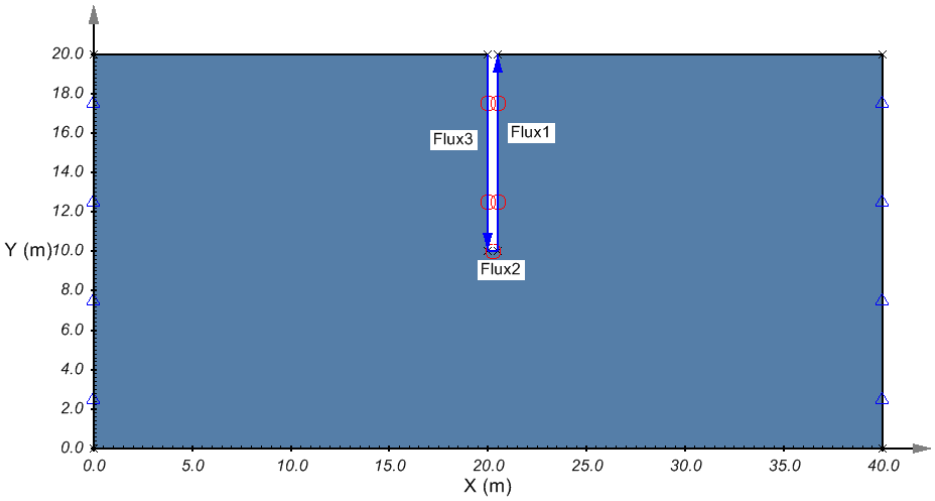

Figure 101 Geometry of geometry-defined well model

The second approach is to simulate the well by using the well function in SVHEAT, as illustrated in the following figure:

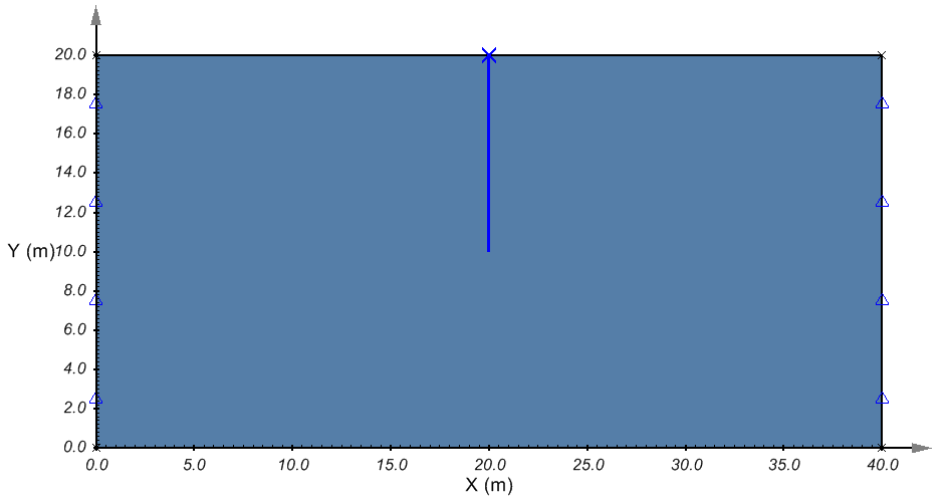

Figure 102 Geometry of heat well model using approach II

The well heat flow rate is set to be -6.15×10^7 J/day (– means heat taken out by the pump). This rate is entered directly for the well object, while for the geometry-defined approach, the corresponding value of (-6.15×10^7/20.5 m = 3×10^6 (J/day/m)) is entered on the boundary condition dialog.

The initial and regional boundary temperatures are both set at 20 °C.

3.9.3 Material Properties

The soil properties are as follows:

Parameters	Values
Thermal conductivity	1.3×10^7 J/day-m-°C
Soil dry density	1,350 kg/m^3
Specific Heat Capacity of Solid Component	760 J/kg-°C

3.9.4 Results and Discussions

The following is the result of the simulation.

3.9.4.1 Steady state analysis

Temperature distribution using the geometry-defined approach is illustrated as follows:

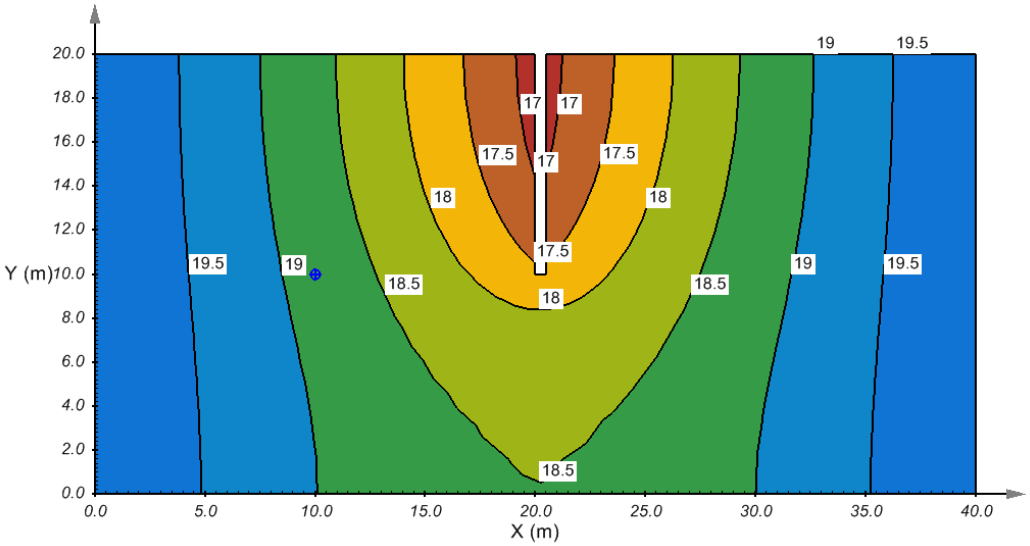

Figure 103 Temperature distribution of steady state analysis using geometry-defined approach

The temperature at point (10, 10) = 18.8 °C.

Temperature distribution using well object approach is as follows:

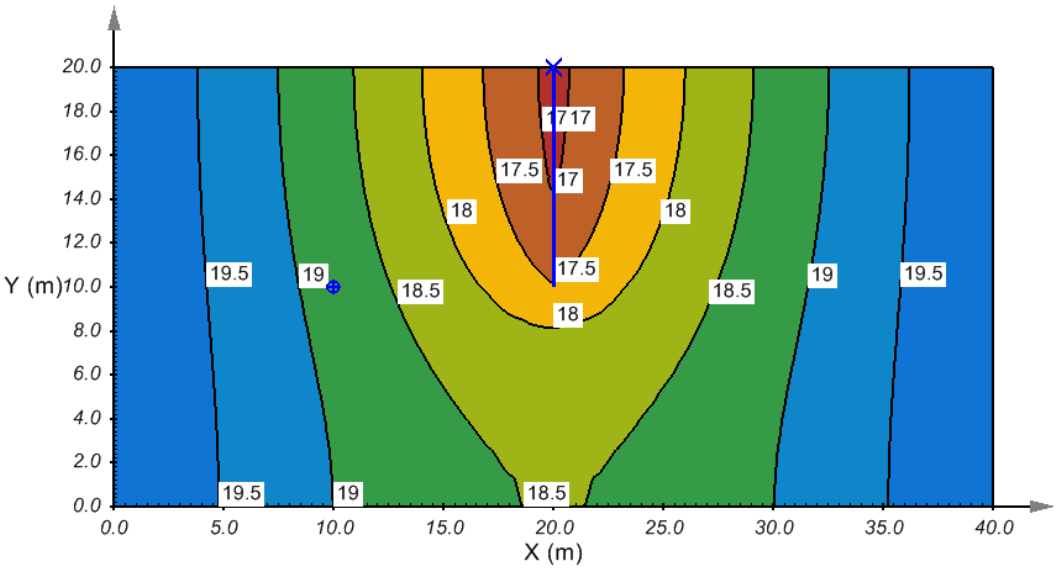

Figure 104 Temperature distribution of steady state analysis using well object approach

The temperature at point (10, 10) = 18.8 °C.

3.9.4.2 Transient analysis verification

Figure 105 shows the temperature distribution at day 400 using the geometry-defined approach:

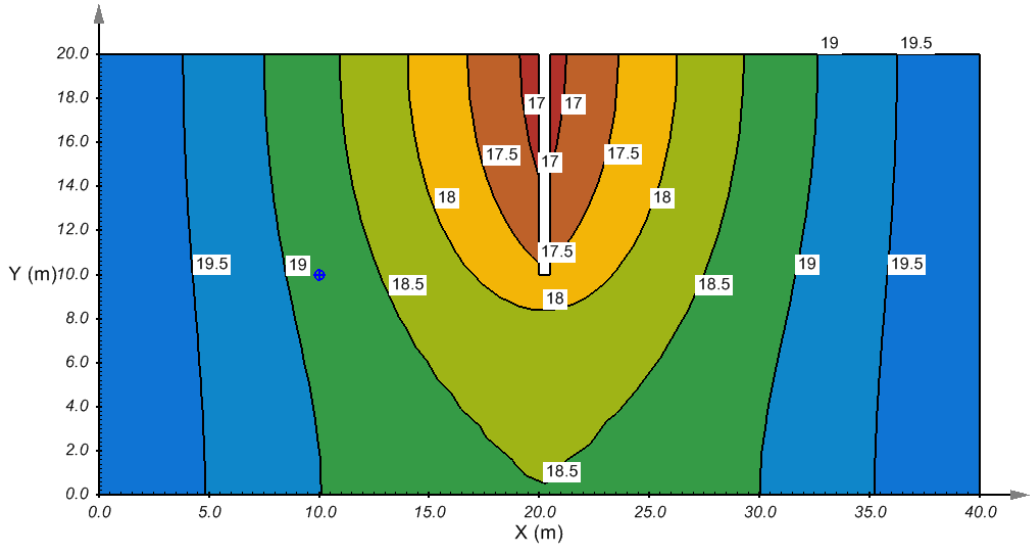

Figure 105 Temperature distribution of transient analysis using geometry-defined approach

The transient state approximates steady state in 150 days as the temperature at point (10, 10) approaches 18.8 °C as shown in Fig. 6:

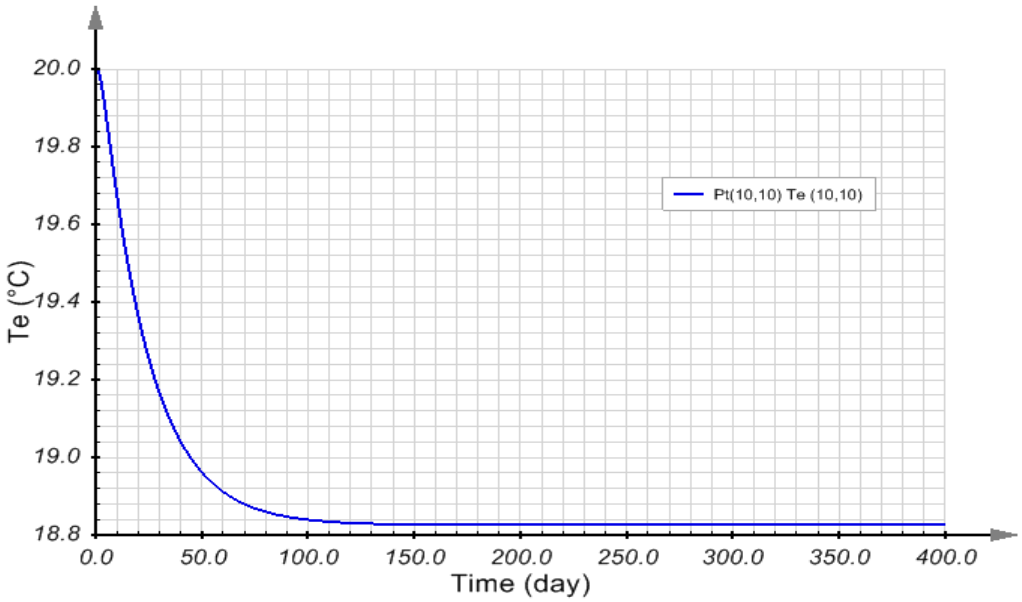

Figure 106 Transient state reaches steady state in 150 days using geometry-defined approach

The heat flow rate is illustrated in the following graph. The constant heat flow rate is -6.15×10^7, which is identical to the input heat flow rate.

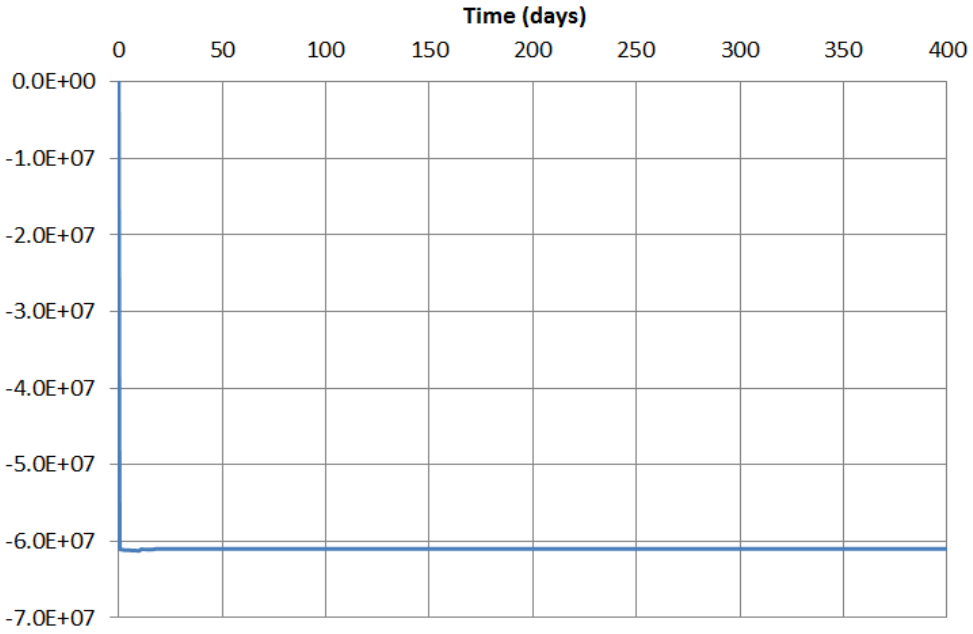

Figure 107 Heat flow rate plot using geometry-defined approach

By using the well object directly, temperature distribution at day 400 can be obtained as follows.

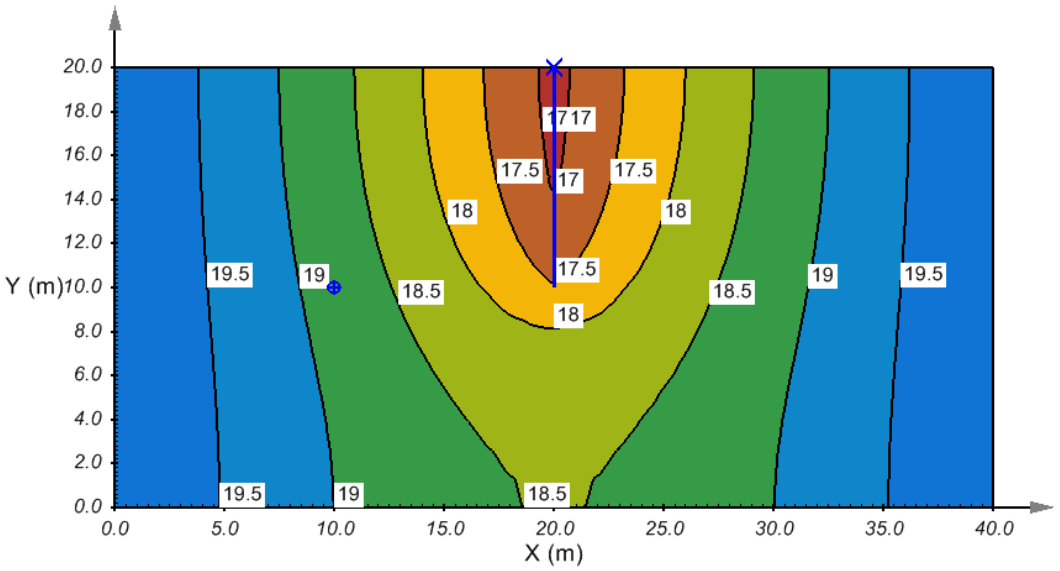

Figure 108 Temperature distribution of transient analysis using well object approach

Figure 109 shows that at the point (10, 10) temperature approaches 18.8 °C after 150 days, which is identical to the geometry-defined approach.

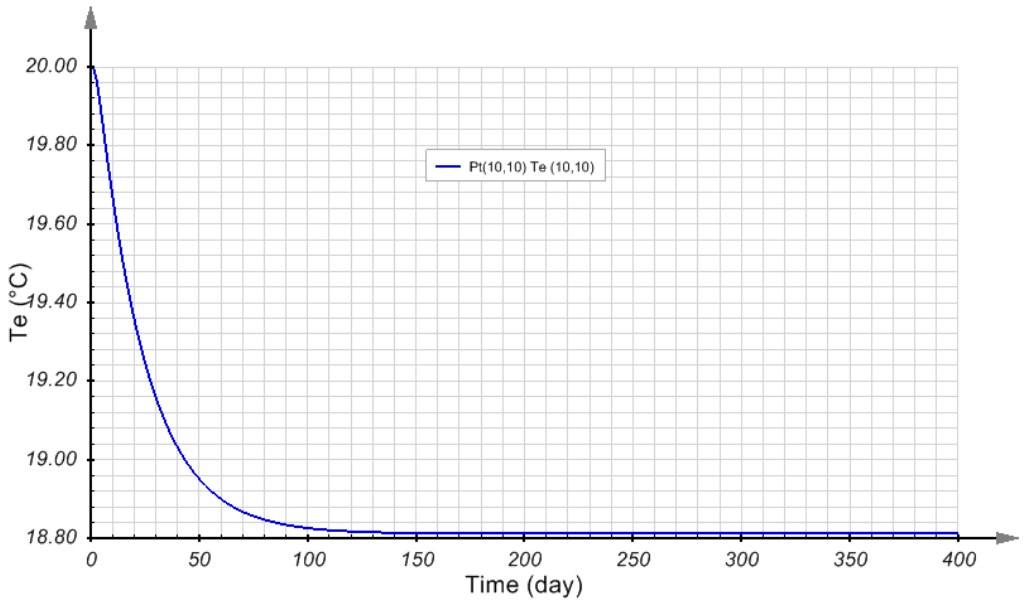

Figure 109 Transient state reaches a steady state in 150 days using well object approach

The well report affirms that the normal flow in (J/day) = -6.15×10^7, which is also identical to the input heat flow rate.

3.9.4.3 Verification of temperature during transient state

In the above verification the thermal conductivity is set to 1.3×10^7 J/day-m-°C. A higher thermal conductivity value 1.3×10^5 J/day-m-°C, will take more time to converge to steady state status. We will examine the results at 400 days, for the two approaches used, to see if the temperature is the same in this part of the verification.

Figure 110 shows the temperature at the point (10, 10) at 400 days using the geometry-defined approach is approximately 11.25 °C.

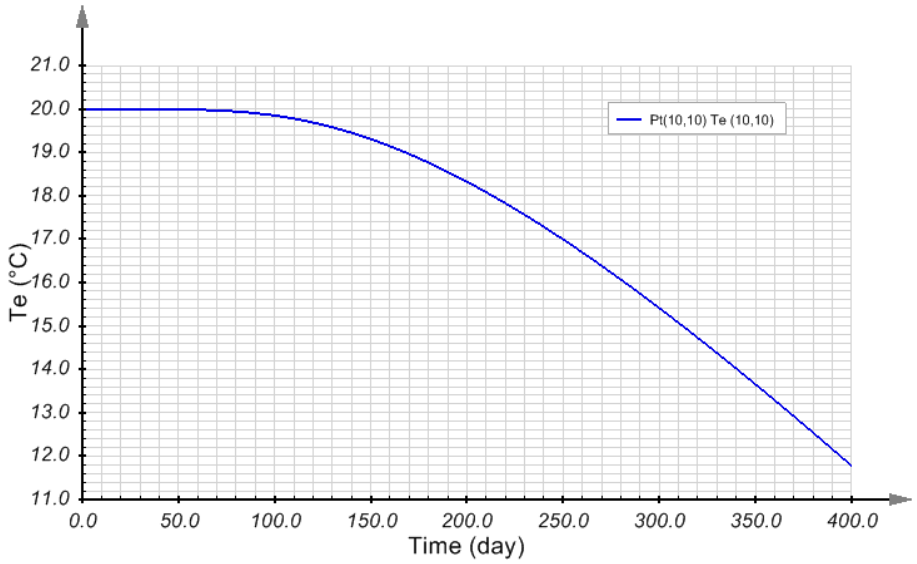

Figure 110 temperature variation versus time using geometry-defined approach

The same result can be achieved using the well object approach at the point (10, 10) as shown in the following Figure 111.

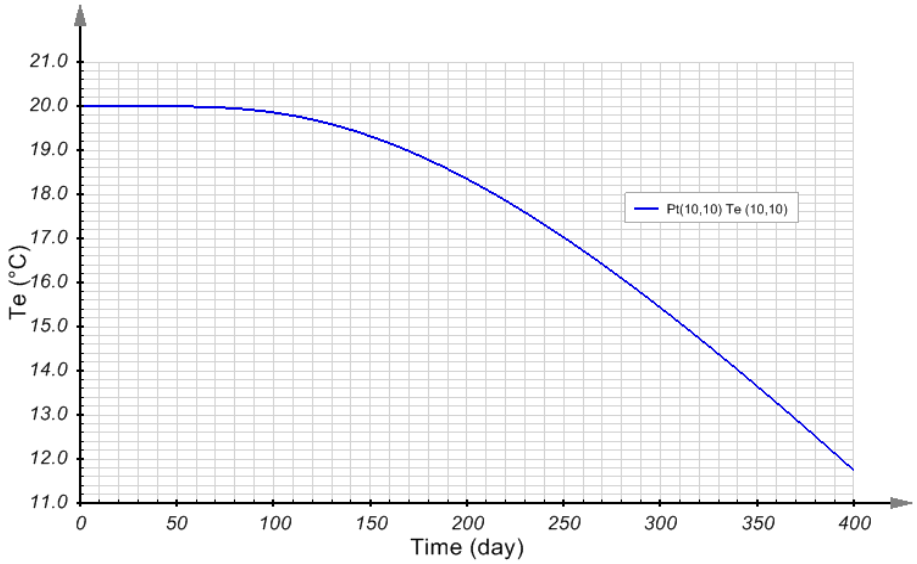

Figure 111 Temperature variation versus time using well object approach

This completes the verification of the well object method in SVHEAT against the geometry-defined method, and can be considered reliable for single well 2-D case. Also, after a sufficient time period, the transient state reaches steady state conditions in this model.

3.10 HAIRPIN THERMOSYPHON

Project: Thermosyphon
Models: HairpinThermoSyphon and HairpinThermoSyphon_Tunnel

The hairpin thermosyphon is a novel design structure for an evaporator and condenser. Both evaporator and condenser are buried under the ground surface (Xu and Goering, 2008).

3.10.1 Purpose

In this verification, two approaches are taken to simulate a thermosyphon. One approach is to simulate the thermosyphon by using region geometry and boundary conditions. Another approach is to use the Tunnel Object function provided by SVHEAT. The goal of these models is to verify that the results of the Tunnel Object method can match the results of the Geometry-Defined thermosyphon method.

3.10.2 Geometry and Boundary Conditions

The model geometry is shown in Figure 112. The road surface is paved with asphalt, and the embankment slope is covered with rocky material. The condenser and evaporator of the thermosyphon are buried under the ground surface. The model with the geometry-defined thermosyphon approach is called HairpinThermoSyphon and is shown in Figure 112. The model with the Tunnel Object approach is called HairpinThermoSyphon_Tunnel and is shown in Figure 113. The models are 2-D transient models and have a duration of one year (or 365 days).

The road surface and the embankment slope have an applied temperature changing with time as shown in Figure 85. Thermal flux is applied to an evaporator section with a value calculated based on thermosyphon performance. The initial temperature of the model domain is 10 °C.

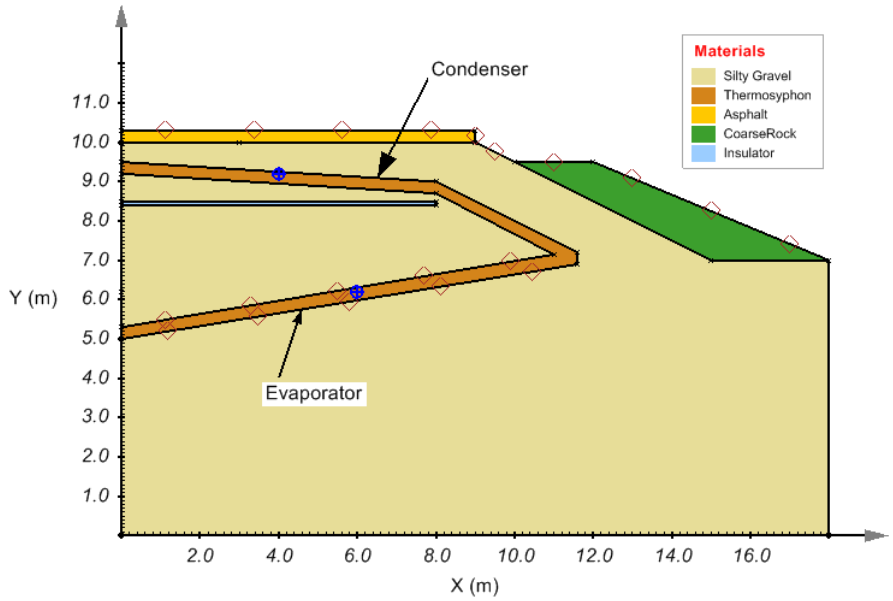

Figure 112 Geometry of the geometry-defined thermosyphon model

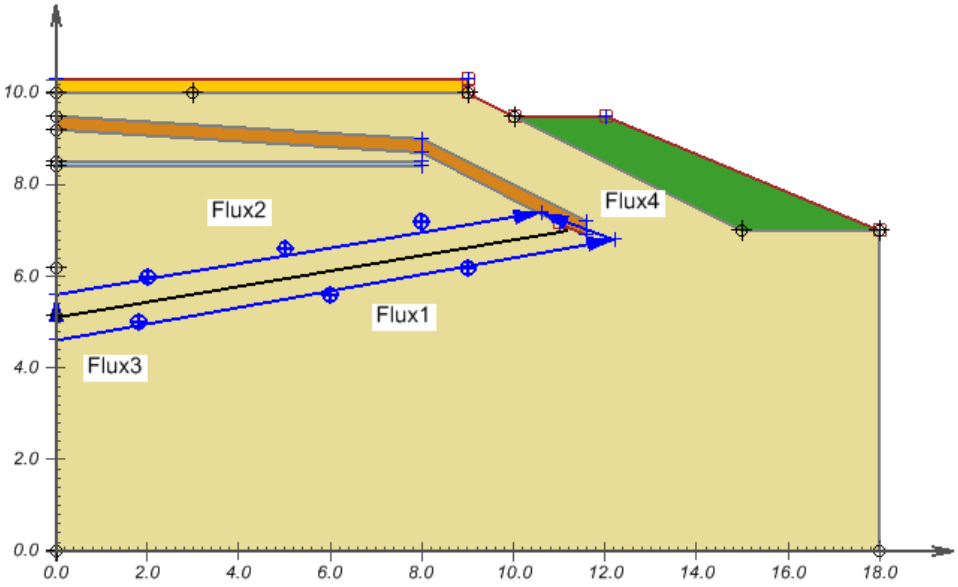

Figure 113 Geometry of the Tunnel Object approach model

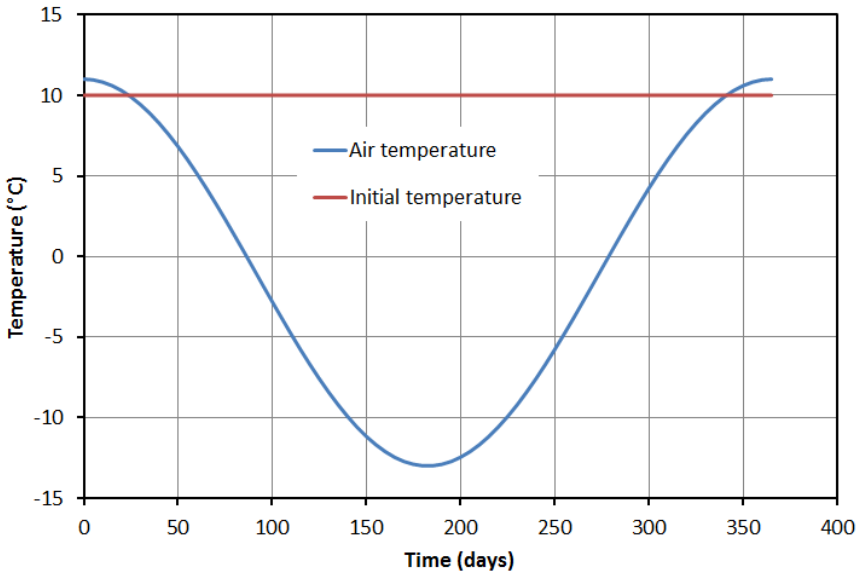

Figure 114 Temperature applied on the ground surface and embankment slope

3.10.3 Material Properties

The thermal properties of all materials used in these models are assumed as follows.

Soil Name	Thermal Conductivity (J / day-m-°C)	Soil Dry Density (kg / m^3)	Specific Heat Capacity (J/ kg-°C)
Silty Gravel	75,168	1,250	750
Thermosyphon	3.5×10^7	N / A	N / A
Asphalt	64,800	N / A	N / A
Coarse Rock	86,400	1,700	800
Insulator	2,419.2	N / A	N / A

3.10.4 Results and Discussions

The most important result of thermosyphon models is the change in temperature. The temperature distributions between the two models on the selected days are shown in the following figures. The temperature distributions of the geometry-defined thermosyphon model HairpinThermoSyphon are shown on the left in the following figures. The results of the models show that the Tunnel Object approach matches the Geometry-Defined thermosyphon approach.

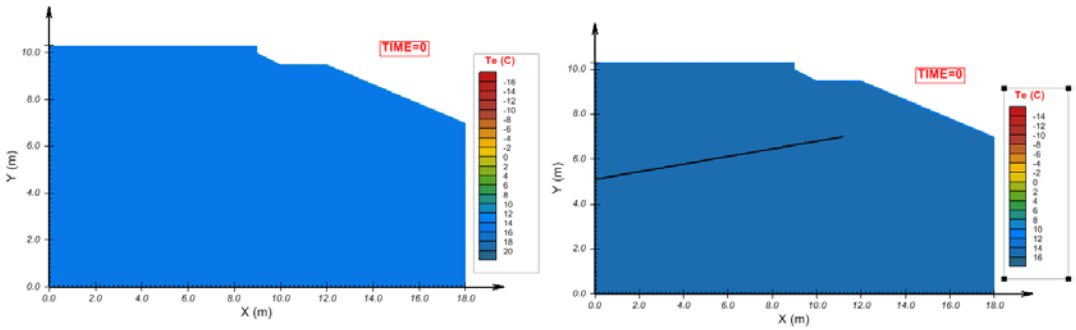

(a) HairpinThermoSyphon Model (b) HairpinThermoSyphon_Tu Model

Figure 115 Temperature distributions in the beginning

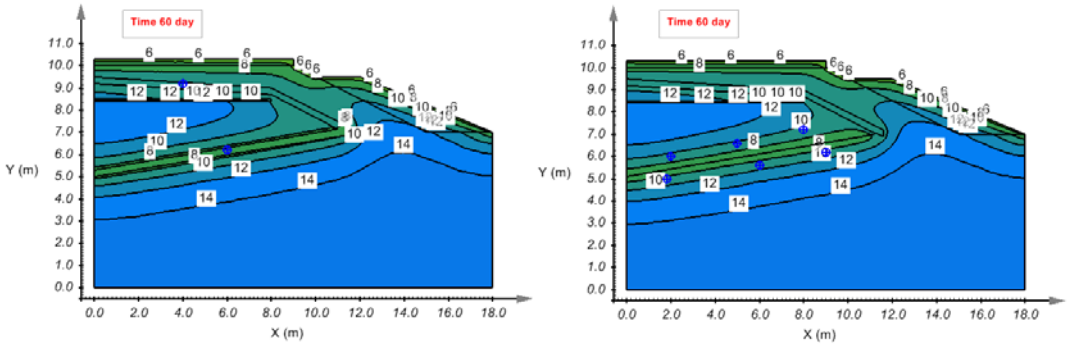

(a) HairpinThermoSyphon Model (b) HairpinThermoSyphon_Tu Model

Figure 116 Temperature distributions on day 60

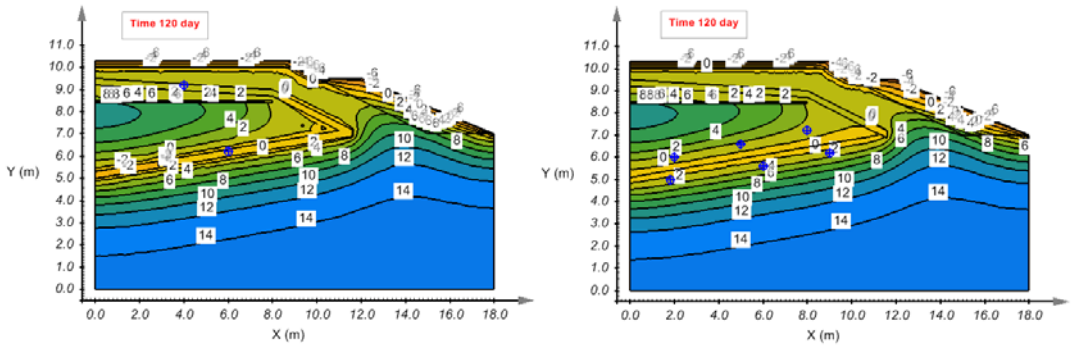

(a) HairpinThermoSyphon Model (b) HairpinThermoSyphon_Tu Model

Figure 117 Temperature distributions on day 120

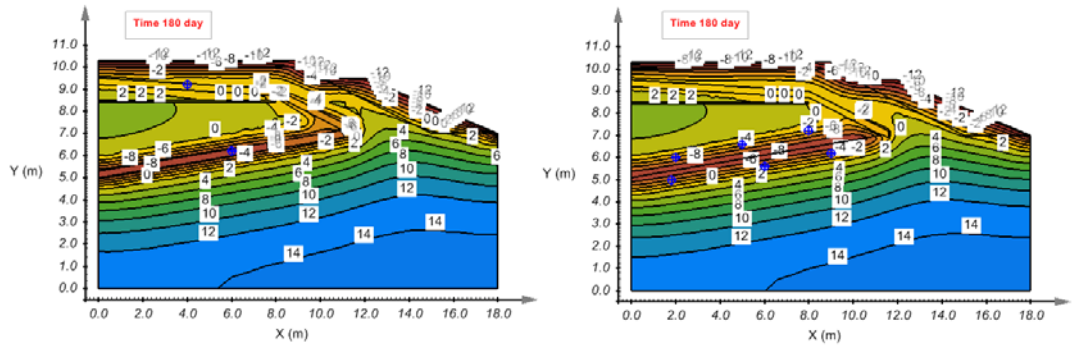

(a) HairpinThermoSyphon Model (b) HairpinThermoSyphon_Tu Model

Figure 118 Temperature distributions on day 180

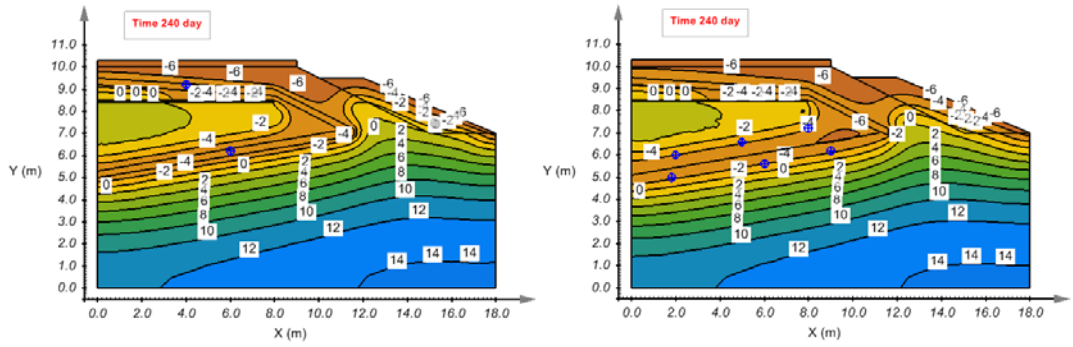

(a) HairpinThermoSyphon Model (b) HairpinThermoSyphon_Tu Model

Figure 119 Temperature distributions on day 240

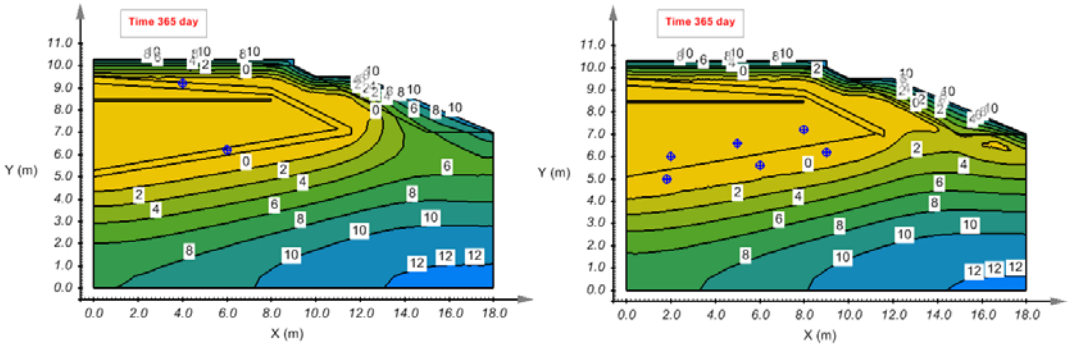

(a) HairpinThermoSyphon Model (b) HairpinThermoSyphon_Tu Model

Figure 120 Temperature distributions on day 365

3.11 TWO PHASE CLOSED THERMOSYPHON

Project: Thermosyphon
Models: SimpleHighwayEmbankmentCooling and
SimpleHighwayEmbankmentCooling_Well

The two phase closed thermosyphon consists of three segments, including the evaporation, adiabatic, and condensation parts. The evaporation part is embedded into the ground where the soil temperature is to be cooled. The condensation part is exposed to air temperature, and adiabatic part connects evaporator and condenser.

3.11.1 Purpose

In this verification, two approaches are taken to simulate a thermosyphon. One approach is to simulate the thermosyphon by using region geometry and boundary conditions. Another approach is to use the Well Object function provided by SVHEAT. The goal of these models is to verify that the results of the Well Object method match the results of the Geometry-Defined thermosyphon method.

3.11.2 Geometry and Boundary Conditions

The model geometry is shown in Figure 121. Region R1 is the schist material, R2 and R3 are subclay, R4 and R5 are natural ground surface, R6 is insulation, and R7 is sandy gravel material. The evaporation parts of the thermosyphon are imbedded under the natural ground surface, and condensation and adiabatic parts are not shown in Figure 121. The model with the geometry-defined thermosyphon approach is SimpleHighwayEmbankmentCooling, and is shown in Figure 121. The model with the Well Object approach is SimpleHighwayEmbankmentCooling _Well, and is shown in Figure 122. The models are 2D transient models for the duration of three months (or 90 days).

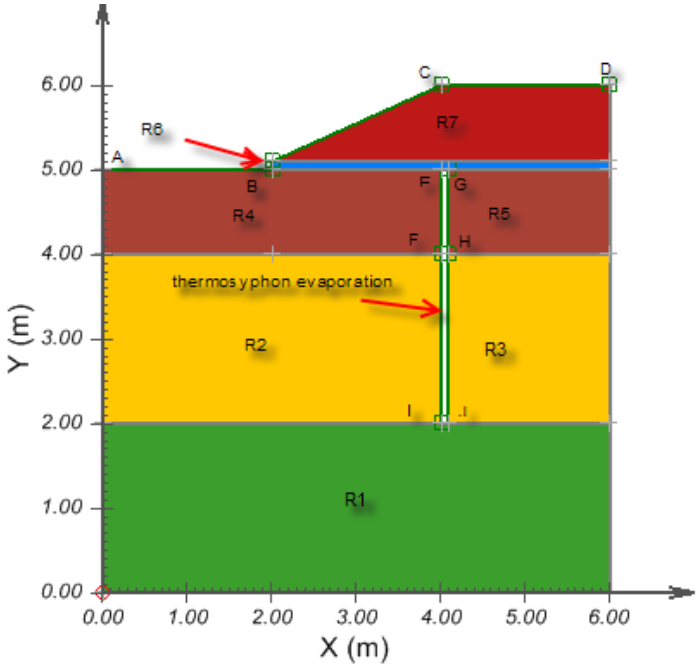

Figure 121 Geometry of the geometry-defined thermosyphon model

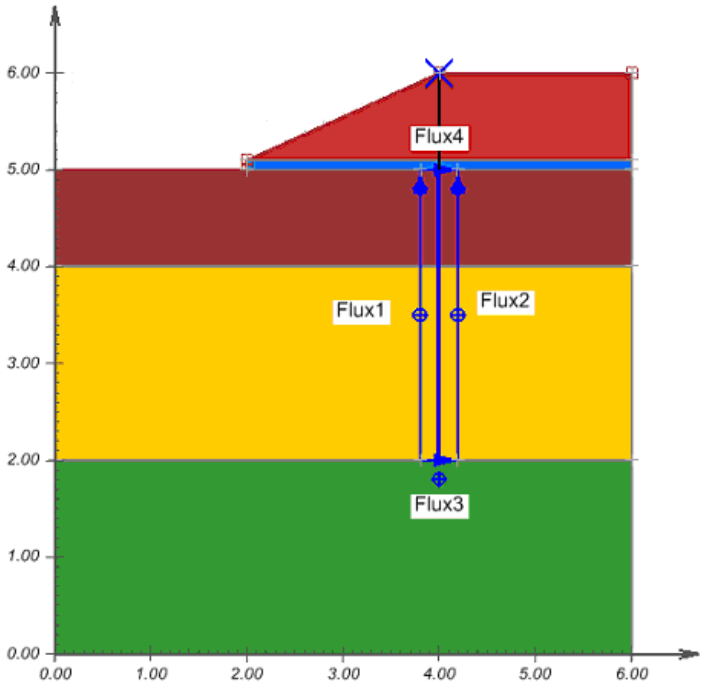

Figure 122 Geometry of the Well Object approach model

The temperature shown Figure 123 expression is applied to the boundary ABCD. The air temperature is changed with a period of 90 days in this conceptual model.

$$T_a = -1 + 12 \sin\left(\frac{2\pi}{30} t + \frac{\pi}{2}\right) \quad \textbf{[1]}$$

where

t = time, day

T_a = air temperature, °C

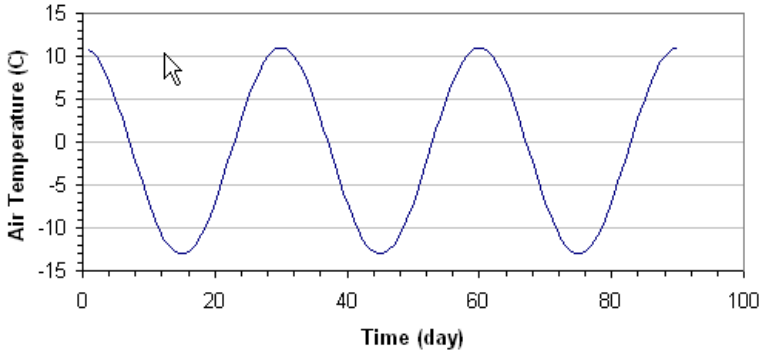

Figure 123 Air temperature applied onto the boundary condition

3.11.3 Material Properties

The thermal properties of all materials used in this model are assumed as following.

Soil Name	Thermal Conductivity (J / day-m-°C)	Soil Dry Density (kg / m^3)	Specific Heat Capacity (J/ kg-°C)
Sandy Gravel	165,801	1,250	750
Coarse sandy gravel	168,480	1,500	730
Silty Gravel	75,168	1,250	750
Schist	127,008	N /A	N / A
Insulator	127,008	N / A	N / A
Thermosyphon	2,419	N / A	N / A

3.11.4 Results and Discussions

The temperature distributions between the two models on the selected days are shown in the following figures. The temperature distributions of the geometry-defined thermosyphon models are shown on the left and the well object models are shown on the right in the following figures. The results of models show that the Well Object approach matches the Geometry-Defined thermosyphon approach.

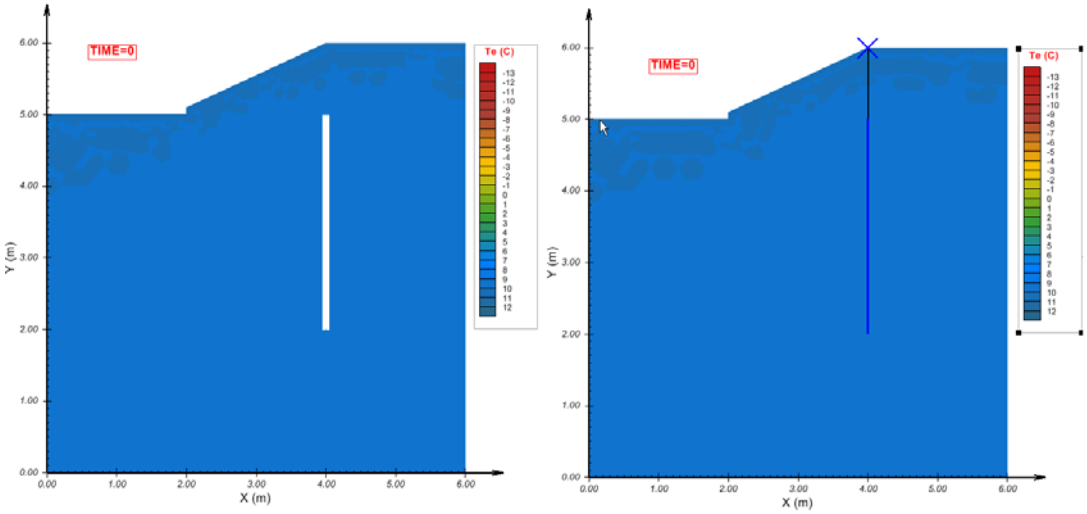

(a)SimpleHighwayEmbankmentCooling Model (b) SimpleHighwayEmbankmentCooling_Well Model

Figure 124 Temperature distributions in the beginning

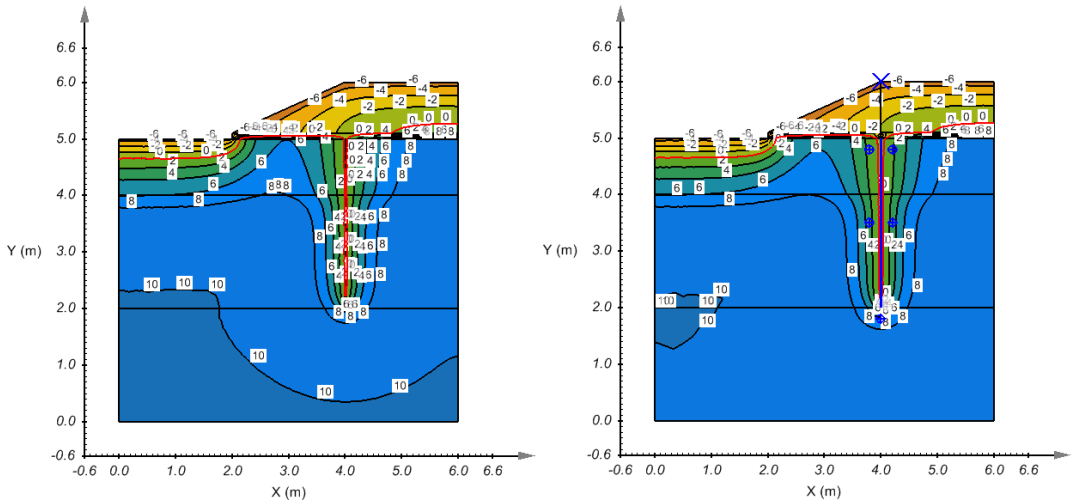

(a) SimpleHighwayEmbankmentCooling Model (b) SimpleHighwayEmbankmentCooling_Well Model

Figure 125 Temperature distributions on day 10

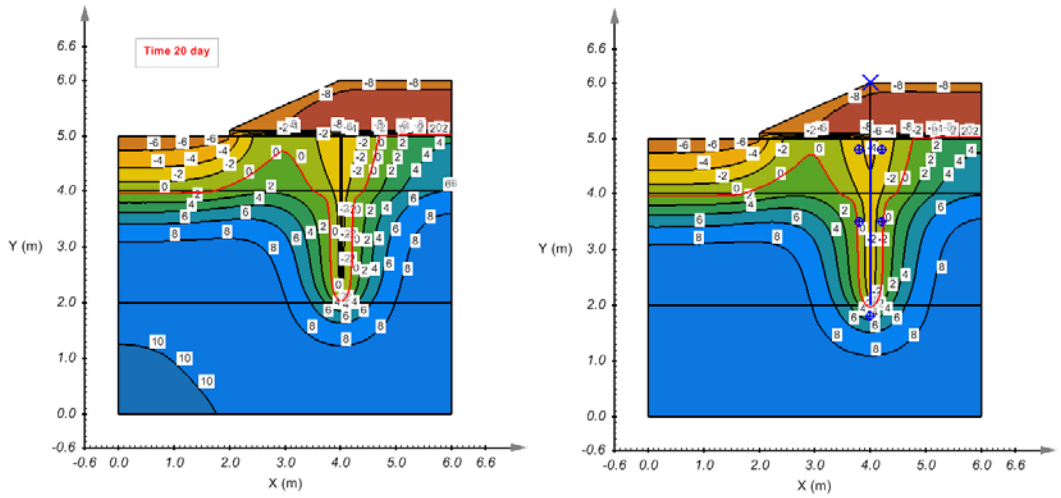

(a) SimpleHighwayEmbankmentCooling Model (b) SimpleHighwayEmbankmentCooling_Well Model

Figure 126 Temperature distributions on day 20

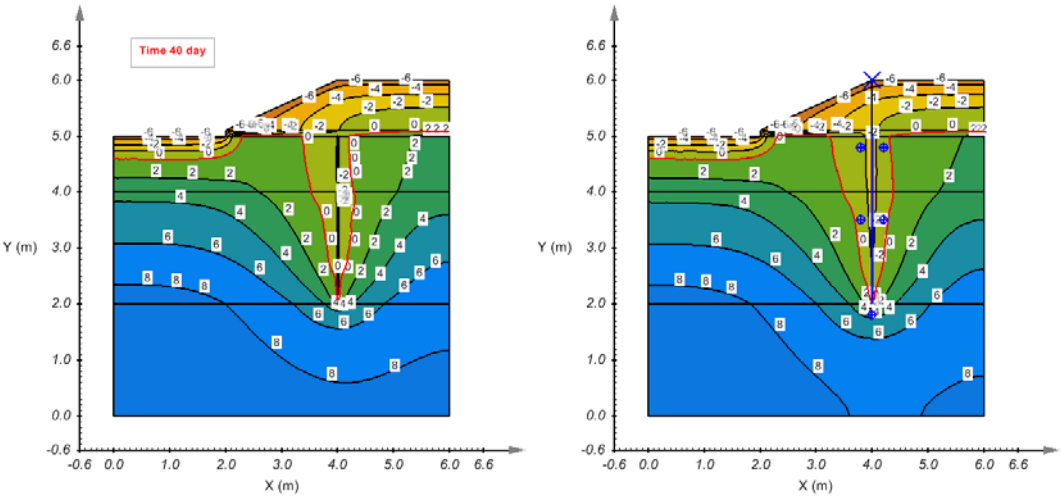

(a) SimpleHighwayEmbankmentCooling Model (b) SimpleHighwayEmbankmentCooling_Well Model

Figure 127 Temperature distributions on day 40

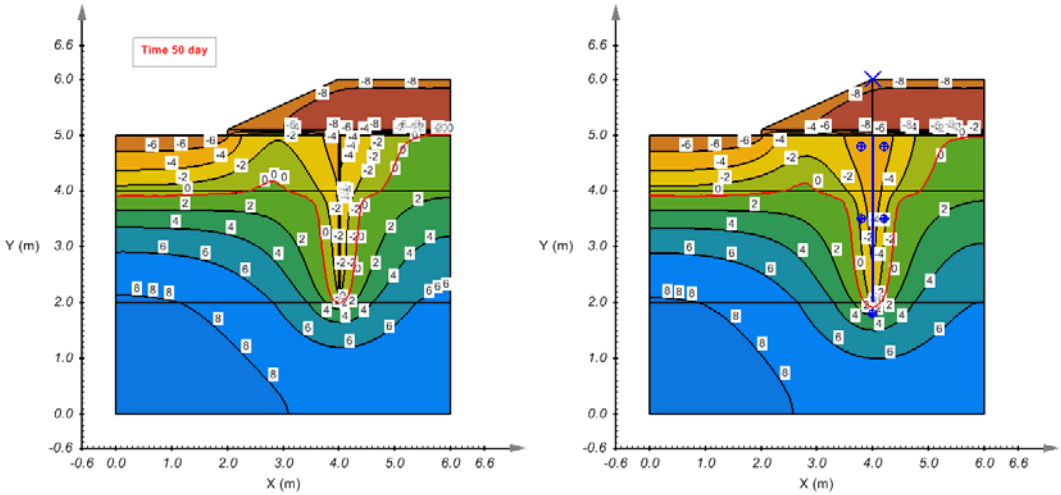

(a) SimpleHighwayEmbankmentCooling Model (b) SimpleHighwayEmbankmentCooling_Well Model

Figure 128 Temperature distributions on day 50

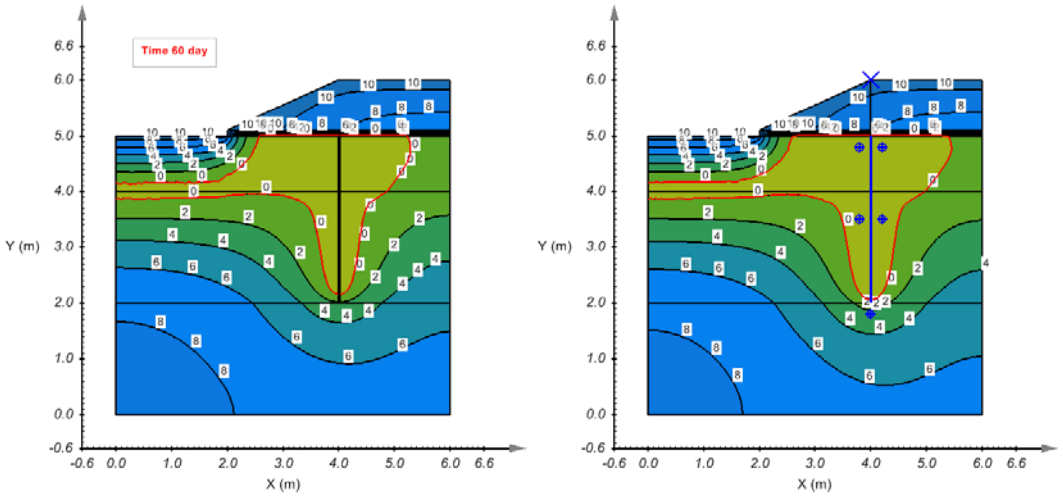

(a) SimpleHighwayEmbankmentCooling Model (b) SimpleHighwayEmbankmentCooling_Well Model

Figure 129 Temperature distributions on day 60

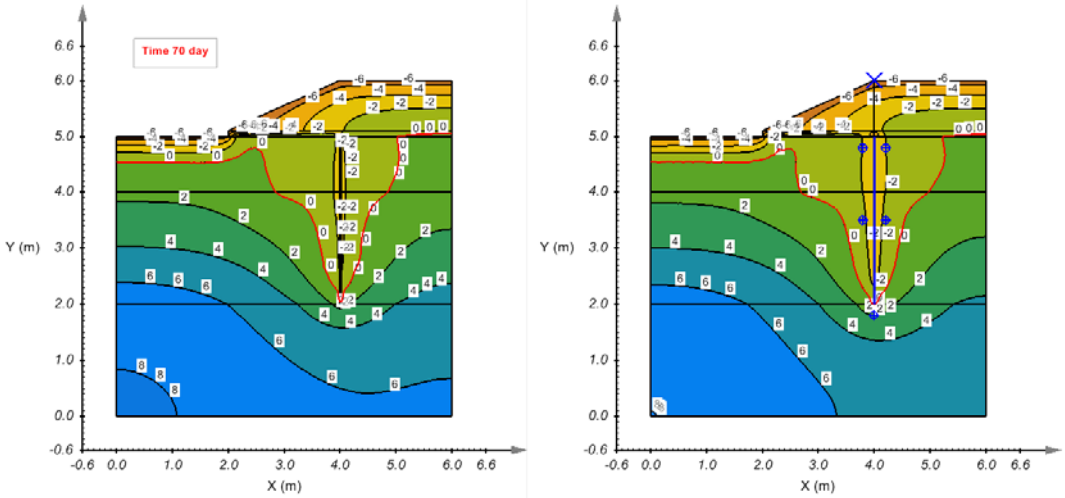

(a) SimpleHighwayEmbankmentCooling Model (b) SimpleHighwayEmbankmentCooling_Well Model

Figure 130 Temperature distributions on day 70

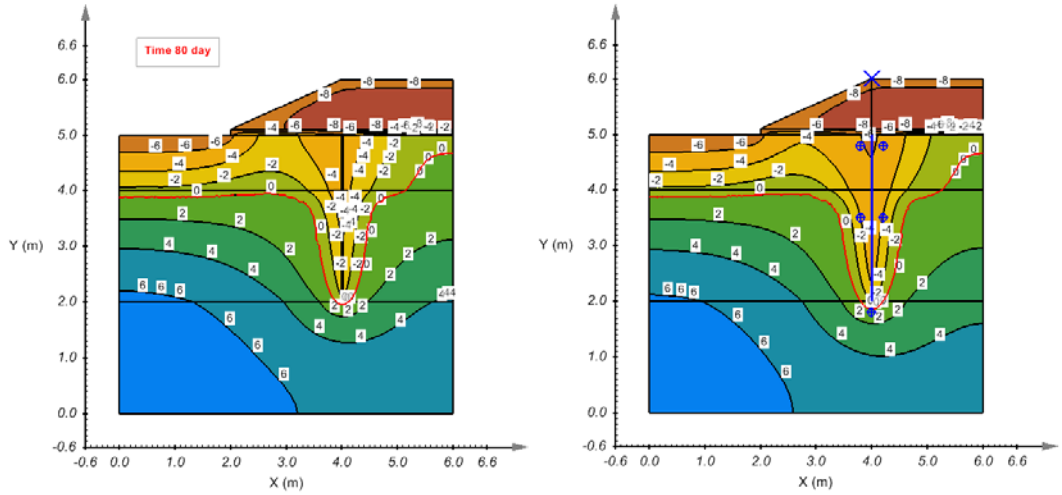

(a) SimpleHighwayEmbankmentCooling Model (b) SimpleHighwayEmbankmentCooling_Well Model

Figure 131 Temperature distributions on day 80

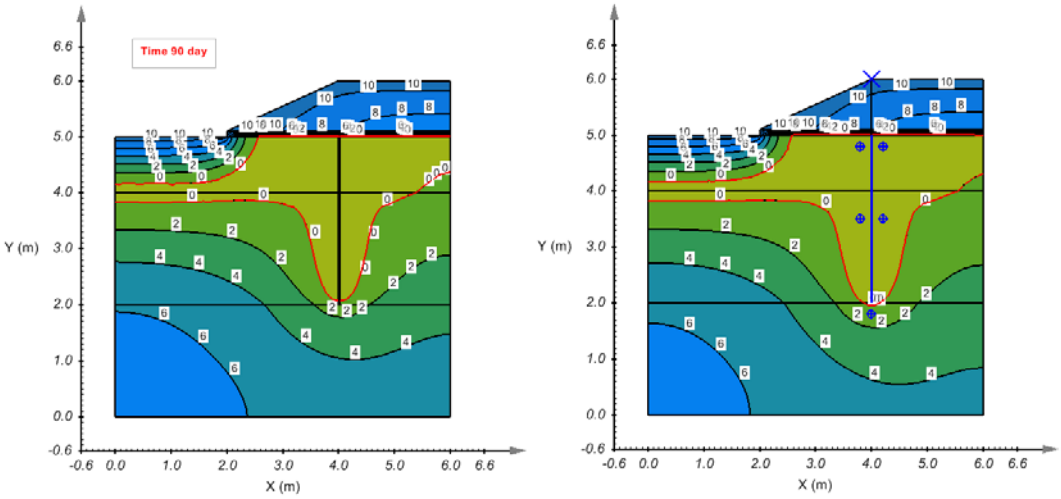

(a) SimpleHighwayEmbankmentCooling Model (b) SimpleHighwayEmbankmentCooling_Well Model

Figure 132 Temperature distributions on day 90

4 THREE-DIMENSIONAL HEAT TRANSFER

4.1 LAI (2004, 2005): VENTILATED CONDUCTION-UNCOUPLED

Project: Geothermal
Model: ventilated_conduct_RailwayEmbankmentCooling

Lai et al. (2004) proposed the analysis of 3-dimensional FEM application in ventilated embankment in permafrost regions.

4.1.1 Purpose

This example illustrates a 3D model used by Lai et al. (2004, 2005) in the analysis of temperature under the ground with the application of ventilated conduct to the train embankment cooling. The purpose is to protect the permafrost table and keep it frozen.

4.1.2 Geometry and Boundary Conditions

The model geometry with ventilated conduct is shown in Figure 133. The ventilated conduct is installed in the embankment above 1 m from natural ground surface. The distance of each ventilated conduct is 2 m. A thermal convection boundary condition is applied to ventilation conduct with a thermal convection coefficient of 15 W/m-°C. The temperature applied onto the top surface, slope, and ventilated conducts are changing with time as sin(x) function, as illustrated in Figure 134.

Permafrost table is located at 2 m from natural ground surface. Initial temperatures are specified depending on different region.

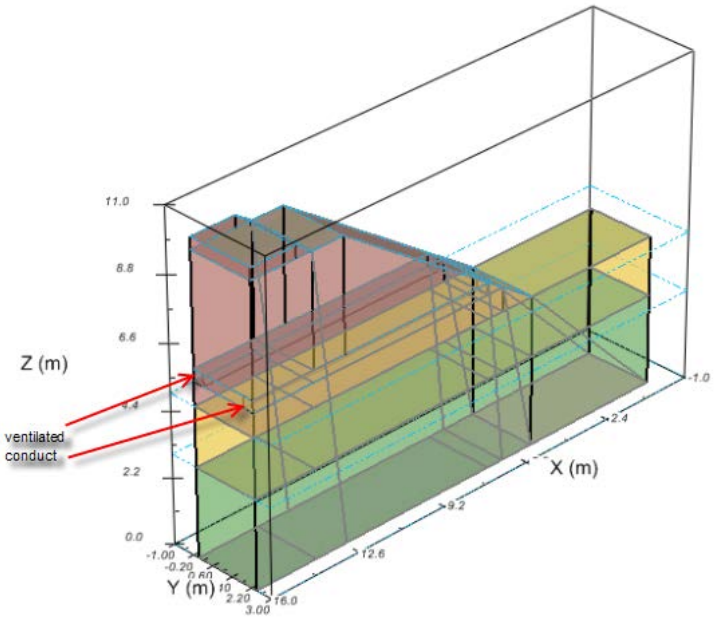

Figure 133 3-D model geometry of ventilated conduct cooling railway embankment

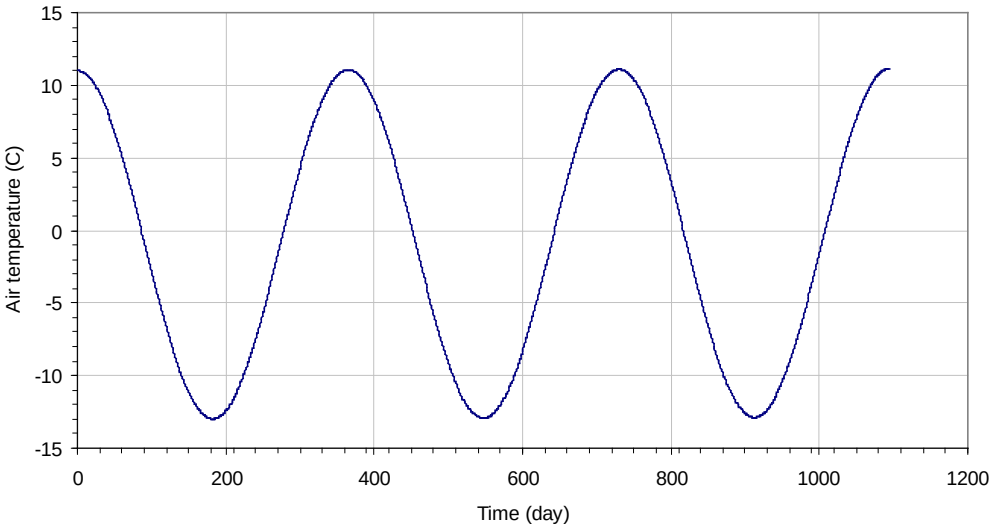

Figure 134 Air temperature

4.1.3 Material Properties

The following material properties are used in the simulation of this example.

Table 15 Material properties used in 3-D ventilated conduct model

Material Name	Thermal properties	Method	Parameters	Values	Unit
Ballast	Thermal conductivity	Constant	λ	29,894	J/day-m-°C
	Heat capacity	Constant	C	1,006,000	J/m^3-°C
	Volumetric water content	Constant	vwc	0	
	SFCC	None			
Gravel and Grid	Thermal conductivity	Constant	λ (unfrozen)	165,801	J/day-m-°C
			λ (frozen)	171,072	J/day-m-°C
	Heat capacity	Constant	C (unfrozen)	2,227,000	J/m^3-°C
			C (frozen)	1,913,000	J/m^3-°C
	Volumetric water content	Constant	vwc	0.11	m^3/ m^3
	SFCC	Expression			
			Tef	-0.01	°C
			Tep	-0.3	°C
Sub clay	Thermal conductivity	Constant	λ (unfrozen)	97,200	J/day-m-°C
			λ (frozen)	116,726	J/day-m-°C
	Heat capacity	Constant	C (unfrozen)	2,357,000	J/m^3-°C
			C (frozen)	1,879,000	J/m^3-°C
	Volumetric water content	Constant	vwc	0.30	m^3/ m^3
	SFCC	Expression			
			Tef	-0.01	°C
			Tep	-0.5	°C
schist	Thermal conductivity	Constant	λ (unfrozen)	157,593	J/day-m-°C
			λ (frozen)	127,353	J/day-m-°C
	Heat capacity	Constant	C (unfrozen)	2,009,000	J/m^3-°C
			C (frozen)	1,846,000	J/m^3-°C
	Volumetric water content	Constant	vwc	0.35	m^3/ m^3
	SFCC	Expression			
			Tef	-0.01	°C
			Tep	-0.4	°C
Thermal	Thermal conductivity	Constant	λ	241	J/day-m-°C

insulator					
	Heat capacity	Constant	C	125,600	J/m^3-°C
	Volumetric water content	Constant	vwc	0.01	m^3/ m^3
	SFCC	None			

The SFCC expression in above table is expressed as
if *Te* > *Tef* then *vwc* else if *Te* > *Tep* then *vwc* / (*Tef* - *Tep*) * (*Te* - *Tep*) + 0.01 else 0.01

The *m2i* expression is expressed as
if *Te* < *Tef* and *Te* > *Tep* then *vwc* / (*Tef* - *Tep*) else 0

4.1.4 Discussion of Results

Figure 135 is the mesh generated in the model. The isothermal surfaces of 0 °C at the initial time and 365 days are illustrated in Figure 136 and Figure 137. The simulated soil temperature distribution only July on XZ plane after running 360 days, 720 days and 1095 days are shown Figure 138, Figure 139, and Figure 140.

The permafrost table simulated with SVHEAT (i.e., an isothermal surface of 0 °C below the natural ground surface) is similar to the result obtained by Lai et al. (2004), as shown in Figure 141 and Figure 142. Please note that the coordinate difference in both figures.

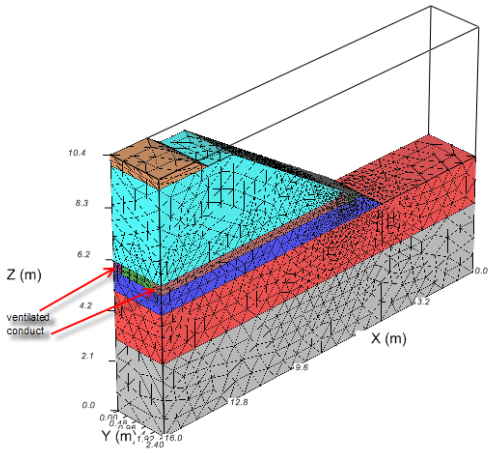

Figure 135 Model mesh generated with SVHEAT in ventilated conduct application

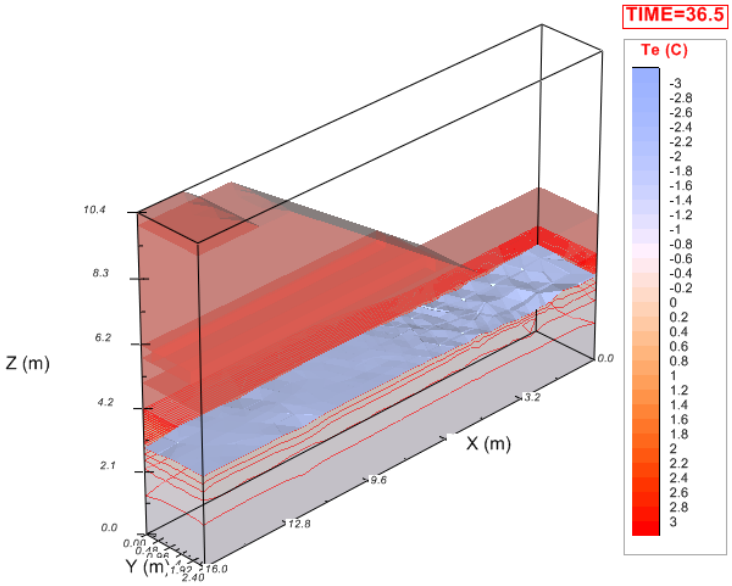

Figure 136 Initial isothermal temperature surface of 0 °C under 2 m from natural ground surface

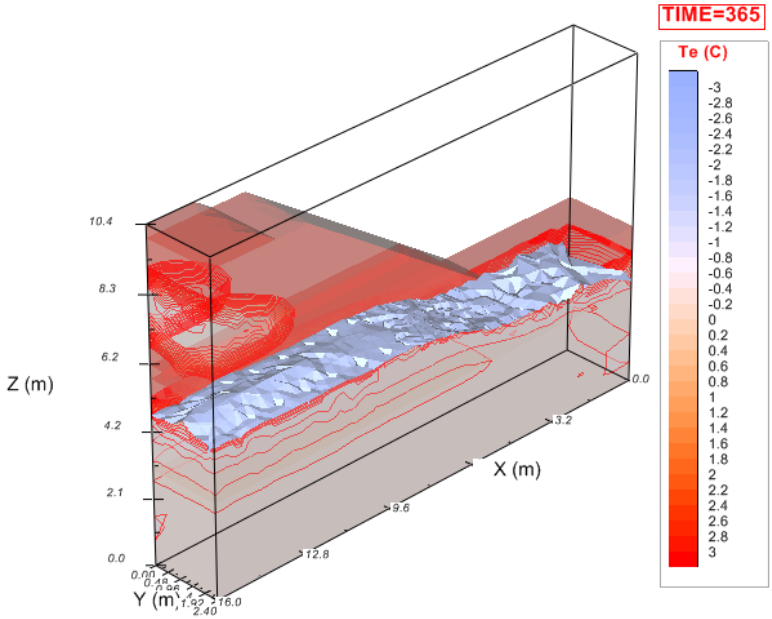

Figure 137 Isothermal temperature surface of 0 °C at time of 365 days

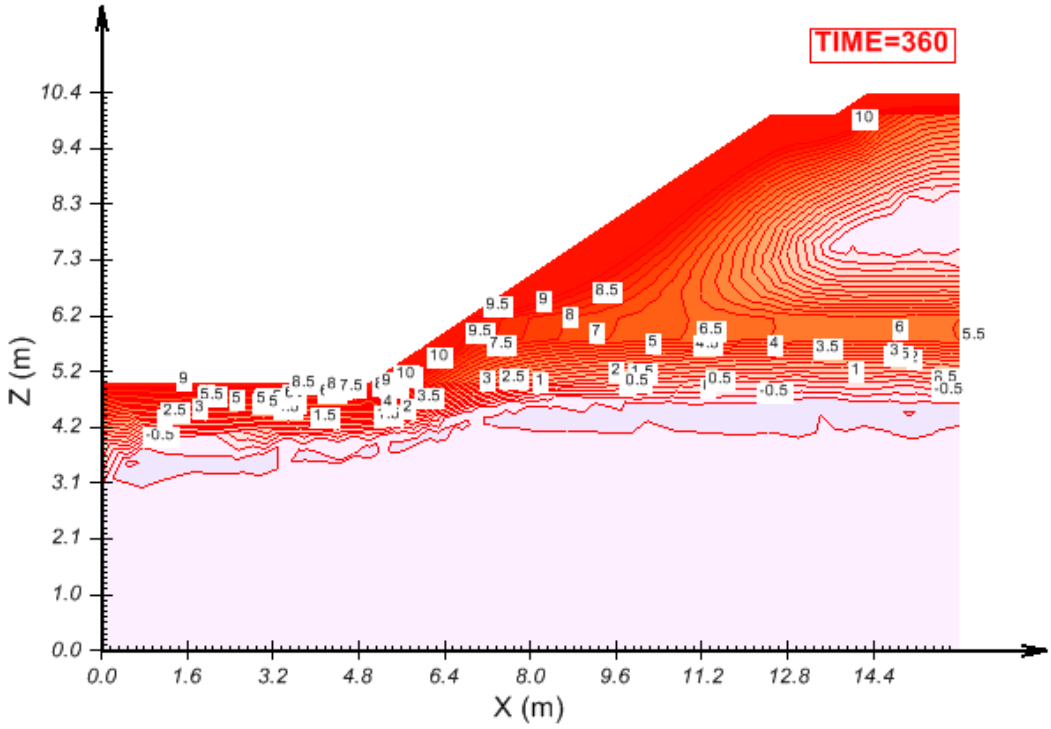

Figure 138 Temperature distribution on July after running 360 days

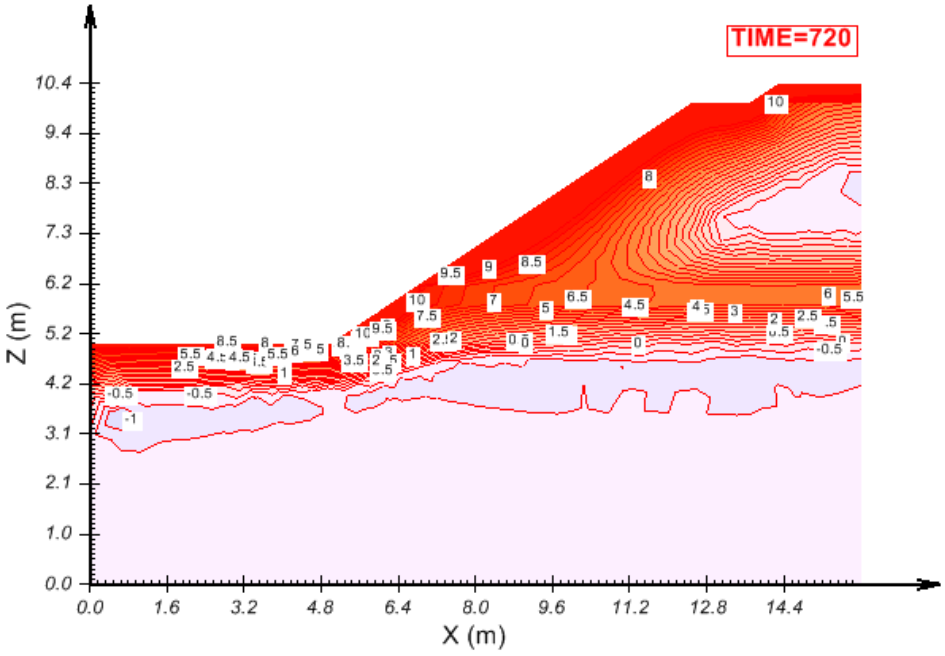

Figure 139 Temperature distribution on July after running 720 days

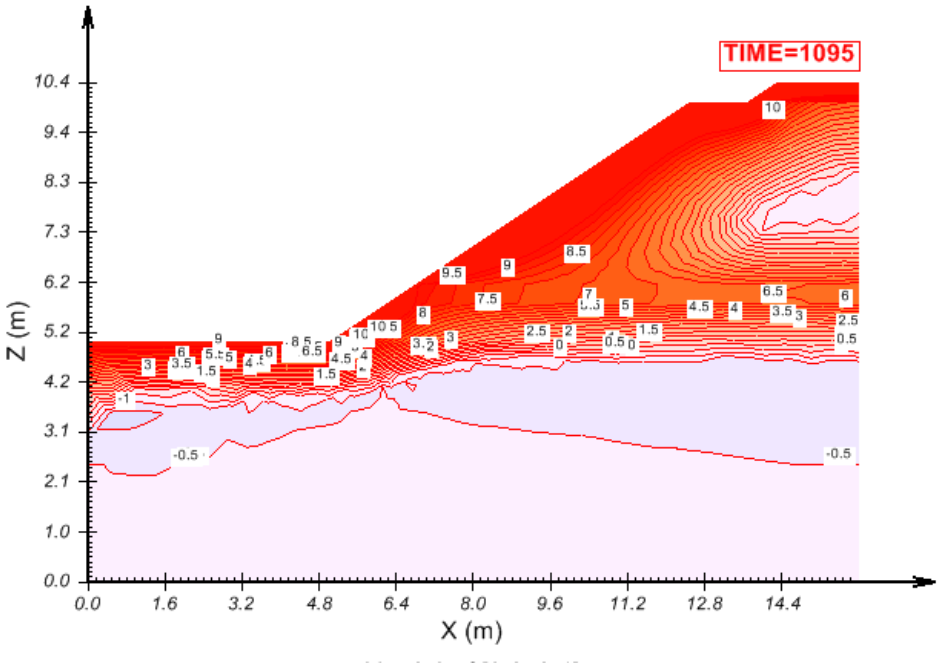

Figure 140 Temperature distribution on July after running 1095 days

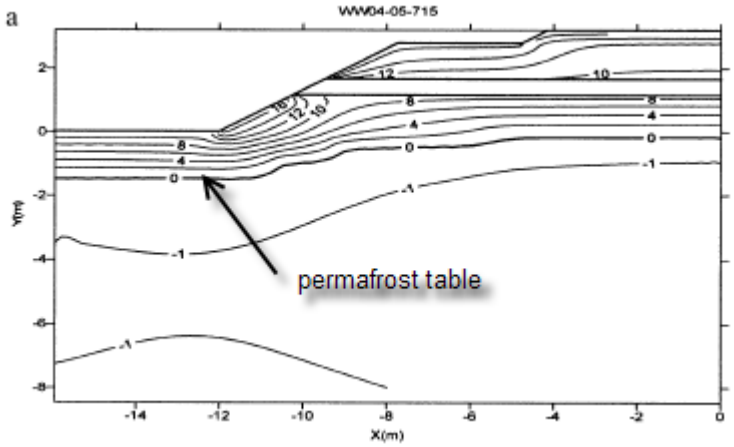

Figure 141 Permafrost table simulated by Lai et al. (2004)

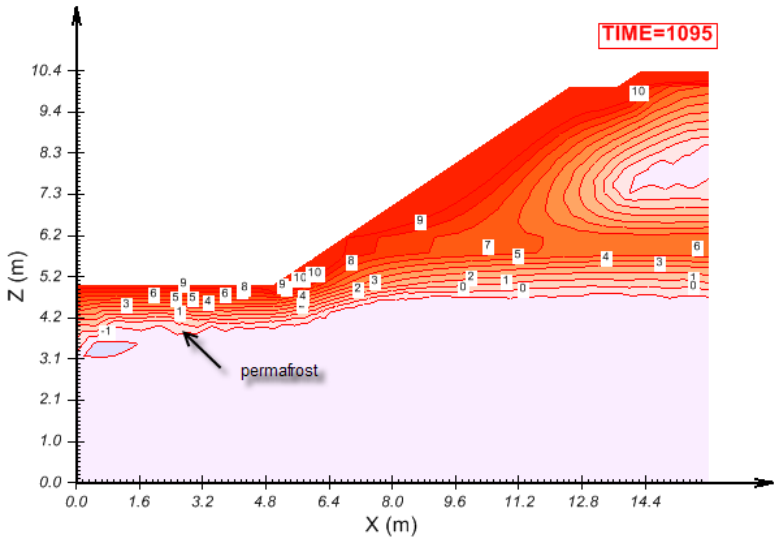

Figure 142 Permafrost table simulated with SVHEAT

4.2 THERMOSYPHON APPLICATION IN COOLING HIGHWAY EMBANKMENT

Project: Thermosyphon
Models: Thermosyphon_highwayEmbankmentCooling and
Thermosyphon_highwayEmbankmentCooling_Well

These models are one of the applications of thermosyphons to the highway embankment cooling.

4.2.1 Purpose

In this verification, two approaches are taken to simulate a thermosyphon. One approach is to simulate the thermosyphon by using region geometry and boundary conditions. Another approach is to use the Well Object function provided by SVHEAT. The goal of these models is to verify that the results of the Well Object method match the results of the Geometry-Defined thermosyphon method.

4.2.2 Geometry and Boundary Conditions

The 3D model geometry is shown in Figure 143. In these models, the evaporation portion of the thermosyphon is embedded the natural ground surface. An insulation layer of 0.1 mm thickness is placed above the evaporation part of the thermosyphon. The model with the geometry-defined thermosyphon approach is called Thermosyphon_highwayEmbankmentCooling (thereafter referred to as the “Geometry Model”) and is shown in Figure 143. The model with the Well Object approach is called Thermosyphon_highwayEmbankmentCooling _Well (thereafter referred as the “Well Object Model”) and is shown in Figure 144. The models are 3-D transient models for the duration of one month (or 30 days).

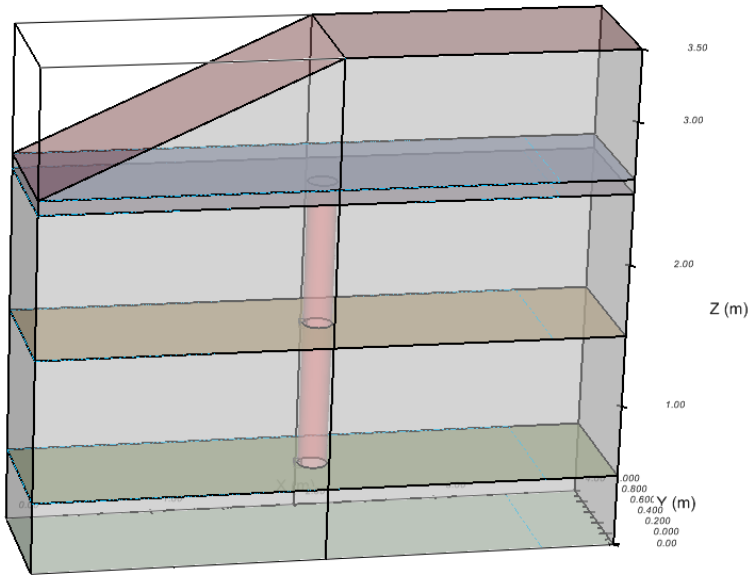

Figure 143 Geometry of the Geometry Model

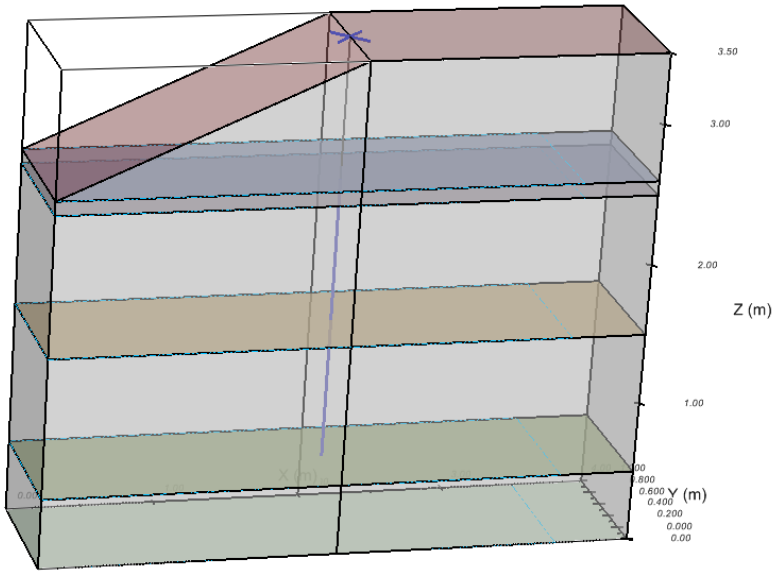

Figure 144 Geometry of the Well Object Model

The thermosyphon boundary condition is applied to the evaporation wall with a performance constant of 432,000 J/day-°C. The top and slope surface are applied the temperature changing with the following equation.

$$T_a = -1 + 12 \sin\left(\frac{2\pi}{30}t + \frac{\pi}{2}\right) \quad \textbf{[1]}$$

where

t = time, day

T_a = air temperature, °C

4.2.3 Material Properties

The thermal properties of all materials used in these models are assumed as following.

Soil Name	Thermal Conductivity (J/day-m-°C)	Soil Dry Density (kg/m^3)	Specific Heat Capacity (J/kg-°C)
Sandy Gravel	165,802	1,330	710
Coarse sandy gravel	168,480	1,500	730
Silty Gravel	75,168	1,250	750
Schist	127,008	N /A	N / A
Insulator	2,419	N / A	N / A
Thermosyphon	3.5×10^7	N / A	N / A

4.2.4 Results and Discussions

The temperature distributions between the two models on the selected days are shown in the following figures. The temperature distributions of the Geometry Model are shown on the left and the Well Object models are shown on the right in the following figures. The results of the models show that the Well Object Model approach matches the results of the Geometry Model approach. The running time of the Geometry Model is about 19 hours and 45 minutes. The running time of the Well Object Model is about 2 hours and 36 minutes. So the latter is much faster than the former (about 7.6 times faster).

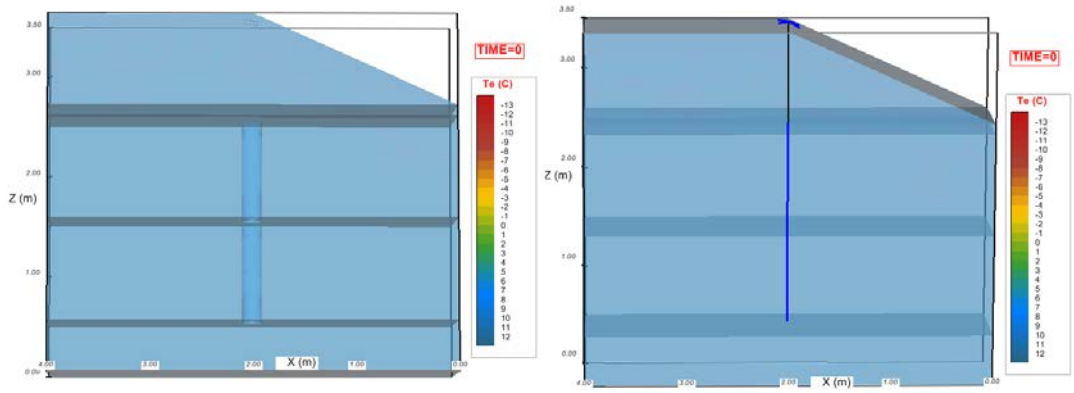

(a) The Geometry Model (b) The Well Object Model

Figure 145 Temperature distributions in the beginning

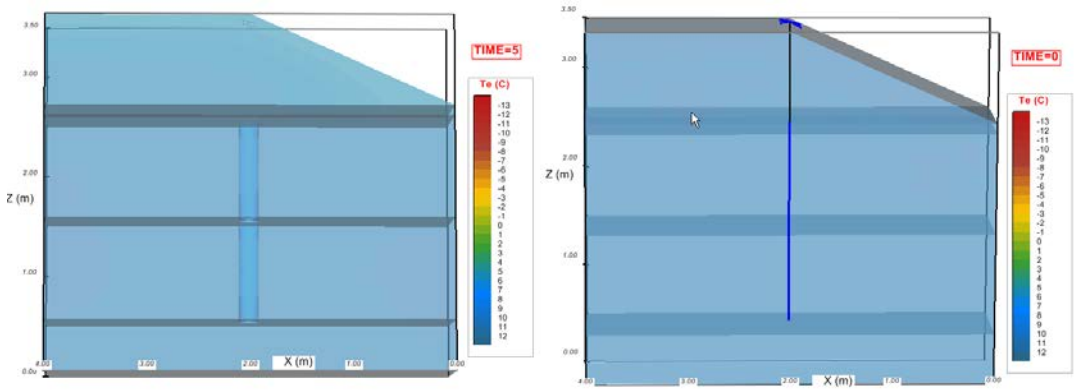

(a) The Geometry Model (b) The Well Object Model

Figure 146 Temperature distributions on day 5

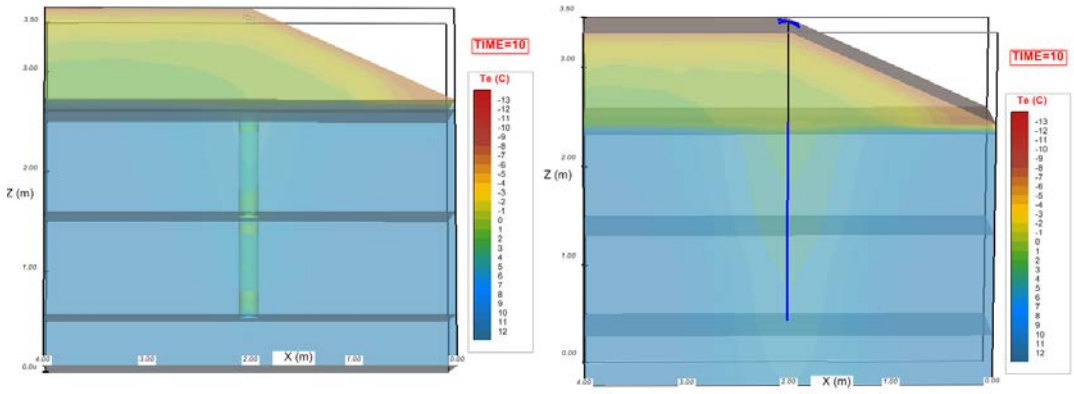

(a) The Geometry Model (b) The Well Object Model

Figure 147 Temperature distributions on day 10

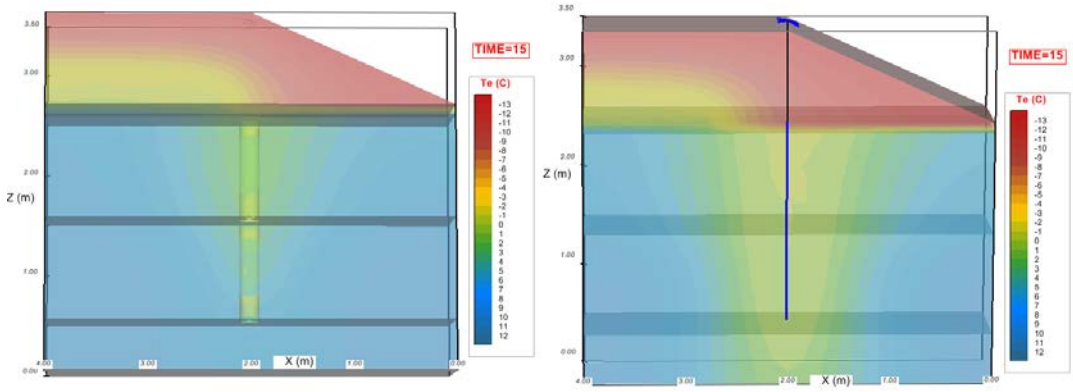

(a) The Geometry Model (b) The Well Object Model

Figure 148 Temperature distributions on day 15

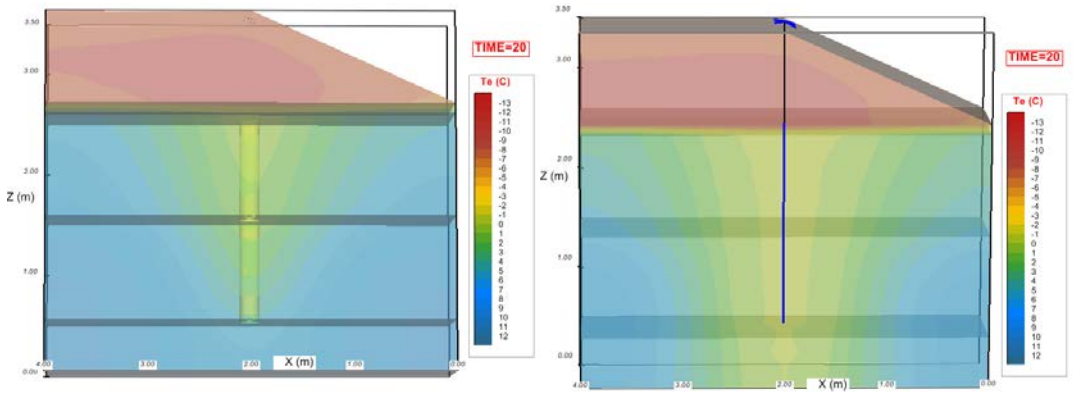

(a) The Geometry Model (b) The Well Object Model

Figure 149 Temperature distributions on day 20

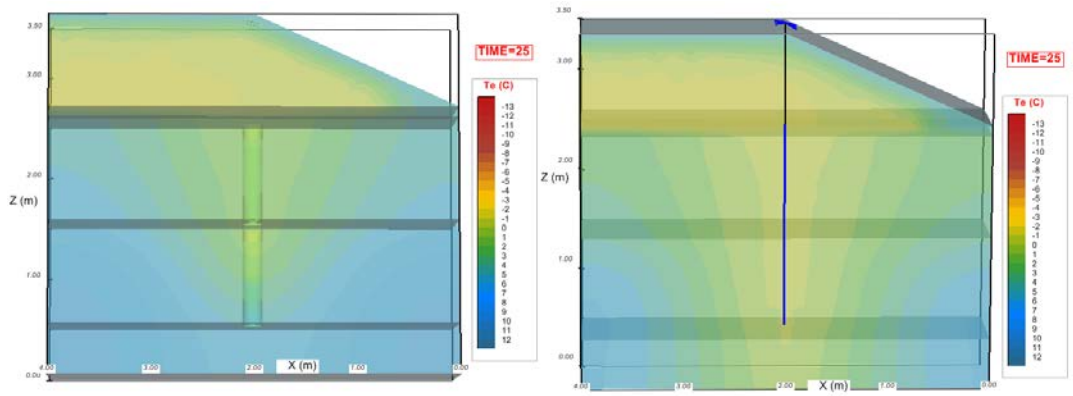

(a) The Geometry Model (b) The Well Object Model

Figure 150 Temperature distributions on day 25

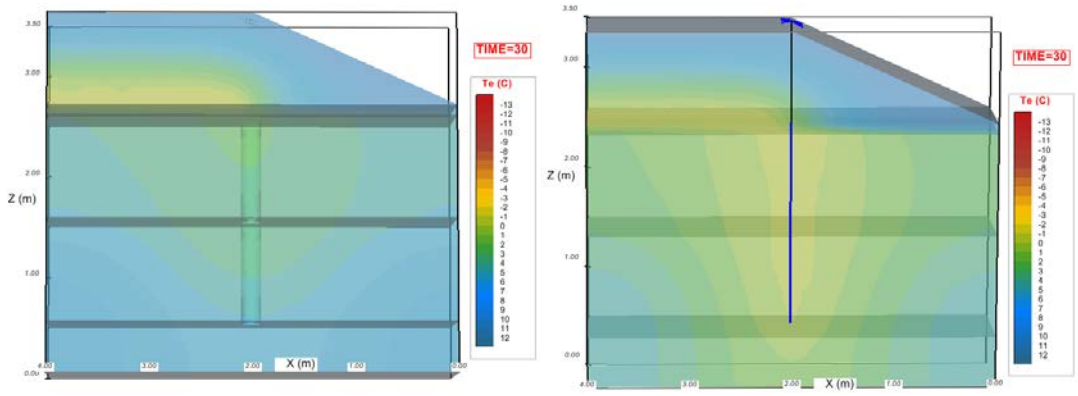

(a) The Geometry Model (b) The Well Object Model

Figure 151 Temperature distributions on day 30

5 REFERENCES

Aldrich, H.P. Jr. (1956). Frost penetration below highway and airfield pavements. Highway Research Board Bull. 135, pp. 124-144.

Coutts, R.J. and J.-M. Konrad (1994). Finite element modeling of transient non-linear heat flow using the node state method. Ground Freezing 94. Balkema, Rotterdam, Netherlands, pp. 39-47.

Dissanayaka, S.H., Hamamoto, S., Kawamoto, K., Komatsu, T., and Moldrup, P. (2012). Thermal Properties of Peaty Soils: Effects of Liquid-Phase Impedance Factor and Shrinkage. Vadose Zone Journal, February 2012, v. 11.

Elder, J.W. (1967). Transient convection in a porous medium. J. Fluid Mech. 27:609 – 623.

Erh, K.T. Nielsen, D.R. and Biggar, J.W. (1971). Two Dimensional heat transfer in porous media with steady-state flow. Soil Sci. Soc. Amer. Proc. 35: 209-214.

FlexPDE 6 (2007). *Reference Manual*, PDE Solutions Inc., Spokane Valley, WA 99206.

FlexPDE 7 (2017). *Reference Manual*, PDE Solutions Inc., Spokane Valley, WA 99206.

Harlan, R.L. and J.F. Nixon (1978). Ground Thermal Regime. In Geotechnical Engineering for Cold Regions, eds. Andersland, O.B. and Anderson, D.M. pp. 103-163.

Jame, Y.W. (1977). Heat and Mass Transfer in Freezing Soil. Ph.D Thesis. University of Saskatchewan, Saskatoon, Canada

Johansen, O. (1975). Thermal Conductivity of Soils. Ph.D. Thesis. Trondheim, Norway. (CRREL Draft Translation 637, 1977)

Lai, Y., Wang, Q. and Niu, F. (2004). Three dimensional nonlinear analysis for temperature characteristic of ventilated embankment in permafrost regions. Cold Regions Science and Technology, 38: 165-184

Liu, Z, and Lai, Y. (2005). Numerical analysis for the ventilated embankment with thermal insulation layer in Qing-Titetan railway. Cold Regions Science and Technology, 42: 177-184.

Li, X. and Koike, T. (2001). A new frozen soil parameterization in land surface scheme. Present and Future of Modeling Global Environmental Change: Toward Integrated Modeling, Eds., T. Mastsuno and H. Kida, pp. 405 – 414.

Lu, S., Ren, T., Gong, Y., and Horton, R. (2007). An improved model for predicting soil thermal conductivity from water content at room temperature. SSSAJ 71 (1):8-14.

Molycorp Seepage Numerical Modeling Report – Part I. 2008. SoilVision Systems Ltd.

Newman, G. P. (1995). Heat and Mass Transfer in Unsaturated Soils during Freezing. Master Thesis. University of Saskatchewan, Saskatoon, Canada

GEO-SLOPE International Ltd. Freezing around a Pipe with Flowing Water.

TEMP/W User's Guide, (1991-2001). GEO-SLOPE International Ltd., Calgary, Alberta, Canada

Zhang, Z.X, Kushwaha R.L. (1998). Modeling soil freeze-thaw and ice effect on canal bank. Can. Geotech. J. 35: 655–665.

Tarnawski, V.R., Momose, T., and Leong, W.H. (2009). Assessing the impact of quartz content on the prediction of soil thermal conductivity. Geotechnique 59(4): 331-338.